

# ABSTRACT

Allen, Angela M. The Interaction of Boronic Acid Based Self-Assembled Monolayers as a Potential Glucose Sensor. (Under the direction of Christopher B. Gorman)

Recognition of sugars such as glucose with phenylboronic acid – terminated self assembled monolayers (SAMs) was the basis for the designing and fabricating a biosensor. Self-assembled monolayers were formed on gold surfaces as shown by infrared spectroscopy. The continuous, repeatable increase of the electrochemical impedance as the concentration of glucose was increased gave indication of binding. This binding could be attributed to the precedent formation of relatively stable esters between phenylboronic acids and sugars. This impedance change upon binding between glucose and a phenylboronic acid-terminated SAM showed promise in the development of a glucose biosensor.

THE INTERACTION OF BORONIC ACID BASED SELF –  
ASSEMBLED MONOLAYERS AS A POTENTIAL GLUCOSE SENSOR

by

ANGELA M. ALLEN

A Dissertation Submitted to the Graduate Faculty of  
North Carolina State University  
in Partial Fulfillment of the  
Requirement for the Degree of  
Doctoral of Philosophy

Department of Chemistry

Raleigh, North Carolina  
November 1, 2004

Approved by:

---

Christopher B. Gorman, Committee Chair

---

Charles B. Boss

---

Kenneth W. Hanck

---

Edmond F. Bowden

# Dedication

*I dedicate this work to my son. Remember you can achieve anything through the will of God.*

*Love,  
Mom*

# BIOGRAPHY

Angela Malelya Allen was born on November 9, 1974 to Theodore and Doris Allen. She has two older sisters: Dr. LaWanda (Eric) Kemp and Ava (Spencer) Moore and a son: John “Trey” Dixon, III. In 1993, she graduated with honors from Dublin High School in Georgia. She attended Albany State University (ASU) to pursue a degree in Chemistry. As an undergraduate, she was a HOPE Scholar and a MARC Scholar. During her years at ASU, she became apart of the Delta Rho Chapter of Delta Sigma Theta Sorority, Inc. She also participated in several other organizations as well. In 1998, she graduated Cum Laude with a Bachelors of Arts in Chemistry. The author taught Physical Science at East Laurens High School (ELHS) in East Dublin, Georgia for a year. After teaching at ELHS, she decided to advance her knowledge in the field of chemistry by applying to several different graduate schools. She was accepted to North Carolina State University (NCSU) Chemistry Department, where she researched under Dr. Christopher Gorman in the area of biosensors. She has successfully her obtained her Ph. D. as of November 2004.

# ACKNOWLEDGEMENTS

First and foremost, I give thanks and honor to God for giving me the strength to have accomplished so much in my life so far.

I would like to thank my family for sacrificing their time and allowing me the opportunity to pursue my dreams. To my parents (Theodore and Doris), there are not enough words to express how special you are to me. To my sisters (LaWanda and Ava), you are the inspiration in your little sister's life. I appreciate each summer that you took my son in as your own. To my son (John, "Trey"), I know at times it was tough but your love is the backbone to my success. And I want to take this moment to let my family know that I am very grateful for their guidance, support, and encouragement.

To my friends (near and far), I thank you for your unchanging friendship. To Chiamaka Porter and Damian Young, we came in together as strangers and we are leaving best friends. I want you to know that knowing you as changed my life and I wish you the best in all that you accomplish. You have been more than my friends; you have been my family. To those who came into the program later (KeAndrea, Donna, Holly, Sofi, Young Rae, and James), it has been a pleasure meeting all of you. From KeAndra and our shopping sprees to Sofi and our interesting discussions, I appreciate you all for the laughs, conversations, and adventures. To Eddie Porter, thank you for stepping in and being the male role model that my son needed. To my friends far away (Erica and Tamika), a telephone is a powerful tool. Thank you for your companionship throughout the years. I hope you all the best in your endeavors.

To those you have gone before me (grandparents and dear friends), sharing this world with you has altered my life tremendously. To my grandparents and Daddy Holeman, I wish you were here today to share this moment with me. Your kindness and consideration will always be remembered.

To my committee, I thank you for your assistance and for challenging my abilities to become a better scientist. Dr. Gorman, it has been a long road and I am pleased to have had the chance to work with you. To Dr. Boss and Dr. Hanck, I would like you to know that you are a blessing to the department. Thank you for never giving up on me and always pushing me in the right directions. To Dr. Gorman's group, it has been a pleasure meeting each and every one of you.

Again, I deeply appreciate everyone who has played a role in supporting my efforts.

# Table of Contents

List of Tables .....	ix
List of Figures .....	x
List of Schemes .....	xvi
CHAPTER 1: SIGNIFICANCE OF RESEARCH.....	1
1.1 Overview .....	1
1.2 References .....	5
CHAPTER 2: BACKGROUND .....	7
2.1 Diabetes .....	7
2.1.1. Type I diabetes .....	9
2.1.2 Type II diabetes .....	9
2.1.3 Evaluation of diabetes.....	10
2.2 Biosensors.....	11
2.2.1 Bioactive materials (bioreceptors).....	12
2.2.2 Transducers.....	14
2.3 Glucose Biosensor .....	16
2.4 Formation of Monolayers.....	21
2.4.1. Self assembled monolayers (SAMs).....	23
2.4.2. Order in self assembled monolayers <sup>50,58-62</sup> .....	24
2.4.3. Characterization of self assembled monolayers <sup>50,58-62</sup> .....	24
2.5 References .....	27
CHAPTER 3: INSTRUMENTAL ANALYSIS .....	29
3.1 Electrochemical Impedance Spectroscopy (EIS) <sup>49,56,63,64</sup> .....	29

3.2 Infrared Spectroscopy (IR) <sup>57,67</sup> .....	36
3.3 Cyclic Voltammetry (CV) <sup>42,64,67</sup> .....	38
3.4 References .....	40
CHAPTER 4: INVESTIGATING THE INTERACTIONS BETWEEN GLUCOSE AND BORONIC ACID BASED SELF ASSEMBLED MONOLAYERS.....	
4.1 Introduction.....	41
4.2 Experimental Section .....	43
4.2.1 Materials and substrates.....	43
4.2.2. Synthesis of N-(3-dihydroxyborylphenyl)-11-mercaptoundecanamide (PBA) .....	43
4.2.3 Pretreatment of gold substrates and formation of SAM .....	44
4.2.4 Spectroscopic measurements.....	45
4.2.5. Electrochemical measurements.....	47
4.3 Results and Discussion .....	49
4.3.1 Characterization of phenylboronic acid-terminated SAMs (PBA-SAM) <sup>77</sup> .....	49
4.2.3 Binding interaction between PBA – SAM and D-glucose <sup>77</sup> .....	54
4.3.3. EIS measurements of the PBA – SAM system .....	59
4.4 Conclusion.....	67
4.5 References .....	69
CHAPTER 5: THE INFLUENCE OF INSERTING ELECTROACTIVE MOLECULES INTO THE PBA – SAMS .....	
5.1 Introduction.....	70

5.2 Experimental Section .....	72
5.2.1. Materials and substrates.....	72
5.2.2. Synthesis of N-(3-dihydroxyborylphenyl)-3-mercaptopropionamide ..	73
5.2.3. Pretreatment of gold substrates and formation of SAM .....	74
5.2.4. Electrochemical measurements.....	75
5.3 Results and Discussion .....	76
5.3.1. Characterization of Fc <sub>11</sub> and PBA <sub>11</sub> coabsorbed on gold surface <sup>79,97</sup>	76
5.3.2. Performance of the mixed SAM .....	80
5.3.4. Binding abilities of boronic acid after incorporating ferrocene – terminated thiol .....	82
5.3.5. Optimizing parameters in order to produce a more proficient biosensor .....	85
5.4 Conclusion.....	91
5.5 References .....	93

## List of Tables

Table 2.1: Complications associated with diabetes.....	7
Table 2.2: Evaluation of the two most common types of diabetes .....	8
Table 2.3: The active materials (biological related) are responsible for binding or interacting with the analyte of interest.....	12
Table 2.4: Some types of transducers that are responsible for converting recognitions to measurable signals.....	14
Table 4.1: Important vibrational mode assignments that corresponds to PBA on a gold surface .....	50
Table 4.2: Two – way ANOVA results on impedance data for PBA <sub>11</sub> -SAMs ....	67
Table 5.1: Two – way ANOVA results on impedance data on Fc <sub>11</sub> /PBA <sub>11</sub> - SAMs .....	91
Table 5.2: Two – way ANOVA results on impedance data on Fc <sub>6</sub> /PBA <sub>11</sub> – SAMs .....	91
Table 5.3: Two – way ANOVA results on impedance data on Fc <sub>6</sub> /PBA <sub>3</sub> – SAMs	91

# List of Figures

Figure 1.1: Schematic approach of the interaction between D-glucose and a boronic acid derivative which forms a boronate ester. ....2

Figure 2.1: (A) Arrangement of a typical biosensor, where the combination of a bioactive material and a transducer is surrounded by analytes. (B) When a bioactive material recognizes a specific analyte, a measurable signal is observed. .... 11

Figure 2.2: Schematic of glucose detection with the enzyme glucose oxidase (Gox). .... 17

Figure 2.3: A picture of the Yellow Spring instrument, YSI 23A Blood Glucose Analyzer. .... 17

Figure 2.4: Schematic of how artificial mediators are used to shuttle electrons, where (ox) is the oxidized formed and the (red) is the reduced formed of the glucose oxidase (Gox) and the mediator (M). .... 18

Figure 2. 5: An example of the home – based glucose sensor , Medisense Pen, used by diabetics. .... 19

Figure 2.6: (A) A picture of a GlucoWatch developed by the Cygnus, Inc., along with (B) sequences of events that occur in the sensor. (From URL: <http://www.brookscoble.com>) .....20

Figure 2.7: A general schematic of an ideal, organized monolayer on a metal substrate (electrode), where the alkane chains are bound to substrate and functional groups are attached to the terminal ends of the alkane chains. ..22

Figure 2.8: Schematic of the self – assembled method. This method involves (A) a substrate and a solution of desired sulfur containing molecule, where (B) the substrate is submerged into the solution for a period of time and (C) a monolayer is formed as a result.....	23
Figure 3.9: The sinusoidal current and voltage (A) for a resistor when the phase shift is zero and (B) for a capacitor when the current lags the voltage.....	30
Figure 3.2: The basic vector diagram used for resistance/capacitance (RC) circuit .....	31
Figure 3. 3: Circuits comprising of a resistor in the DC method (A)series and (B) parallel that can be related to the total impedance when the AC method is in (C) series and (D) parallel.....	32
Figure 3.4: The simplest circuit used in electrochemical cells (systems). .....	33
Figure 3.5: An example of a Bode plot representing a gold electrode in 0.1 HClO <sub>4</sub> solutions from a BAS IM6 instrument.....	34
Figure 3.6: Example of a complex plot for a simple electrochemical system .....	35
Figure 3.7: An example of cyclic voltammetric excitation signal used to obtain voltammogram .....	38
Figure 3.8: An example of a surface bound voltammetry for one – electrode redox couple; scan rate of 100 mV/s in 0.1 HClO <sub>4</sub> aqueous solution.....	39
Figure 4.1: A picture of the Bowden cell use for electrochemical measurements, along with a schematic of the cylindrical cavity; the working electrode (gold substrate) is secured at the bottom of the cell, the counter electrode	

(platinum wire) is coiled around the reference electrode (silver/silver chloride).....	47
Figure 4.2: The PM-IRRAS spectra of a monolayer PBA on a gold surface in the low (A) and high (B) wavenumber region, respectively.....	50
Figure 4.3: Single – pass ATR – FTIR spectra of a 3 mM PBA solution in ethanol allowed to evaporate on the ATR element in the low (A) and high (B) wavenumber region. ....	52
Figure 4.4: Cyclic voltammogram overlay of bare gold (A) and boronic acid terminated-SAM (B). Experiments were performed in 1.0 M HClO <sub>4</sub> and at room temperature. Scan rate, 100 mV/s; electrode area, 0.32 cm <sup>2</sup> .....	54
Figure 4.5: PM – IRRAS spectra of a PBA – SAM exposed (solid spectrum) to 3 mM glucose solution for 30 minutes and a PBA – SAM not exposed (dashed spectrum).....	55
Figure 4.6: Single-pass ATR-FTIR spectra of a 3 mM solution of PBA (solid), 3 mM solution of glucose (short dashed), and the 1:1 molar ratio of both in the low (A) and high (B) wavenumber region. All solutions were allowed to evaporate on the ATR element.....	57
Figure 4.7: Representations of Bode plots by the Thales software. Plots represent impedance on bare gold (A) and impedance on a PBA – SAM (B). All experiments were performed in 0.1 M HClO <sub>4</sub> at 5mV amplitude.....	60
Figure 4.8: Graph representing the changes that occur in the absence and the presence of glucose in the intermediate region. An experiment ran in 0.1 M HClO <sub>4</sub> at 5 mV amplitude and at room temperature. ....	62

Figure 4.9: Plot of impedance against glucose concentration. The experiment was done in 0.1 M HClO<sub>4</sub> solution at 5 mV amplitude and at room temperature. Data obtained at 1.47. Hz. ....63

Figure 4.10: Comparisons of impedance plots for mercaptoundecanoic acid – terminated SAM (blue) and phenylboronic acid –terminated SAM (red) at different glucose concentrations. Impedance measurements done at an amplitude of 5 mV and at room temperature. Plots were taken at 1.47 Hz. .64

Figure 4.11: Graphs representing comparisons of PBA – SAMs. Experiments done in 0.1 M HClO<sub>4</sub> at an amplitude of 5 mV and room temperature.....65

Figure 4.12: A plot of how each cell differs in percent as different glucose concentrations are added. Each cell is represented by the same color as in Figure 4.11.....66

Figure 5.1: PM – IRRAS spectra of a mixed SAM, having a 50/50 feed ratio, on gold in the (A) low and (B) high wavenumber regions, respectively.....77

Figure 5.2: An overlay of cyclic voltammograms of (red) ferrocenylthiolate on gold and (black) a 50/50 feed ratio of a mixed SAM [PBA<sub>11</sub> and Fc<sub>11</sub>]; experiment done in 0.1 M NaClO<sub>4</sub> (pH 11 w/ 10 mM NaOH) at a scan rate of 100 mV/s and at room temperature. ....78

Figure 5.3: Comparisons of cyclic voltammograms in high pH (red) and low pH (black) electrolyte solutions for Fc<sub>11</sub>/PBA<sub>11</sub> SAMs. Experiments done at scan rate of 100 mV/s and at room temperature. (Data for graphs were taken at different times) .....81

Figure 5.4: Overlays of Fc – SAM cyclic voltammograms at different glucose concentrations: 0 mM (black), 5 mM (red) and 20 mM (green); scan rates at 100 mV/s .....83

Figure 5.5: Graph of the percent change in the impedance data obtained in 0.1 NaClO<sub>4</sub> (pH 11, adjusted with 10 mM NaOH); observed at 1.5 Hz .....83

Figure 5.6: Plots that represent the reproducibility of Fc<sub>11</sub>/PBA<sub>11</sub> – SAMs; experiments done in pH 11 solution at an amplitude of 5 mV and at room temperature. ....84

Figure 5.7: A graph representing the cells from Figure 5.5 (with respect to colors) of the impedance changes in the presence of glucose .....84

Figure 5.8: Cyclic voltammogram of a Fc<sub>6</sub>/PBA<sub>11</sub> - SAM on a gold surface in pH 11 solution; scan rate of 100 mV/s at room temperature. ....86

Figure 5.9: Cyclic voltammogram of a Fc<sub>6</sub>/PBA<sub>3</sub> - SAM on a gold surface in pH 11 solution; scan rate of 100 mV/s at room temperature. ....87

Figure 5.10: Bode plots of both mixed monolayers: (A) Fc<sub>6</sub>/PBA<sub>11</sub> – SAM and (B) Fc<sub>6</sub>/PBA<sub>3</sub> – SAM. ....88

Figure 5.11: Impedance plots of representative data from Fc<sub>6</sub>/PBA<sub>11</sub> – SAMs at different glucose concentrations. Impedance measurements done at an amplitude of 5 mV and at room temperature. Plots were taken at 1.47 Hz. .89

Figure 5.11: Impedance plots of representative data from Fc<sub>6</sub>/PBA<sub>3</sub> – SAMs at different glucose concentrations. Impedance measurements done at an amplitude of 5 mV and at room temperature. Plots were taken at 1.47 Hz. .89

Figure 5. 12: A proposed circuit model to investigate the physical characteristics of the mixed SAMs; which includes four components: uncompensated solution resistance,  $R_s$ , film capacitance,  $C_f$ , charge transfer resistance,  $R_{ct}$ , and pseudocapacitance,  $C_a$ . .....90

## List of Schemes

Scheme 4.1: Synthesis of N-(3-dihydroxyborylphenyl)-11-mercaptoundecanamide (PBA).....	45
Scheme 5.1: Synthesis of N-(3-dihydroxyborylphenyl)-3-mercaptopropionicamide) (abbreviated PBA <sub>3</sub> ).....	74
Scheme 5.2: Molecules used in the formation of mixed monolayers in order to optimize the organization of the SAM. ....	85

# CHAPTER 1: SIGNIFICANCE OF RESEARCH

---

## **1.1 Overview**

Over the last few years, there has been a growing interest in developing biosensors that are selective for sugar (saccharide or diol) detection.<sup>1-11</sup> The advancements in this field offer promising outlooks in many important applications related to sugars such as managing diabetes by monitoring the levels of glucose concentration in the blood. Majority of commercially available glucose biosensors are enzyme – based, which requires frequent collection of blood samples. There are several problems related to this type of method. The first one is the pain from pricking a finger via a small needle. Second, the frequent pricking can be an inconvenience that affects a patient's daily routine. Despite some advancement in using enzyme – based sensors, there are still several other approaches that can be explored. Lately, studies have focused on the development of continuous glucose monitoring to improve the management of monitoring glucose levels and to provide instant feedback for diabetic patients. In recent works, boronic acids have been chosen as good candidate for sensors due to their ability to bind with sugars.<sup>25</sup> Boronic acid reacts with sugars to form boronate esters when the hydroxyl groups on a diol (sugar) are in the 1,2 or 1,3 orientation.<sup>26-28</sup> Figure 1.1 shows a boronic acid derivative binding to the 1,2 – hydroxyl positions of a glucose molecule. The initial goal of this research was to design and fabricate a self – assembled

monolayer containing a boronic acid derivative thiolate on a gold electrode that will communicate electrochemically upon concentration of glucose addition.

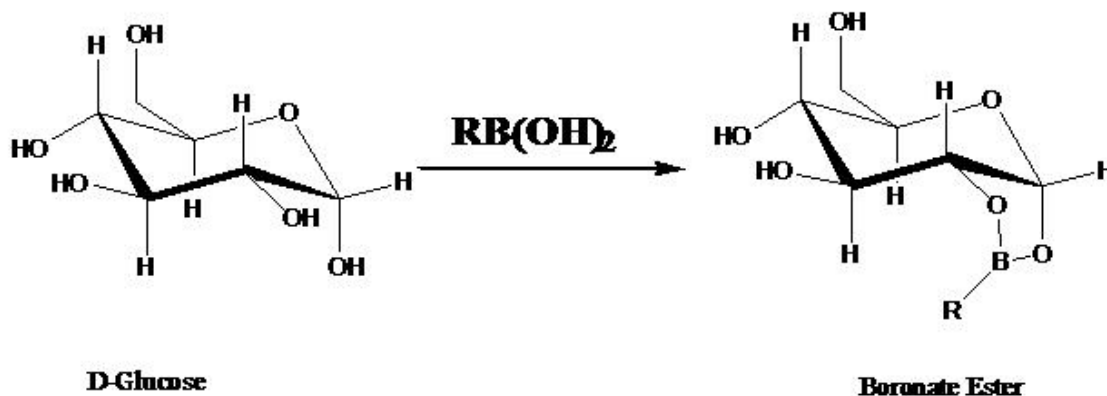


**Figure 1.1: Schematic approach of the interaction between D-glucose and a boronic acid derivative which forms a boronate ester.**

Boronic acid is a Lewis acid that reversibly combines with sugars such that it demonstrates potential applications for the development of a glucose biosensor. A broad range of techniques (such as adsorption, fluorescence, Raman, etc.) has been used to study these abilities.<sup>29-36</sup> DiCesare and Lakowicz incorporated a boronic acid group in resonance with an azo dye and studied the color change upon addition of sugars through absorption.<sup>33</sup> Hayashita et al. designed a fluorescent probe containing a fluorescent pyrenyl group and an arylboronic acid moiety in order to recognize sugars selectively.<sup>37</sup> James et al. designed a diboronic acid system that be employed in an electrochemical detection of sugars.<sup>30</sup> Further recognition of sugars such as glucose with a self assembled monolayer (SAM) containing a phenylboronic acid derivative has been the basis for designing and fabricating a biosensor in some studies. For

instance, Kanayama and Kitano formed monolayers with disulfides carrying boronic acid groups on a gold colloid or a gold electrode and showed the detection of sugar binding by UV – vis adsorption change and by cyclic voltammetry (respectively) using an electroactive marker.<sup>38,39</sup> Nakashima et al. extended the use of SAMs by studying a sugar sensor based on a phenylboronic acid – terminated redox active SAM on a gold electrode by electrochemical means.<sup>36</sup>

It was hypothesized that electrochemical impedance spectroscopy could be capable of detecting the interaction between glucose and a surface bound boronic acid – terminated thiol. The technique would offer rapid acquisition of data and provide accurate measurements without destroying the system. An incentive for selecting electrochemical impedance spectroscopy for this study of phenylboronic acid – terminated self – assembled monolayers was because it furnished electrochemical information regarding the binding ability of phenylboronic acids to glucose without the need of an electroactive molecule or a molecule that can be reduced or oxidized (Chapter 4). Alternatively, combining an electroactive molecule, ferrocene – terminated self – assembled monolayer, with a non – electroactive species, boronic acid - terminated self – assembled monolayer launched other ways to study sugar binding extensively (Chapter 5). Furthermore, characterizing the surface before and after inserting ferrocene – thiol was examined through means of surface infrared spectroscopy (IR) and cyclic voltammetry (CV).

The binding phenomenon between the boronic acid derivative and glucose offers promising approaches in the development of innovating types of glucose biosensors. In our research, the ease of preparation for self – assembled monolayers appeared to be a promising way to design versatile surface bound molecules that would exhibit characteristics of molecular recognition. Infrared spectroscopy gave a handle on characterizing the modified gold surfaces containing phenylboronic acid self – assembled monolayers. Cyclic voltammetry was used in the investigation of how the monolayers formed on the gold substrates by making the interfacial capacity available for quantitative values. Overall, we were interested in using electrochemical impedance spectroscopy to reveal information on SAMs containing a phenylboronic acid derivative during sugar detection.

## 1.2 References

- (1) Clark, L. *Biosens. Bioelectron.* **1993**, *8*, iii.
- (2) Cass, A.; Davis, G.; Francis, G.; Hill, H.; Aston, W.; Hlggins, I.; Plotkin, E.; Scott, L.; Turner, A. *Anal. Chem.* **1984**, *56*, 667.
- (3) Hunter, I.; Jones, L.; Kanigan, T.; Brenan, C.; Sambol, L.; Sosnowski, L. In *MIT Home Automation and Healthcare Consortium*, 2000.
- (4) Mohanty, S. At URL: <http://citeseer.ist.psu.edu/mohanty01biosensor.html>
- (5) Ohara, T.; Rajagopalan, R.; Heller, A. *Anal. Chem.* **1994**, *65*, 2451-2457.
- (6) Reach, G.; al., e. *Anal. Chem.* **1996**, *68*, 3822-3826.
- (7) Rishpon, J.; Gottesfeld, S.; Campbell, C.; Davey, J.; Zawodzinski, T. *Electroanalysis* **1994**, *6*, 17.
- (8) Vo-Dinh, T.; Cullum, B. *Fresenius J. Anal. Chem.* **2000**, 366, 540.
- (9) Wang, J. *Electroanalysis* **2001**, *13*, 983.
- (10) Wisniewski, N.; Moussy, F.; Reichert, W. *Fresenius J. Anal. Chem.* **2000**, 366, 611-621.
- (11) Woedtke, T.; Julich, W.; Hartmann, V.; Stieber, M.; Abel, P. *Biosensors & Bioelectronics* **2002**, *17*, 373-382.
- (12) Badugu, R.; Lakowicz, J.; Geddes, C. *Anal. Chem.* **2004**, *76*, 610-618.
- (13) Claremont, D.; Penton, C.; Pickup, J. *J. Biomed. Eng.* **1986**, *8*, 272.
- (14) McDonald, W.; Kopeland, R. At URL: <http://www.ieee.org/organizations/pubs/newsletters/leos/apr98/invitro.htm>
- (15) Kobos, R. *Trends Anal. Chem.* **1987**, *6*, 6.
- (16) Clark, L.; Lyons, C. *Ann. NY Acad. Sci.* **1962**, *102*, 29.
- (17) Frew, J.; Hill, H. *Anal. Chem.* **1987**, *59*, 933A.
- (18) He, B. At URL: [www.glue.umd.edu](http://www.glue.umd.edu)
- (19) Rinken, T.; Tenno, T. *Biosens. Bioelectron.* **2001**, *16*, 53.
- (20) Murray, R.; Ewing, A.; Durst, R. *Anal. Chem.* **1987**, *59*, 379.
- (21) Tierney, M.; Kim, H.; Burns, M.; Tamada, J.; Potts, R. *Electroanalysis* **2000**, *12*, 666.
- (22) Wang, J. *Electroanalysis* **1991**, *3*, 255.
- (23) Vreeke, M. At URL: <http://www.devicelink.com>
- (24) Wink, T.; Zuilen, S.; Bult, A.; Benneken, W. *The Analyst* **1997**, *122*, 43R.
- (25) Lorand, J.; Edwards, J. *J. Am. Chem. Soc.* **1959**, *24*, 769.
- (26) Springsteen, G.; Ballard, E.; Gao, S.; Wang, W.; Wang, B. *Bioorg. Chem.* **2001**, *29*, 259.
- (27) Springsteen, G.; Wang, B. *Tetrahedron* **2002**, *58*, 5291.
- (28) Yang, W.; Gao, X.; Wang, B. *Med. Res. Rev.* **2003**, *23*, 346.
- (29) Adhikiri, D.; Heagy, M. *Tetrahedron Lett.* **1999**, *40*, 7893.
- (30) Arimori, S.; Ushiroda, S.; Peter, L.; Jenkins, A.; James, T. *Chem. Commun.* **2002**, 2368.
- (31) Carey, R.; Folkers, J.; Whitesides, G. *Langmuir* **1994**, *10*, 2228.
- (32) Czarnik, A. *J. Am. Chem. Soc.*, 117.
- (33) DiCesare, N.; Lakowicz, J. *Org. Lett.* **2001**, *3*, 3891.
- (34) Gabai, R.; Sallacan, N.; Chegel, V.; Bourenko, T.; Katz, E.; Willner, I. *J. Phys. Chem. B* **2001**, *105*, 8196.

- (35) Karnati, V.; Gao, X.; Gao, S.; Yang, W.; Ni, W.; Sankar, S.; Wang, B. *Bioorg. Med. Chem. Lett.* **2002**, *12*, 3373.
- (36) Murakami, H.; Akiyoshi, H.; Wakamata, T.; Nakashima, N. *Chem. Lett.* **2000**, 940.
- (37) Tong, A.; Yamauchi, A.; Hayashita, T.; Zhang, Z.; Smith, B.; Teramae, N. *Anal. Chem.* **2001**, *73*, 1530.
- (38) Kitano, H.; Morokoshi, S.; Ohhori, K.; Gemmei-Ide, M.; Yokoyama, Y.; Ohno, K. *J. Colloid Interface Sci.* **2004**, *273*, 106.
- (39) Kanayama, N.; Kitano, H. *Langmuir* **2000**, *16*, 577.

# CHAPTER 2: BACKGROUND

## 2.1 Diabetes

An overall definition for diabetes is a group of diseases characterized by high levels of blood glucose resulting from a flaw in the insulin production.<sup>40</sup> The disease is related to amount of sugar (glucose) in the blood. Insulin is a pancreatic hormone that allows for cells to uptake glucose, which is present in the blood.<sup>40</sup> When there is a change in the insulin production, the amount of glucose (whether too much or too little) in the blood ultimately affects the function of several organs. Too much insulin (low level of glucose) causes a person's ability to reason to become impaired, resulting in a coma; and not enough insulin (high level of glucose) causes a person to have diabetes.<sup>40,41</sup>

Table 2.1: Complications associated with diabetes

Complication	Description
Heart disease and stroke	Heart disease leading cause of diabetes – related deaths Risk of stroke is 2 out of 4 times higher
High blood pressure	Greater cases and must take prescription medicine for hypertension
Blindness	Leading cause of blindness among adults 20 – 74 years old
Kidney disease	Over 100,000 people with diabetes undergo dialysis or kidney transplantation
Amputations	Over 80,000 cases of lower – limb amputations
Nervous system disease	Damages sensations in feet/hands, slow digestion process, and other problems
Dental disease	Commonly at risk for periodontal or gum disease, which cause loss of teeth

As of 2002, there are a total of 13 million people in the United States that have been diagnosed with diabetes, and there are about 5 million more that have not been diagnosed.<sup>42</sup> Diabetes has several different causes and it causes complication in several different organs of the body (Table 2.1). Complications such as strokes, blindness, high blood pressure, and kidney disease can occur; even premature death in some cases.<sup>43</sup> In 2000, diabetes was the sixth leading cause of death in the United States. Direct and indirect costs of this illness are constantly rising in order to control glucose levels in patients (diabetics).<sup>42</sup>

**Table 2.2: Evaluation of the two most common types of diabetes**

<b>Characteristic</b>	<b>Type I</b>	<b>Type II</b>
<b>Level of insulin secretion</b>	<b>None or very little</b>	<b>Normal or exceed normal</b>
<b>Age of on - set</b>	<b>Common in childhood</b>	<b>Common in adulthood</b>
<b>Defect</b>	<b>Destruction of pancreatic <math>\beta</math> cells</b>	<b>Decrease in sensitivity of insulin</b>
<b>Obesity related</b>	<b>No</b>	<b>Typically</b>
<b>Genetic related</b>	<b>Yes</b>	<b>Yes</b>
<b>Management</b>	<b>Insulin intake</b>	<b>Increase in exercise regimen Dietary control Oral medication</b>

When the insulin production is normal, the blood sugar level is somewhere between 60 – 115 mg/dl or 3.3 – 6.4 mM (to convert mg/dl to mM, divide by 18).<sup>41</sup> When the insulin production is abnormal, some type of insulin therapy is required in which constant measurements of glucose levels are needed. In the early days, physicians relied on tasting the urine for diagnosing diabetes; and one would be

diagnosed if the urine tasted sweet.<sup>41</sup> Nowadays testing of the blood is used for diagnosing; one would be diagnosed if the level of glucose after 10 hours of eating a meal were around 126 mg/dl.<sup>41</sup> In addition, other reasons for diagnosing people rely on symptoms related to the disease such as excessive thirst, excessive urination, and general fatigue.<sup>40,41</sup> After being diagnosed, the physician must decide what type of diabetes a patient has. The most common types of diabetes today are Type I and Type II diabetes.<sup>40,41,43-45</sup>

### **2.1.1. Type I diabetes**

In this type of diabetes, there is a destruction of the pancreatic beta ( $\beta$ ) cells (insulin production). The deficiency in insulin production leads to life long dependency on insulin treatments. Type I diabetes accounts for almost 10% of all cases of diabetes. Known by the lack of insulin secretion, Type I diabetes was previously called juvenile on – set diabetes. This case usually occurs in younger people such as children and young adults (up to 30 years of age) that are not necessarily overweight.

### **2.1.2 Type II diabetes**

In Type II diabetes, insulin secretion can be normal or exceed normal but the  $\beta$  cells just do not use the insulin properly because a person typically secretes an excess of insulin that flows over into the blood, which leads to insulin resistance (body cells resist insulin). Over a period of time, a need for insulin intake may arise in a patient due to the increase of insulin production in the pancreas, wherein this increase causes the pancreas to gradually stop producing insulin. Characterized as a non – insulin dependant type, Type II diabetes is also

identified as adult on – set diabetes. This type of diabetes usually occurs in people over the age of 40. However, it is common in overweight people and those who have a history of diabetes in their families. Type II diabetes is higher in those who ethnic groups which includes African Americans, Hispanic Americans, Native Americans, and Asian Americans. Over 90% of diabetic cases are diagnosed as Type II. Recently, there have been more cases of Type II diabetes in children and adolescents.

### **2.1.3 Evaluation of diabetes**

These are not the only types of diabetes, but they are the most common cases in the United States (Table 2.2). Diabetes can lead to major complications that cause people to adjust their lifestyles. Diabetics, persons who have been diagnosed, can learn to control this disease with appropriate medical care. Those with Type I can control diabetes with the proper intake of insulin by the use of pump or injections. And those with Type II can control diabetes by increasing their exercise regimen, managing their eating habits, and taking the necessary oral medication. Nevertheless, checking the glucose levels in the blood (for either type of diabetes) is the essential way in preventing complications associated with diabetes. Regulating the flow of insulin can slow the process of severe complications that occur with the disease. Therefore, the future of diabetes research is leaning towards the field of sensors for monitoring the glucose levels. Researchers are trying to develop sensors that can continuously monitor glucose levels with the hopes in lessening the disruption of diabetic patients' daily lives. In addition, research has improved sensors by allowing patients to monitor their

glucose levels in their individual homes. This advantage allows for untrained people to be able to monitor their glucose levels with little or minimum human error. Increasing people's knowledge and understanding of diabetes can aid in approaching this disease with new and innovative ways to control it.

## 2.2 Biosensors

Biosensors are defined as devices that combine analytical active materials with transducing systems in hopes to recognize specific analyte.<sup>4,8,9,46-48</sup> They react in response to specific biological molecular recognition of analyte, which are in turn measured by a variety of transduction techniques that convert the event into measurable signals (Figure 2.1).

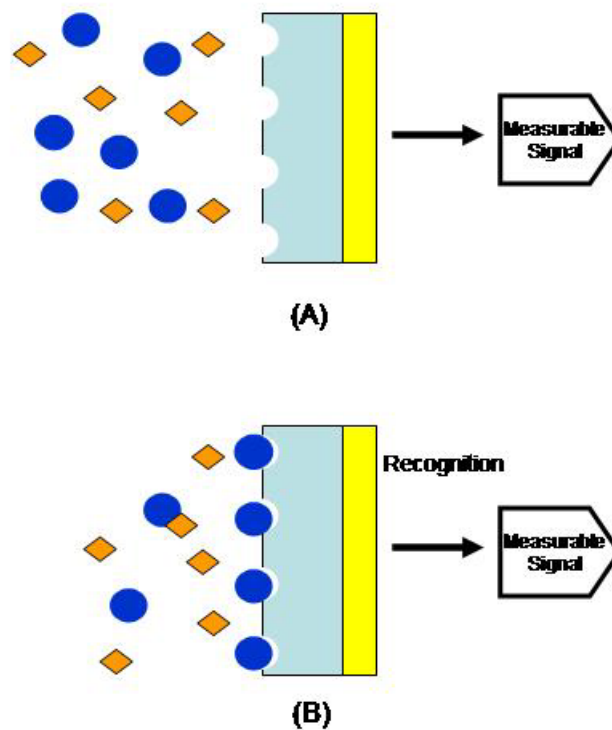


**Figure 2.1: (A) Arrangement of a typical biosensor, where the combination of a bioactive material and a transducer is surrounded by analytes. (B) When a bioactive material recognizes a specific analyte, a measurable signal is observed.**

The aim of biosensors is to produce continuous signals wherein the quantities are related to the amount of analyte.<sup>4,8,9,46-48</sup> Various kinds of biosensors exist have an application in the chemical regime. Biosensors are often classified either by their recognition pattern or the technique that is used for recognition.

### 2.2.1 Bioactive materials (bioreceptors)

The bioactive materials are responsible for the molecular recognition or the binding that occurs with the specific analyte that the sensor would measure. The specific selectivity between the active material and analyte of choice determines the precision of the sensor. Table 2.3 lists some types of bioreceptors (bioactive materials) that are commonly used in sensors. Bioactive materials are grouped into several categories, for example, nucleic acids, antibody, and enzymes.

**Table 2.3: The active materials (biological related) are responsible for binding or interacting with the analyte of interest.**

<b>Types of Bioreceptors</b>	<b>Recognitions based on</b>
<b>Nucleic acid</b>	<b>Hybridization between DNA/ RNA and a probe</b>
<b>Antibody/antigen</b>	<b>Binding affinity of antibody to antigen</b>
<b>Enzymatic</b>	<b>Catalytic information</b>
<b>Cellular</b>	<b>The rate of cellular respiration activity</b>

*2.2.1a) Nucleic acids:* This bioreceptor recognizes the hybridization of two single strands, one complementary strand, and another deoxyribonucleic acid (DNA) or ribonucleic acid (RNA) strand. In this sensor, the biorecognition forms a basis for pairing a DNA single stranded molecule and a synthesized complementary molecule, called a probe. The probe is often labeled with some sort of optical molecule (often fluorescence). The overall event involves unwinding a double stranded DNA to give two single strands, then a probe is added and the complementary ends of both strands are hybridized. When there is a sufficient amount of binding, the amount can be detected optically. Usually the detections are made possible by the use of fluorescent probes. The binding to the complementary sequences led to sensors often called genosensors.\*

*2.2.1b) Antibody/antigen:* Another example of recognition happens when the bioactive material, antibody, binds to antigens. The response is often known as a lock and key effect. Antibodies are defense proteins in the immune system that unite with specific geometrical configurations of antigens. This recognition event of sensors is called immunosensors.

*2.2.1c) Enzyme:* Typically, enzymes are attractive due to their binding capabilities and catalytic activities in recognition mechanisms.\* Biologically, enzymes are proteins that specialize in catalyzing specific metabolic reactions that lower the limit of detection. The recognition of binding is detected by reactions that are catalyzed by enzymes that remain unchanged during detection. Some enzymes require the use of coenzymes when there is a need for additional chemical components.

## 2.2.2 Transducers

Transduction techniques convert signals from a recognition event to signals that are understandable to a human observer. One method for transducers is to determine the concentration of analytes proportional to the concentration of the bioactive material observed in the process of detection. There are a variety of transducers used today and many more being studied for future use (Table 2.4). Two of those transducers employed in glucose sensor research are the optical and electrochemical methods of detection.

**Table 2.4: Some types of transducers that are responsible for converting recognitions to measurable signals.**

<b>Types of Transducers</b>	<b>Recognitions based on</b>
<b>Optical detection</b>	<b>Measurement of lights by different types of spectroscopy</b>
<b>Electrochemical detection</b>	<b>Measurements of current by amperometry and voltammetry</b>
<b>Mass detection</b>	<b>Measurements of mass by quartz crystal microbalance (QCM)</b>

*2.2.2a) Optical transducers:* The signal that optical transducers yield measures the output of light in biosensors. The optical transducers are known to use different kinds of spectroscopic techniques (examples are absorption, fluorescence, Raman, refraction, etc.). Biosensors based on the characteristics of absorbed or reflected light such as energy and polarization that establish the understanding of these transductions. For example, the absorption technique provides information when energy measure changes as the analyte vibrates in its

surroundings. Another case involves molecules on fixed surfaces. The measurements of how polarization change as light are emitted to the surface gives vital information on the molecules attached. Usually optical transducers can be associated with the ability of the bioreceptors to fluoresce either directly or indirectly. For instant, these transducers recognize the interactions between analytes to bioactive materials, in which the interactions then cause quenching to occur or cause a reduction in quenching.

*2.2.2b) Electrochemical transducers:* The biosensor that detects electrochemical measurements relies on the change in electrical properties whereupon ions or electrons are produced or consumed in chemical reactions. Unlike the optical detection, electrochemical detection is very useful when the analytes of interest do not fluoresce or when the use of a tagged fluorescent molecule is difficult to handle. The results from electrical signals provide information about the interactions between the specific analytes and bioactive material used. Among the most common methods are amperometric and voltammetric, where two or three electrode systems are applied. Amperometric measurements monitor the current flow within a cell at a given potential. Voltammetric measurements observe the current change within a cell as different potentials are scanned across a cell. The most common glucose sensors available today are amperometric based sensors.

Biosensors have achieved great accomplishments throughout the years in many areas. They have uncovered a vast deal of information ranging from

medicine to biotechnology. However, there is still more investigations needed to construct more sophisticated and reliable devices.

### **2.3 Glucose Biosensor**

Since the 1960's, the introduction of biosensors has opened the doors for many areas of technology; especially, glucose research.<sup>16</sup> Those who have been diagnosed with diabetes perform several tests to monitor their glucose levels on a daily basis that can be painful and time consuming. Therefore, the focuses have been on developing devices that can be pain – free and monitor glucose levels continuously. A variety of methods have been explored when it comes to improving devices for diabetes control.<sup>9,46</sup> Even though there are many challenges to encounter, there have been advancements over the years with glucose biosensors.

The history of biosensors began with Leland Clark who studied the detection of oxygen using a platinum wire that eventually led to the basis for glucose sensors.<sup>16</sup> Then, along with Lyons, the first idea of a glucose biosensor based on an enzyme electrode was introduced for clinical use. The biosensor consisted of an enzyme that was incorporated at a close proximity to a platinum electrode, a piece of dialysis membrane on the other side of the enzyme that caused the enzyme to be trapped.<sup>16</sup> Figure 2.2 illustrates the detection scheme of glucose involving the enzyme known as glucose oxidase (Gox). In the presence of oxygen, glucose oxidase reacts with glucose and yields gluconic acid and hydrogen peroxide. It is the formation of hydrogen peroxide that is significant

because hydrogen peroxide is reduced. This reduction is detected by amperometric means.

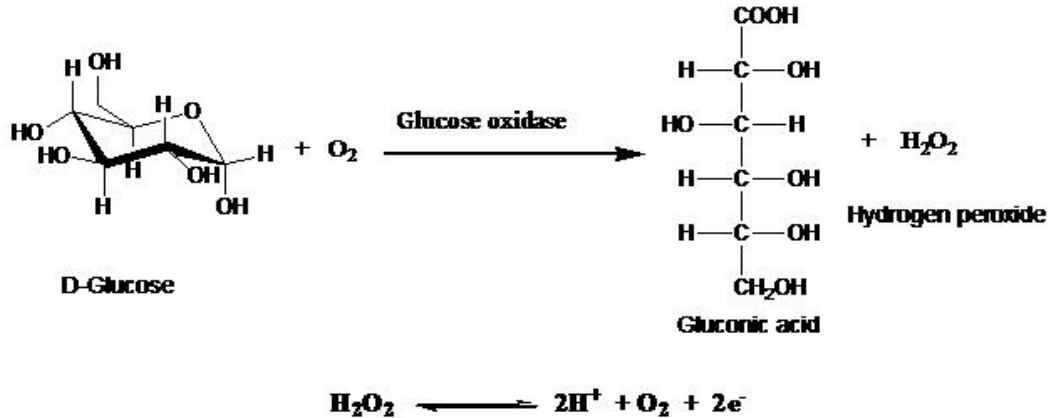


Figure 2.2: Schematic of glucose detection with the enzyme glucose oxidase (Gox).

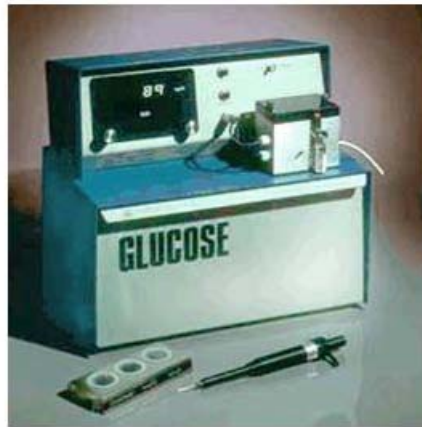
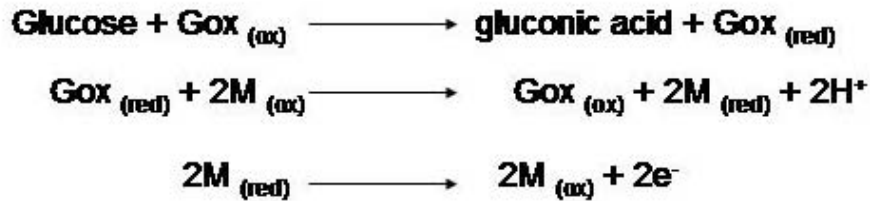


Figure 2.3: A picture of the Yellow Spring instrument, YSI 23A Blood Glucose Analyzer.

The release of hydrogen peroxide in the reaction is monitored amperometrically at the platinum electrode, so as hydrogen peroxide is produced it shows a relationship parallel to glucose concentration. Clark and Lyons eventually sold their idea to the Yellow Spring Instrument Company, wherein the company took their idea and improved the sensor by adding another electrode. In

1975, the company launched the first commercially available glucose biosensor for clinical use (Figure 2.3).<sup>8,9,46</sup>



**Figure 2.4:** Schematic of how artificial mediators are used to shuttle electrons, where (ox) is the oxidized form and the (red) is the reduced form of the glucose oxidase (Gox) and the mediator (M).

The variation of oxygen in the blood limits the detection of glucose since the consumption of oxygen is needed to react with glucose to form the necessary products for detection. So to compensate for this limitation, a non – physiological electron acceptor (artificial mediator) was studied in order to replace the dependency of oxygen.<sup>2,8,9,13,46</sup> Artificial mediators were useful because it allowed electrons to travel back and forth from the enzyme center to the electrode during its oxidized and reduced forms (Figure 2.4). Artificial mediators such as ferrocene derivatives, ferrocyanide, conducting organic salts or quinone compounds have been used extensively.<sup>2,8,9,13,46</sup> In the selection of mediators, they should be stable molecules that possess good electrochemical properties. In addition, the mediators should be capable of reacting with the enzyme in order for the sensor to function effectively.



**Figure 2. 5: An example of the home – based glucose sensor , Medisense Pen, used by diabetics.**

Glucose sensing was taken one step further in order to establish electrical contact between the mediator and electrode surfaces. Chemically modifying electrodes eliminate the act of diffusion that occurs in free solution, while stabilizing the movement of the mediator on the electrode, which offers high current outputs.<sup>8,20,24</sup> All of these advancements on electrochemical biosensors led them into becoming marketable for home use. Commercially available glucose sensors for home use involve a patient pricking his/her finger frequently on a daily basis. Once a droplet of blood is drawn, the blood is applied to a reagent strip where the enzyme is located. Then a glucose monitor relays a reading of the glucose concentration in the blood. In the late 1980's, Medisense, Incorporated launched the first home based glucose sensor, The Medisense Pen, for diabetics (Figure 2.5).<sup>9,46</sup>

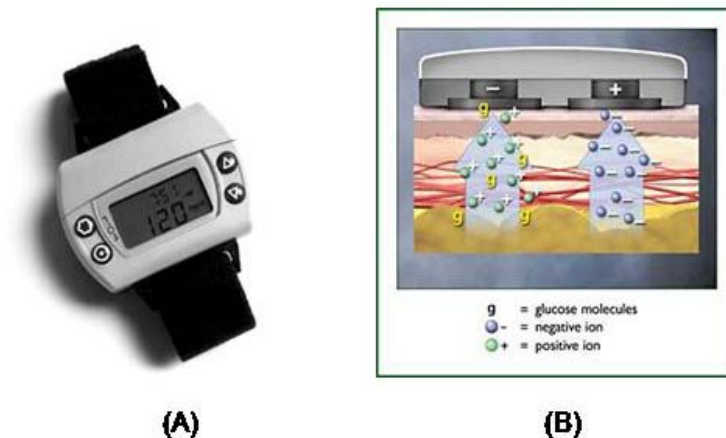


**Figure 2.6: (A) A picture of a GlucoWatch developed by the Cygnus, Inc., along with (B) sequences of events that occur in the sensor. (From URL: <http://www.brookscole.com>)**

Lately, research has shifted focus from in vitro testing with reagent strips to continuous monitoring with noninvasive testing.<sup>3,9,12,46</sup> Remarkable progress has been made towards the development of wearable sensors that are capable of making frequent measurements. The wearable sensors have capabilities that could limit the disruptions that diabetics face on a daily basis. In 1999, a company named Minimed designed a continuous subcutaneous glucose device (not shown). This amperometric sensor can be worn for up to three days at a time.<sup>3,9,12,46</sup> While inserted into the tissue, the levels of glucose concentration are recorded every ten seconds as an average of readings is stored every five minutes. However, this sensor did not limit the finger pricking process, as a matter of fact; it still required several tests of finger pricking daily for calibration purposes. In addition, the patient did not get feedback during use, but feedback was stored for seventy-two hours and the information stored had to be downloaded by a physician. Another company, named Cygnus, Inc., developed a

way to monitor glucose concentration based on reverse iontophoresis (Figure 2.6).<sup>3,9,12,46</sup> Figure 2.6a shows an example of the device that is capable of taking readings at least three times in one hour for twelve hours, at the same time reducing the need of finger pricking from several times a day to once a day for calibration purposes. The process of reverse iontophoresis applies a low amplitude electrical current; glucose molecules are pulled through the skin (Figure 2.6b). The glucose molecules are trapped in gel discs containing the enzyme, glucose oxidase. Then the electrochemical sensor detects the glucose concentration level, and a reading appears digitally on a watch display. This noninvasive approach represents promising ways toward continuous glucose monitoring; however, there are still challenges in this research.

The improvement and enhancement towards the development of dependable continuous glucose monitoring with the reduction of frequent finger pricking are currently being investigated. In spite of all the progressions in this area, there are still challenges correlating to the stability and reliability of glucose biosensors. For that, there is a need to continue the research efforts for the success of glucose blood monitoring.

## ***2.4 Formation of Monolayers***

Further improvements include the use of chemically modified substrates (electrodes) that involve the attachment of specific molecules. For over 30 years, scientists studied modified electrodes for the expansion of electrochemical research.<sup>49</sup> Lane and Hubbard explained studying chemically modifying substrates as a way to obtain fundamental information about the mechanism of

electron transfer at electrode surfaces.<sup>49</sup> Others described it as the ability to convey greater selectivity to electrode surfaces that are limited to unmodified electrodes.<sup>49</sup> Modified electrodes consist of a layer of molecules bound to a metal surface, in which they create what is known as monolayers (Figure 2.7).<sup>50-53</sup>

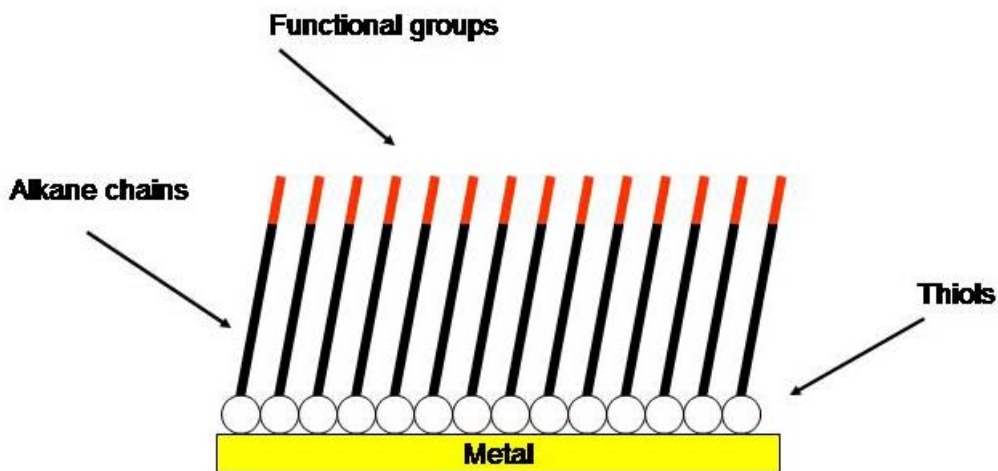


**Figure 2.7: A general schematic of an ideal, organized monolayer on a metal substrate (electrode), where the alkane chains are bound to substrate and functional groups are attached to the terminal ends of the alkane chains.**

An ideal monolayer exhibits well – ordered, packed alkane chains (methylene groups –  $\text{CH}_2$ ) that are chemisorb to an electrode. Chemisorption entails of an adsorptive interaction between a sulfur-containing molecule of various lengths of alkane chains and an electrode.<sup>50-53</sup> The most common interaction is formed with sulfur containing molecules (sulfides, disulfides, and thiols) and metal surfaces (gold, silver, and platinum). It is possible to attach a wide range of functional groups to the terminal ends of alkane chains without disrupting the formation of monolayers. Mixed monolayers can be assembled by attaching different functional groups simultaneously or sequentially.<sup>54</sup>

### 2.4.1. Self assembled monolayers (SAMs)

Generally there are two methods in the formation of monolayers: Langmuir – Blodgett transfer and self – assembly.<sup>55</sup> Compared to the other method, the self – assembled method produces more versatile monolayers with stronger adsorption of sulfur – substrate (particular gold) bonds; therefore, this method will be pursued in the following study.<sup>56,57</sup> The self – assembled method deposits thiols onto a substrate by forming monolayers spontaneously upon exposure to the substrate (Figure 2.8). Self – assembled monolayers (SAMs) can be deposited onto the surface of a substrate within minutes, which results into a strong thiolate – substrate bond that is partially irreversible.<sup>56,57</sup> The chemisorption reaction between the gold electrode and the alkylthiol occurs after the electrode is immersed into a diluted thiol solution, wherein yielding packed and ordered monolayers.

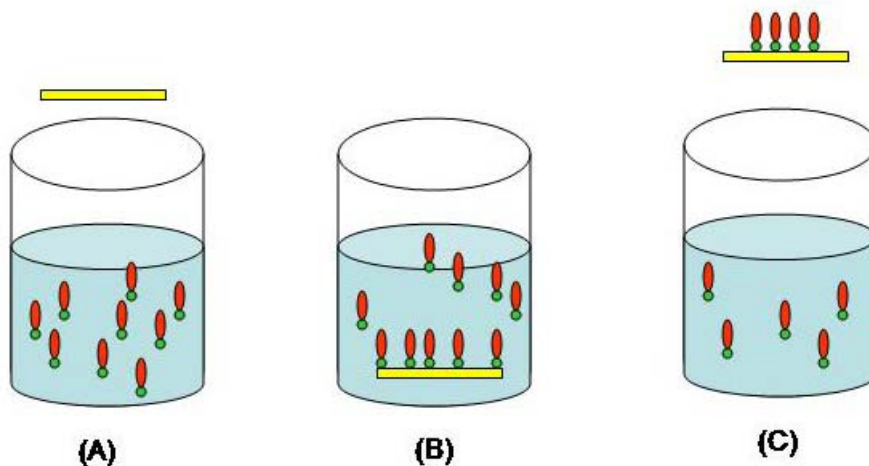


**Figure 2.8: Schematic of the self – assembled method. This method involves (A) a substrate and a solution of desired sulfur containing molecule, where (B) the substrate is submerged into the solution for a period of time and (C) a monolayer is formed as a result.**

#### **2.4.2. Order in self assembled monolayers<sup>50,58-62</sup>**

Consequently, the nature of the SAMs maybe altered due to the length of the alkane chains or the functional groups. The length of the alkane chain can determine how well ordered monolayers are formed. And the functional groups influence how densely packed monolayers are formed. In a sensor, the functional group acts the bioreceptor, and it is commonly immobilized on or in close proximity to the surface of the transducer. The distance between the functional group and the surface depends on the length of the alkane chain. The height of the monolayer serves as a boundary between the molecular recognition and the means of collecting data, which in turn is responsible for the sensitivity and selectivity of sensors. Porter et al. showed that long alkanethiols (number of methylene groups > 10) form well-ordered monolayers. A reduction in that number can lead to less ordering. This order can be maintain as long as the functional group is relatively small (<5 Angstroms). The packing and ordering density of a SAM can be decreased as the functional group becomes bulkier. When a mixed SAM is formed, there are no distinct phases; suggesting that there is random ordering occurring.

#### **2.4.3. Characterization of self assembled monolayers<sup>50,58-62</sup>**

The electrochemical behaviors of monolayers are divided into two categories according to terminal end groups of the alkane chain: nonelectroactive and electroactive. Nonelectroactive terminal end groups produce monolayers that block electrons from interacting with an electrode. The blocking characteristics of these monolayers can characterize the interfacial capacitance on the substrate or block out faradaic processes is affected (discussed later in Chapter 4). Faradaic

processes involve the exchange of electrons between the electrode and molecules that can be reduced and oxidized. Also, it allows for a closer evaluation of electrodes with the purpose of revealing any defects, such as pinholes. Electroactive terminal end groups produce monolayers based on how well electrons exchange with the electrode creating. For instance, the distance of a reduction/oxidation (redox) couple gives rise to experiments that look at how electrons are transfer. In the case of a reversible system, the responses studied are governed by thermodynamics rather than kinetics. An example of an ideal monolayer containing electroactive molecules can be characterized by a method called cyclic voltammetry (will be discussed in Chapter 5).

The use of modified electrodes is growing in the marketplace as practical devices for biosensors. The ease of formation can be quick and result in well ordered monolayers that consist of a wide variation of functional groups. The capability in characterizing and quantifying biomolecules deposited on electrodes provides significant applications for various types of biosensors. Bioanalytical molecules (or receptors) immobilized on electrode's surfaces or near the surfaces which link them to a transducer. When the immobilized bioanalytical molecule recognizes an analyte, a signal is created which is related to the concentration of the analyte. Applications for self – assembled monolayers focus mainly on techniques such as electrochemical, optical, and quartz crystal microbalance that generate information about specific properties or functions. Forming monolayers via the self – assembled method are easy to prepare, ordered, and packed all within reasonably deposition times. The monolayers

utilize biological molecules that are immobilized on electrodes for the advancement of biosensors. In addition, binding events on SAMs that are reversible and selective are of interest.

## 2.5 References

- (1) Sherwood, L. *Human Physiology: From cells to systems*; Second ed.; West Publishing Company, 1993.
- (2) Saudek, C.; Rubin, R.; Shump, C. *The John Hopkins guide to diabetes for today and tomorrow*; The John Hopkins University Press: Baltimore, 1997.
- (3) Prevention, C. f. D. C. a. At URL: <http://www.diabetes.org> Accessed: 2003.
- (4) Gough, D.; Armour, J. *Diabetes* **1995**, *44*, 1005.
- (5) Heller, A. *Annu. Rev. Biomed. Eng.* **1999**, *1*, 153.
- (6) At URL: <http://www.fraserclan.com/biosen2.htm> Accessed: 2002.
- (7) Centre, C. B. At URL: <http://www.cranfield.ac.uk/biotech/sensors/events.htm> Accessed: 2004.
- (8) Mohanty, S. At URL: <http://citeseer.ist.psu.edu/mohanty01biosensor.html>
- (9) Tonnesen, C.; Withrow, G. At URL: <http://www.hitl.washington.edu/scivw/EVE/I.D.1.c.Biosensors.html> Accessed: 2002.
- (10) Vo-Dinh, T.; Cullum, B. *Fresenius J. Anal. Chem.* **2000**, *366*, 540.
- (11) Wang, J. *Electroanalysis* **2001**, *13*, 983.
- (12) Clark, L.; Lyons, C. *Ann. NY Acad. Sci.* **1962**, *102*, 29.
- (13) Cass, A.; Davis, G.; Francis, G.; Hill, H.; Aston, W.; Hlggins, I.; Plotkin, E.; Scott, L.; Turner, A. *Anal. Chem.* **1984**, *56*, 667.
- (14) Claremont, D.; Penton, C.; Pickup, J. *J. Biomed. Eng.* **1986**, *8*, 272.
- (15) Wink, T.; Zuilen, S.; Bult, A.; Benneken, W. *The Analyst* **1997**, *122*, 43R.
- (16) Murray, R.; Ewing, A.; Durst, R. *Anal. Chem.* **1987**, *59*, 379.
- (17) Badugu, R.; Lakowicz, J.; Geddes, C. *Anal. Chem.* **2004**, *76*, 610.
- (18) Hunter, I.; Jones, L.; Kanigan, T.; Brenan, C.; Sambol, L.; Sosnowski, L. In *MIT Home Automation and Healthcare Consortium*, 2000.
- (19) Kissinger, P.; Heineman, W. *Laboratory Techniques in Electroanalytical Chemistry*; 2nd ed.; Marcel Dekker, Inc, 1996.
- (20) Bain, C.; Whitesides, G. *Angew. Chem. Int. Ed. Engl.* **1989**, *28*, 5897.
- (21) Brett, O.; Brett *Electrochemistry*; Oxford University Press: New York, 1998.
- (22) Chidsey, C.; Loiacono, D. *Langmuir* **1990**, *6*, 682.
- (23) Finklea, H., Ed. *Self-assembled monolayers on electrodes*; John Wiley & Sons Ltd., 1997.
- (24) Bain, C.; Whitesides, G. *J. Am. Chem. Soc.* **1989**, *111*, 7164.
- (25) Schreiber, F. *Prog. Surf. Sci.* **2000**, *65*, 151.
- (26) Vassos, B.; Ewing, G. *Electroanalytical Chemistry*; John Wiley & Sons, Inc., 1983.
- (27) Gunzler, H.; Williams, A. *Handbook of Analytical Techniques*; Wiley-VCH, 2001; Vol. II.
- (28) Bain, C.; Troughton, E.; Tao, Y.; Evall, J.; Whitesides, G.; Nuzzo, R. *J. Am. Chem. Soc.* **1989**, *111*, 321.
- (29) Flink, S.; van Veggel, C.; Reinhoudt, D. *Adv. Mater.* **2000**, *12*, 1315.
- (30) Ju, H. *Phys. Chem. Chem. Phys.* **1999**, *1*, 1549.

- (31) Oldham; Myland *Fundamentals of Electrochemical Studies*, 1994.
- (32) Porter, M.; Bright, T.; Allara, D. *J. Am. Chem. Soc.* **1987**, *109*, 3559-3568.

## CHAPTER 3: INSTRUMENTAL ANALYSIS

---

### **3.1 Electrochemical Impedance Spectroscopy (EIS)<sup>49,56,63,64</sup>**

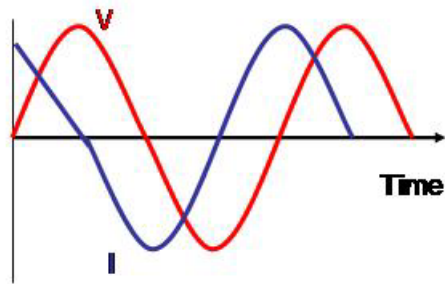
Electrochemical impedance spectroscopy (EIS) is a technique that provides useful information into physical and chemical properties of SAM – modified surfaces (or a system). In impedance spectroscopy, a sinusoidal varying potential (V) with a known frequency is applied across a system. The response to this stimulus is an alternating current (I) through the system, and the quantity of interest is the impedance (Z) of the system.

$$V = IZ \quad (1)$$

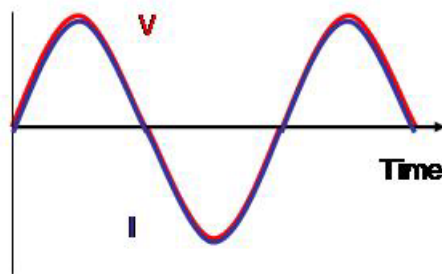
This application of applying a potential across a system, while generating a current, can be related to the Ohm's Law. The law relies on a constant potential (V) that is applied across a resistance (R), which in turn induces a constant current (I).

$$V = IR \quad (2)$$

In other words, the impedance of a system is a ratio of voltage applied over the current response. This value of this ratio can also be related to resistors, capacitors, and inductors. Induction is not relevant to this research as it deals with the rate at which energy is drawn from a source when the flow of electricity is produced within a cell. Therefore, the research focuses on the properties of capacitance (permits storage of charge) and resistance (opposes current to pass through).



(A)



(B)

**Figure 3.9: The sinusoidal current and voltage (A) for a resistor when the phase shift is zero and (B) for a capacitor when the current lags the voltage.**

In Figure 3.1A, when the applied potential and the current response are in phase with each other, it is said that the system is behaving like a resistor.

Resistance is defined as a barrier to the flow of electronic charge. When there is no capacitive component, the resistance,  $R$ , equals the impedance. The

impedance of a resistor is given by the equation:

$$Z = R \quad (3)$$

In figure 3.1B, when the applied potential and the current response are out of phase with each other, it is said that the system is behaving like a capacitor. In other words, the result of the applied potential and the current response being out of phase is due to the time needed to charge or discharge the capacitor.

Capacitance is defined as the ability to retain or store charge. The impedance of capacitor is given by the equation:

$$Z = 1/\omega C = X_c \quad (\omega = 2\pi f) \quad (4)$$

As a result of altering current in an electrical circuit, the energy needed to charge the fields connected to the flow of electrons develops a counterforce known as reactance. Hence, capacitance is represented by the term,  $X_c$ ; therefore, capacitance is a function of frequency.

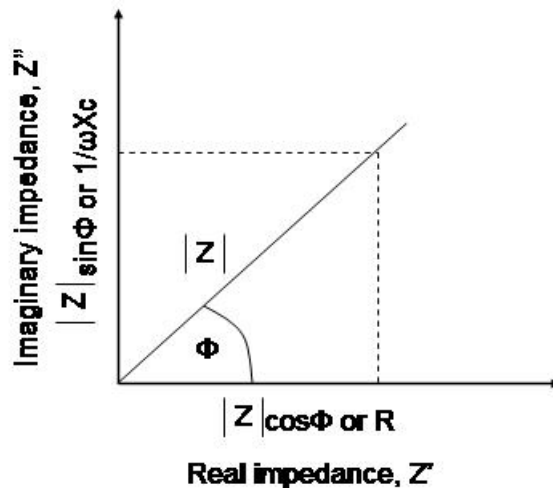


**Figure 3.2: The basic vector diagram used for resistance/capacitance (RC) circuit**

Total opposition to the current, any impedance of resistors and capacitors, must be added because of the phase differences; therefore, impedance comprises of a real and an imaginary terms ( $Z'$  and  $Z''$ , respectively) (Figure 3.2). They are related by the following equation:

$$Z = Z' - jZ'' \quad (\text{where } j = \sqrt{-1}) \quad (5)$$

Hence, impedance is a complex number. The symbol,  $|Z|$ , is given for the overall impedance or magnitude. Once the values of the magnitude,  $|Z|$ , and the phase

angle,  $\Phi$ , are obtained, the real and imaginary components can be generated. In figure 3.2, the length of the vector stands for the magnitude ( $|Z|$ ) and the angle ( $\Phi$ ) produced by the vectors, which are related to the real and imaginary parts.

$$|Z| = \sqrt{Z'^2 + Z''^2} \quad (6)$$

$$\text{and } \tan\Phi = Z''/Z' \quad (7)$$

$$\text{or } Z' = |Z|\cos\Phi \quad (8)$$

$$\text{and } Z'' = |Z|\sin\Phi \quad (9)$$

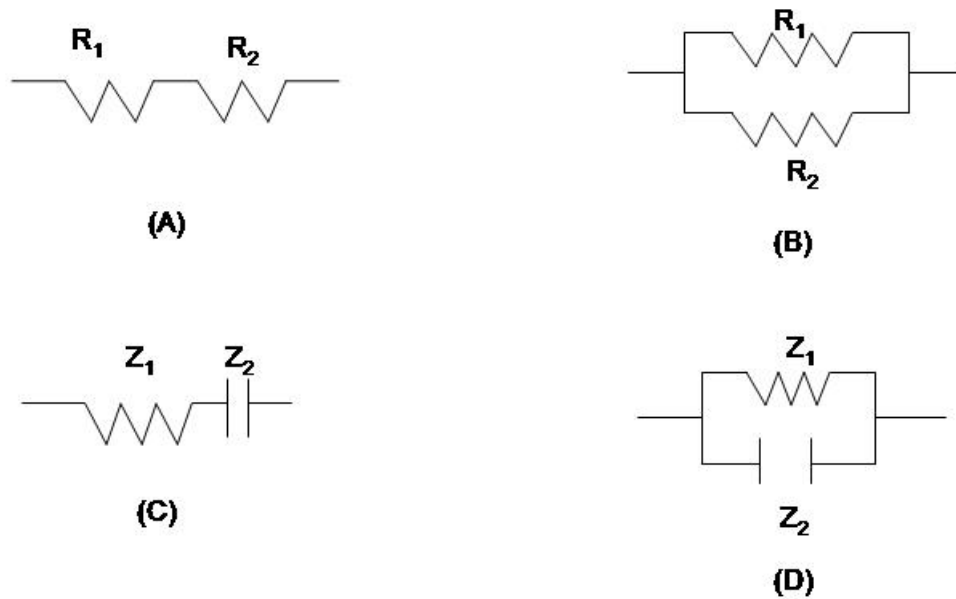


**Figure 3. 3: Circuits comprising of a resistor in the DC method (A)series and (B) parallel that can be related to the total impedance when the AC method is in (C) series and (D) parallel.**

As a result, the real impedance,  $Z'$ , behaves like a resistor and the imaginary impedance,  $Z''$ , behaves like a capacitor. As described previously, the impedance in the alternating current (AC) method is related to the resistance in the direct current (DC) method of the Ohm's Law. The relationship between the methods can be seen further when the components behave in combinations as

shown in the equivalent circuits (Figure 3.3). The calculations for the total resistance are as followed:

$$R_t = R_1 + R_2 + \dots + R_n \text{ (series)} \quad (10)$$

$$1/R_t = 1/R_1 + 1/R_2 \dots + 1/R_n \text{ (parallel)} \quad (11)$$

Noting that Z is the same as R, and capacitance is not considered. The calculations for the total impedance are as followed:

$$Z_t = Z_1 + Z_2 + \dots + Z_n \text{ (series)} \quad (12)$$

$$1/Z_t = 1/Z_1 + 1/Z_2 + \dots + 1/Z_n \text{ (parallel)} \quad (13)$$

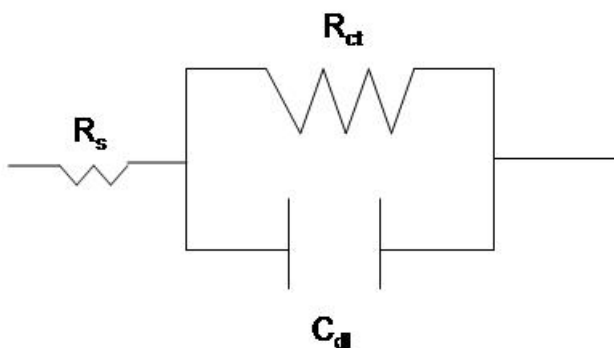


**Figure 3.4: The simplest circuit used in electrochemical cells (systems).**

An equivalent circuit is a useful way to elucidate the electrical behavior of a cell that is stimulated by resistors and capacitors. Total impedance is determined by the combination of resistors and capacitors that makes up an equivalent circuit that can aid in determining measurements for impedance. Equivalent circuits are the cores of impedance analysis where systems are dissected among different electrodes (for examples, working, reference, or counter electrodes) setup in an electrochemical cell. Unlike the simple electrochemical cell with just a resistor and a capacitor, there are systems that

add another resistance, due to the electrolyte solution between the reference and working electrodes. Therefore, the simplest circuit for an electrochemical system contains a charge resistance,  $R_{ct}$ , and a double layer capacitance,  $C_{dl}$ , in parallel together and in series with a solution resistance,  $R_s$  (Figure 3.4).

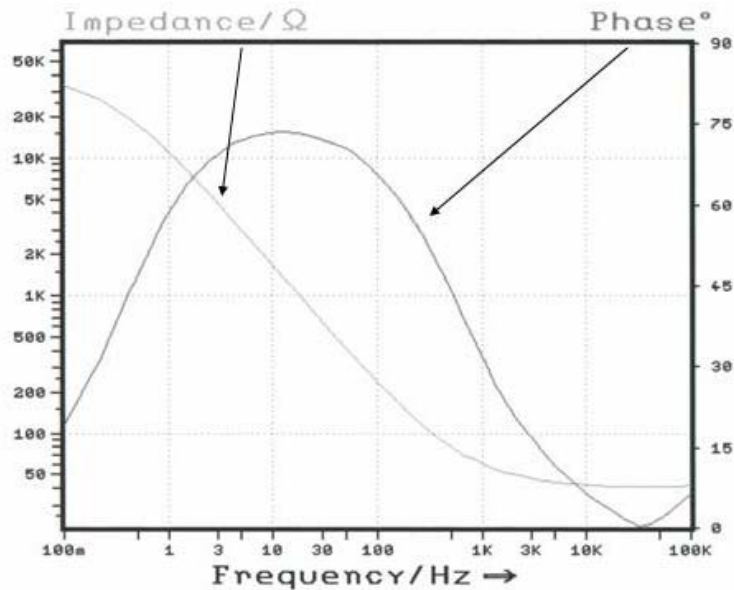


**Figure 3.5: An example of a Bode plot representing a gold electrode in 0.1 HClO<sub>4</sub> solutions from a BAS IM6 instrument.**

From the equivalent circuits, impedance analysis can be interpreted by a variety of plots, which show how simple circuits behave in combination. One way to analyze impedance is through Bode plots. The Bode plot displays graphs that have axes of total impedance (magnitude) and phase angle as a function of frequency. The latter axis, frequency, gives this plot an advantage over the other plots associated with real and imaginary axes because it's easier to see how frequency influences the impedance. Usually the axes are represented by a log  $|Z|$  versus  $\log \omega$  so that extrapolating the values of resistances,  $R_s$  and  $R_{ct}$ ,

becomes easier. Figure 3.5 shows an example of a Bode plot of a gold electrode in 0.1 HClO<sub>4</sub> electrolyte solutions. In this example, there are three distinct domains: a low frequency domain, mid frequency domain, and high frequency domain. Recall, the phase shifts for resistance (0°) and capacitance (90°) are in phase and out of phase with the applied AC bias, respectively. Observing the Bode plot, there are two domains that the phase angle approaches 0° and the impedance level out. These domains signify the cell behaving like a resistor. The domain where the phase angle approaches 90° and the impedance values increase linearly creating a straight line signifies the cell behaving like a capacitor. This mid domain will be the focus of the research since it furnishes an understanding of what is occurring on the surface.

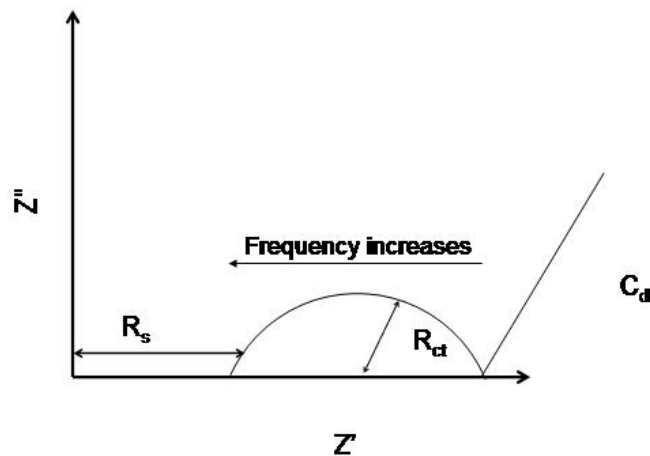


**Figure 3.6: Example of a complex plot for a simple electrochemical system**

Another way to analyze impedance is through the real,  $Z'$ , and imaginary,  $Z''$ , components computed from impedance measurements with the respect to magnitude impedance,  $|Z|$ , and frequency,  $\omega$ . The formats developed from these

axes are known as complex plots. Other plots using the same axes are known as Nyquist plots or Cole – Cole plots (differing in how the axes are calculated). The impedance data are plotted with the imaginary component against the real component of impedance at each frequency excitation (Figure 3.6). The expected plot shows a semicircle (represents the resistance component) and a linear line at the rightmost end of the semicircle (represents the capacitance component). Complex plots are utilized primarily for the ease of revealing the effects of the ohmic resistance in cells; wherein, the shape of the semicircle does not change when the position of the reference electrode alters the resistance. However, the values of frequency are not obvious in the appearance of the plots. Even though it is easy to extrapolate resistance directly from the complex plots, it is difficult to calculate the capacitance without knowing the frequency. Therefore, the Bode plot will be used in the research.

The impedance technique holds some advantages over DC techniques such as cyclic voltammetry and amperometry. One advantage is the use of variable amplitude to facilitate minimal perturbation throughout the electrochemical cell that in turns reduces the errors in measurements. Another advantage is the information impedances provide such as the mechanistic information on capacitance and charge – transfer of electrochemical systems.

### **3.2 Infrared Spectroscopy (IR)<sup>57,67</sup>**

The application of IR conveniently gives a way to identify organic compounds that are distinguished by different absorption patterns (in other words, each compound possesses unique fingerprints). Infrared covers a range

of radiation from  $\sim 12,800$  to  $10\text{ cm}^{-1}$  or from  $\sim 0.78$  to  $1000\ \mu\text{m}^{-1}$ . In most instances, several analytical applications analyze these compounds in what is called the mid – IR region, which extends from  $\sim 4,000$  to  $400\text{ cm}^{-1}$ . The process of identifying different compounds those possess dipole moments takes place when the absorption of infrared radiation causes small energy differences that exist between various vibrational states. When the vibrational states alter the dipole moments, the magnitude of the energy variation caused by the distance between centers of charges determines the absorbed radiation. This technique can also be employed in the study of surface chemistry.

In this research, polarization modulation - infrared reflection adsorption spectroscopy (PM-IRRAS) was used for the characterization of modified surfaces and the binding ability between SAMs and other molecules. This method of IR has advantages over conventional IR. For instance, interferences associated with the atmosphere when using two different gold surfaces are essentially eliminated, allowing for spectral acquisition in the mid – IR fingerprint region and the use of a reference sample for background subtraction purposes is eliminated. Problems such as contamination of the surfaces from handling the gold surfaces and variability of sample positions from placing and removing from instrument can be eliminated.

A typical spectrum produces outputs such as transmittance versus wavelength and absorbance versus wavelength or wavenumbers. In this research, the data will be represented as absorbance versus wavenumber because the wavenumber is directly proportional with both energy and frequency.

### 3.3 Cyclic Voltammetry (CV)<sup>42,64,67</sup>

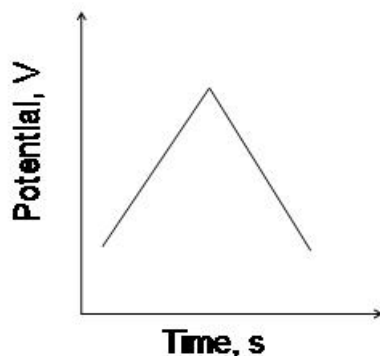


**Figure 3.7: An example of cyclic voltammetric excitation signal used to obtain voltammogram**

Cyclic voltammetry is generally used for studying mechanisms and rates of reduction/oxidation (redox) reactions. Hence, the application of cyclic voltammetry is commonly the first technique to use when dealing with electrochemical studies. In CV, current response of a system arises from a triangular potential waveform seen in Figure 3.7. First the potential is ramped linearly from an initial potential to a final potential. Once the final potential is reached, the potential is scanned in the reverse direction until it is returned to its original potential. The resulting plot of current versus potential applied is known as a cyclic voltammogram. The shape of the CV typically consists of peak formations seen in both scan directions if there are electroactive species present. The position and shape of the peaks produces insightful information that differentiates the kinetics and thermodynamics of a system.

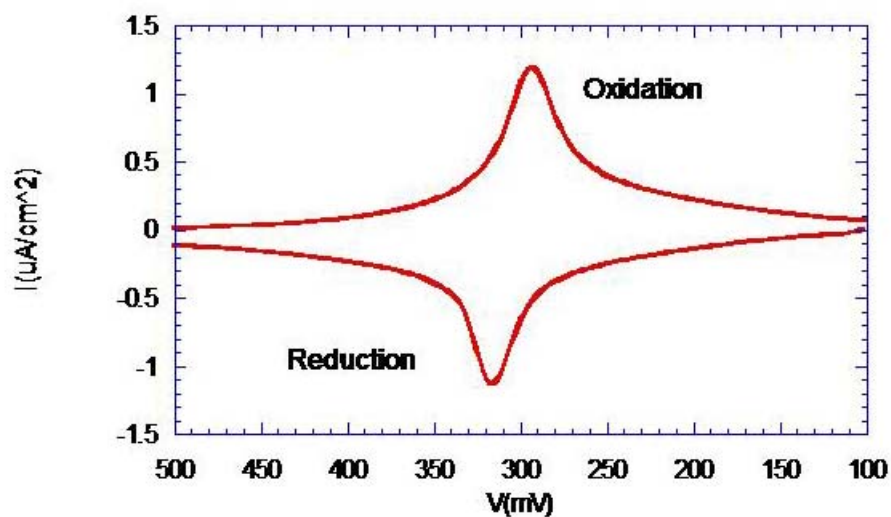


Figure 3.8: An example of a surface bound voltammetry for one – electrode redox couple; scan rate of 100 mV/s in 0.1 HClO<sub>4</sub> aqueous solution.

Figure 3.8 illustrates a plot of the current response subjected to an applied potential when a redox couple is bound to a surface or when electroactive species are present. During an experiment, an initial potential is scanned in a positive direction. Throughout the scan, the electroactive species begin to be reduced at the working electrode. When majority of the species have been reduced, a peak is observed. Next the potential is scanned in the opposite direction causing the current to decay until a potential is reached where the oxidation of the electroactive species begin to occur. Then, another peak is observed. At this time, the potential cycle has been complete. In this research, CV will be used in the investigation of electron transfer processes that transpire between ferrocenylalkanethiols and gold surfaces as a function of glucose concentration.

### 3.4 References

- (1) Kissinger, P.; Heineman, W. *Laboratory Techniques in Electroanalytical Chemistry*; 2nd ed.; Marcel Dekker, Inc, 1996.
- (2) Monk, P. *Electroanalytical Chemistry*; John Wiley & Sons, Inc., 2001.
- (3) Vassos, B.; Ewing, G. *Electroanalytical Chemistry*; John Wiley & Sons, Inc., 1983.
- (4) Wang, J. *Analytical Electrochemistry*; 2nd ed.; Wiley-VCH, 2000.
- (5) Sawyer, D.; Sobkowiak, A.; Roberts, J. *Electrochemistry for Chemists*; Second ed.; John Wiley & Sons, Inc.
- (6) Macdonald, J. *Impedance Spectroscopy*, 1987.
- (7) Yoo, J.; Park, S. *Anal. Chem.* **2000**, 72, 2035.
- (8) Gunzler, H.; Williams, A. *Handbook of Analytical Techniques*; Wiley-VCH, 2001; Vol. II.
- (9) Skoog, D.; Holler, F.; Nieman, T. *Principles of Instrumental Analysis*; Fifth ed.; Saunders College Publishing, 1998.
- (10) Kissinger, P.; Bott, A. *Current Separations* **2002**, 20, 2.

# CHAPTER 4: INVESTIGATING THE INTERACTIONS BETWEEN GLUCOSE AND BORONIC ACID BASED SELF ASSEMBLED MONOLAYERS

---

## ***4.1 Introduction***

The detection of glucose with high sensitivity and accuracy is important for the field of biomedical research. The use of modified surfaces through monolayer formation has led to an explosion in the area of biosensor technology. The formation of a self – assembled (SAM) based on a strong covalent binding between thiols ( $R - SH$ ) and a metal surface is an ideal way to obtain ordered and packed monolayers.<sup>50,52,53</sup> The ability to equip any metal surface with an alkane chain and a functionalized tail group is essential in constructing a biosensor that can detect glucose. Many commercially types of sensors have been constructed to date, but none have been successful in monitoring glucose continuously. The fundamental phenomenon of molecular recognition plays an important role in this process of detection. Phenylboronic acids are known in literature as recognition molecules for sugars.<sup>26-28</sup> The interaction between phenylboronic acid derivative bound to a metal surface, as the active material, and sugar, as the analyte, has been investigated through several techniques such as infrared spectroscopy, cyclic voltammetry, SPR spectroscopy, and Raman spectroscopy.<sup>29,30,33-36,38,39,68-74</sup> Other research efforts have been examined with this interaction by means of other optical and electrochemical methods using boronic acid derivative SAMs to detect different sugars.

The goal is to fabricate self-assembled monolayers based on a thiol – modified phenylboronic acid compound that will communicate electrochemically upon the addition of glucose by way of impedance spectroscopy. Olliff et al. designed a phenylboronic acid – terminated SAM on gold electrodes, characterized the SAM formation by Fourier transform infrared spectroscopy (FTIR), and studied the response to nicotinamide adenine dinucleotide through means of surface plasmon resonance (SPR).<sup>75</sup> Koh et al. constructed SAMs, containing different carbon chain lengths of phenylboronic acid derivative thiols, for the molecular recognition of monosaccharides by SPR.<sup>74</sup> Whitesides et al. investigated the interfacial properties of boronic acid – terminated SAMs through means of wettability and x-ray photoelectron spectroscopy (XPS).<sup>76</sup> The efforts of these researches have opened the door into employing the use of boronic acid moieties incorporated into the formation of SAMs as molecular sensing devices for sugars. Previously, our group with collaboration with the Franzen group characterized the formation of PBA – SAMs on gold surfaces by means of surface IR.<sup>77</sup> This work proposes a new method for detecting binding between aminophenylboronic acid – terminated self assembled monolayers and sugars by electrochemical impedance spectroscopy. Impedance spectroscopy gives information on the interfacial capacitance of a system without the need of a faradaic reaction.<sup>65</sup>

The first goal of this work was to synthesize the necessary phenylboronic acid- terminated thiol and to characterize the formation of the self – assembled monolayers by means of polarization modulation infrared reflectance absorption

spectroscopy (PM – IRRAS) and cyclic voltammetry (CV). The second goal was to investigate the change in impedance that occurs upon changing glucose concentration and the reproducibility of the monolayer by means of electrochemical impedance spectroscopy (EIS).

## **4.2 Experimental Section**

### **4.2.1 Materials and substrates**

3-Aminophenylboronic acid hemisulfate was purchased from Acros Organics. Other chemicals and reagents for the synthesis of N-(3-dihydroxyborylphenyl)-11-mercaptoundecanamide (PBA) were commercially available and purchased from either Acros Organics or Sigma-Aldrich. Synthesis and characterization of PBA can be found in the appendix section. Glucose and other sugars (all D chirality) were also purchased from Sigma-Aldrich. Milli-Q grade deionized water ( $18 \text{ M}\Omega \cdot \text{cm}$ ) was used for the rinsing of solutions and monolayers. Absolute ethanol (200 proof) was also used for the preparation of the monolayer formation and solutions.

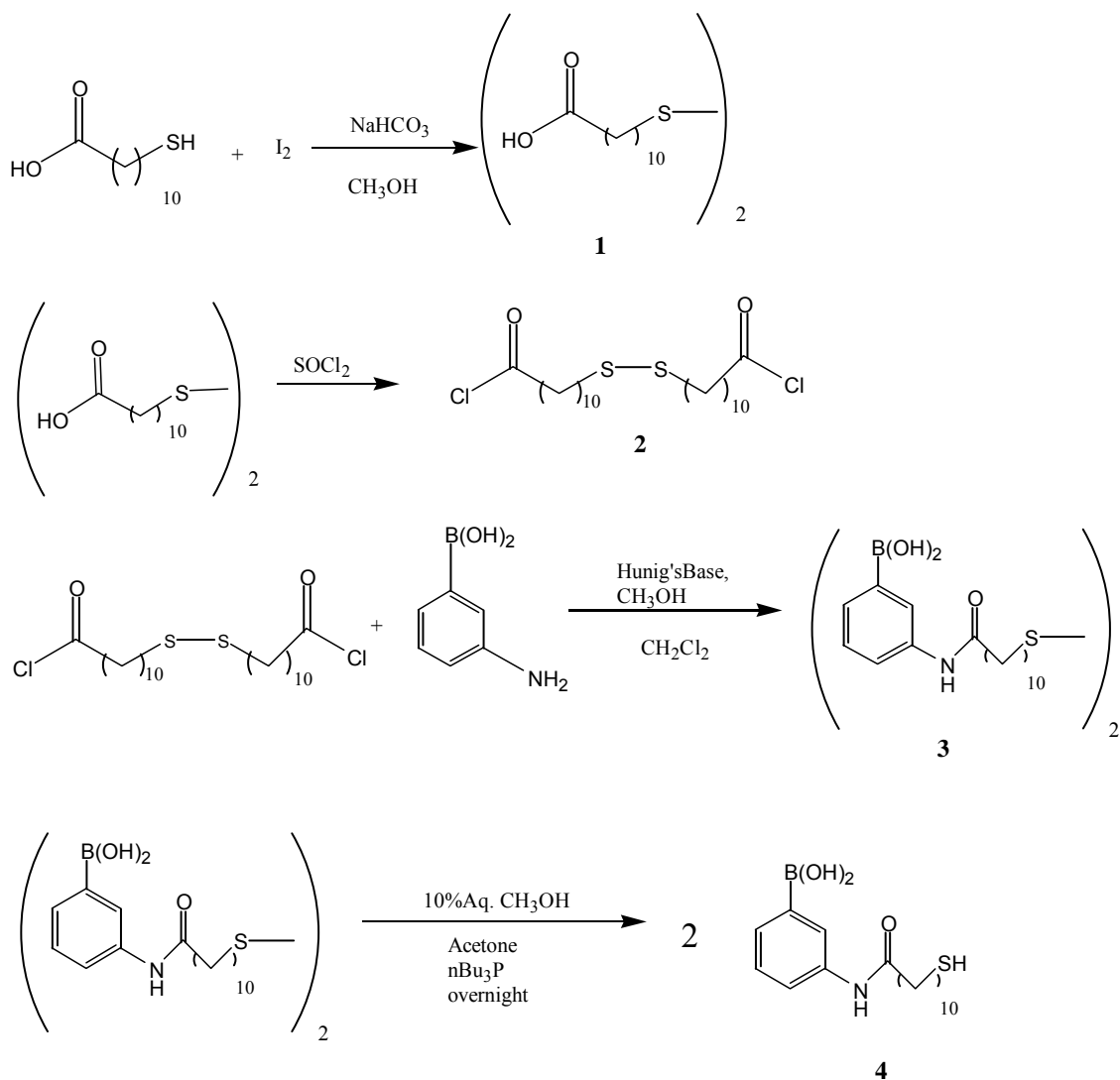
### **4.2.2. Synthesis of N-(3-dihydroxyborylphenyl)-11-mercaptoundecanamide (PBA)**

The synthesis of N-(3-dihydroxyborylphenyl)-11-mercaptoundecanamide) (abbreviated PBA) is shown in Scheme 4.1. 11-mercaptoundecanoic acid (5g, 22.9mmol) was added to a suspension of methanol (5ml), sodium bicarbonate (5.77g, 68.7mmol) and molecular iodine (2.91g, 11.4mmol) to yield disulfide **1** which precipitated from solution and was used without further purification. This molecule (4g, 9.2mmol) was converted to the bis-acid disulfide **2** by refluxing for 30 minutes in thionyl chloride (21.89g, 184.0mmol). The excess thionyl chloride

was removed by distillation. Subsequently a substitution reaction was performed to give the bis-amide disulfide **3** where the brownish oil of **2** (4g, 8.48mmol) was added to a mixture containing 3-aminophenylboronic acid hemisulfate (3.16g, 17mmol) and Hunig's base (7mL). Separation of **3** (1g, 1.6mmol) with tributylphosphine (1.58mL) yielded the final product **4**. The identity and purity of the final product was confirmed by:  $^1\text{H}$  NMR [( 400 MHz,  $\text{CD}_3\text{OD}$ ,  $\delta$ ) 1.33 (s,12H), 1.67 (m, 4H), 2.36 (t, 2H,  $J = 7.3$  Hz), 2.66 (t, 2H,  $J = 7.2$  Hz), 7.30 (m, 1H), 7.48 (m,1H), 7.61 (m, 1H), 7.78 (m, 1H)], and elemental analysis<sup>32</sup>.

#### **4.2.3 Pretreatment of gold substrates and formation of SAM**

Evaporated gold substrates (with Ti adhesion layer) were purchased from Evaporated Metal Films, Inc. All gold substrates used to prepare the monolayers were first cleaned in a piranha solution (3:1 ratio of concentrated  $\text{H}_2\text{SO}_4$  and 30%  $\text{H}_2\text{O}_2$ ) for approximately 30 seconds (CAUTION: piranha solution reacts violently with organic chemicals), immediately rinsed with 18  $\text{M}\Omega \cdot \text{cm}$  deionized water and dried under  $\text{N}_2$  gas. The freshly cleaned gold substrates were then directly immersed in an ethanol solution of thiol for incubation at room temperature. During this time the phenylboronic acid –terminated thiol (PBA) was immobilized on the gold surface. The monolayers were then rinsed with ethanol and water, and then dried under  $\text{N}_2$  gas prior to measurements.



**Scheme 4.1: Synthesis of N-(3-dihydroxyborylphenyl)-11-mercaptoundecanamide (PBA)**

#### 4.2.4 Spectroscopic measurements

For surface analysis (mainly used for evidence of phenylboronic acid terminated-SAM formation), infrared spectroscopy was used. Polarization modulation infrared reflection absorption spectroscopy (PM-IRRAS) spectra were performed on a Digilab FTS 6000 spectrometer equipped with a step scan interferometer, a liquid nitrogen cooled narrow band MCT detector, a global source, and a UDR – 4 filter. The IR radiation was typically phase modulated at frequencies of 400 or 800 Hz at an amplitude of 1.0 or 2.0  $\lambda$  HeNe while stepping

at 0.5 – 2.5 Hz. A gold polarizer was used to obtain either s- or p-polarized radiation before reflecting off the sample at an incident angle of 80 degrees from the surface normal. All spectra were done at room temperature at a resolution of  $4\text{ cm}^{-1}$  with a spectral range of  $900 - 4000\text{ cm}^{-1}$ . For infrared measurements, the freshly cleaned gold substrates were then directly immersed in a 3mM ethanol solution of PBA for overnight incubation at room temperature. During this time the phenylboronic acid –terminated thiol was immobilized on the gold surface. The monolayers were then rinsed with ethanol and water, and then dried under  $\text{N}_2$  gas prior to measurements. The digital signal processing (DSP) algorithm incorporated into the Digilab spectrometer software was used to obtain the spectra, which eliminated the need for a separate reference gold slide.

To confirm findings with the surface IR, the solution single – pass attenuated total reflection Fourier transform infrared spectroscopy (ATR – FTIR) of phenylboronic acid – thiol solution was taken using a PIKE Technologies single – pass ATR attachment attached to a Digilab FTS 3000 FTIR spectrometer equipped with a germanium crystal for single – pass attenuated total reflection (ATR). The spectrometer was equipped with liquid nitrogen cooled MCT/A detector, and the spectra were recorded at a resolution of  $4\text{ cm}^{-1}$  with a spectral range of  $650 - 4000\text{ cm}^{-1}$ . The solutions were allowed to concentrate on the ATR element to increase the absorptive features of the molecule of interest. The absorption spectra were the result of 64 scans and were recorded at room temperature.

#### 4.2.5. Electrochemical measurements

Electrochemical experiments were performed using a single compartment cell. This electrochemical cell, originated by the Bowden group of North Carolina State University, was made to accommodate a gold substrate by exposing an area of  $0.32 \text{ cm}^2$  via a cylindrical cavity (Figure 4.1).<sup>78</sup> After piranha cleaning, the substrate was further cleaned in a solution of  $0.01 \text{ M KCl}$  in  $0.1 \text{ M H}_2\text{SO}_4$ , rinsed with deionized water and absolute ethanol before adding the necessary  $1 \text{ mM}$  (PBA) alkanethiol ethanol solutions. Incubation times varied (2 hours, 4 hours, and overnight) in the attempts to achieve the maximum formation time of the self assembled monolayers. After incubating at room temperature, the monolayers were rinsed again with absolute ethanol and deionized water prior to measurements.



**Figure 4.1:** A picture of the Bowden cell use for electrochemical measurements, along with a schematic of the cylindrical cavity; the working electrode (gold substrate) is secured at the bottom of the cell, the counter electrode (platinum wire) is coiled around the reference electrode (silver/silver chloride)

Also in Figure 4.1, the necessary electrolyte, counter electrode (platinum wire), and reference electrode (Ag/AgCl) was placed within the cylindrical cavity of the glass middle piece. The BAS CV – 50W system was used to perform cyclic voltammetric (CV) experiments at room temperature. The electrolyte varied depending on each run. The voltammograms were performed in electrolyte with glucose concentrations of 0 mM, 5 mM, and 20 mM. Spectra of potential versus current were acquired from voltammograms that used potential sweep rate of either 50 mV/s or 100 mV/s in the range of 0 to 600 mV (potentials). Data were analyzed in either the Origin Pro or KaleidaGraph software, which provided cyclic voltammograms.

Impedance spectroscopy experiments were done on a BAS – Zahner IM6e impedance analyzers, in which the same type of electrochemical cell and electrodes as above were used. The cell was enclosed in the Faraday cage, whereupon any outside electrical noise was reduced. Impedance measurements were performed at a bias potential of 300 mV (an arbitrary value) and in a frequency range from 100 mHz to 100 kHz (and then the frequency range was decreased to 400 mHz to 4 Hz), using an alternating voltage, 5 mV. The impedance spectra were collected and interpreted through Bode plots. From the magnitude and phase values of the Bode plots, the complex plane,  $Z'$  and  $-Z''$ , data could be derived and interpreted. The data from the software program was analyzed using the Origin Pro software or Excel.

In addition, the use of analysis of variance (ANOVA) provided a statistical based technique capable of indicating which factors studied here had a statistical

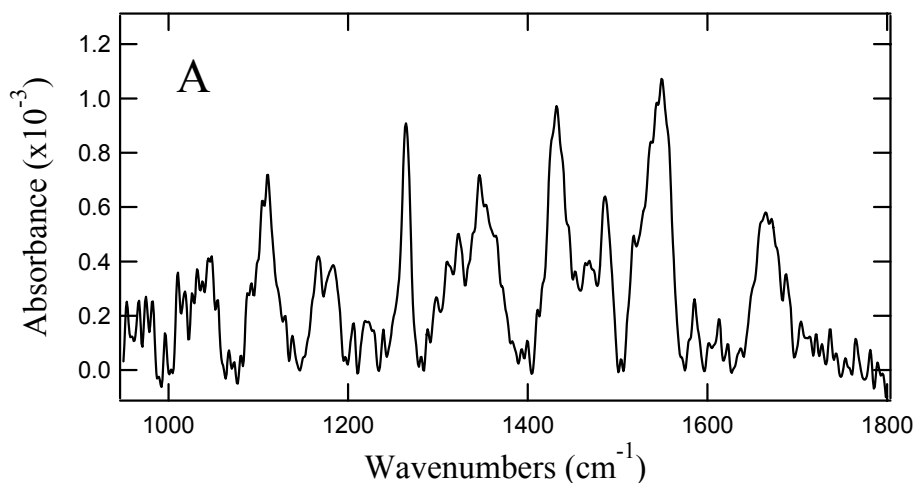
significance. A two – way ANOVA analysis using Excel was selected to investigate factors that affect reproducibility of cells and response to different glucose concentration. ANOVA was performed on impedance data after measurements were taken on cells after the addition of different concentrations of glucose. The aim of this analysis was to determine if the variations were due to random error or not. In ANOVA, the F – test value is the statistic used to test the hypothesis that the variation observed is real. In other words, if the variance factor (F) is smaller than the variance limit ( $F_{crit}$ ), then the variation is due to random error. However, if F is larger than  $F_{crit}$ , then the variation is not due to random error and the effects are real.

### 4.3 Results and Discussion

#### 4.3.1 Characterization of phenylboronic acid-terminated SAMs (PBA-SAM)<sup>77</sup>

##### 4.3.1a) Surface IR

After incubation with PBA in ethanol solution, formation of the PBA – SAM was confirmed by polarization modulation infrared reflectance absorption spectroscopy (PM-IRRAS). The PM-IRRAS spectra exhibit intense and apparent stretching modes that reveal the composition of PBA – SAM on the gold (Au) surface (Figure 4.2).



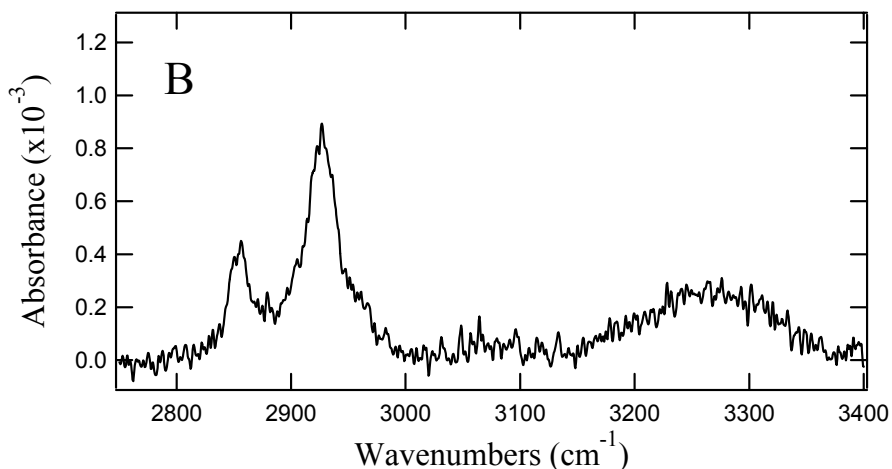


**Figure 4.2: The PM-IRRAS spectra of a monolayer PBA on a gold surface in the low (A) and high (B) wavenumber region, respectively**

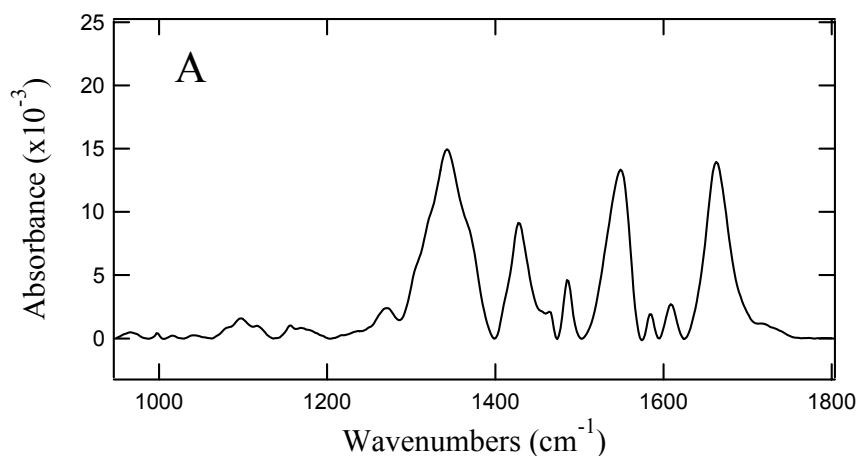
**Table 4.1: Important vibrational mode assignments that corresponds to PBA on a gold surface**

Vibrational modes (cm <sup>-1</sup> ) for Experimental Results		
(PM) – IRRAS	solution ATR – FTIR	mode assignment
1663	1663	C = O stretch
1580	1549	N – H bending
1430	1427	C-C stretch (phenyl ring, B –O stretching)
1342	1342	B – O stretch
2856	2853	Symmetric CH <sub>2</sub> stretch
2927	2926	Asymmetric CH <sub>2</sub> stretch
3263	3304	O – H stretch

T

The stretching modes illustrated in Figure 4.2A and 4.2B were found in the 950 – 1800 cm<sup>-1</sup> region and 2750 – 3400 cm<sup>-1</sup> region, respectively. Table 4.1 lists several important peak assignments of the IR vibrational modes that are indicative of the presence of PBA –SAM on the gold surface. These peak assignments are within the IR modes of other papers for PBA – SAMs.<sup>79,80</sup> Figure

4.2A has several stretching modes, such as a C=O ( $1663\text{ cm}^{-1}$ ) and B-O ( $1342\text{ cm}^{-1}$ ), that support the formation of a SAM. The primary N-H bending mode is seen at  $1580\text{ cm}^{-1}$ , while the peak at  $1430\text{ cm}^{-1}$  is likely due to a mixture of C-C and B-O stretching. The mode at  $1264\text{ cm}^{-1}$  is possibly due to imperfections in the gold surface allowing the silicon oxide modes of the glass substrate to be observed while the mode at  $1111\text{ cm}^{-1}$  is likely due to ring deformation modes. Figure 4.2B shows predominant modes at  $2856\text{ cm}^{-1}$  and  $2927\text{ cm}^{-1}$  that are due to the symmetric and asymmetric stretching motions of the methylene groups in the alkane chain of the PBA. The broad mode centered at  $3263\text{ cm}^{-1}$  is the result of O-H stretching motions of the  $\text{B}(\text{OH})_2$  moiety of PBA.



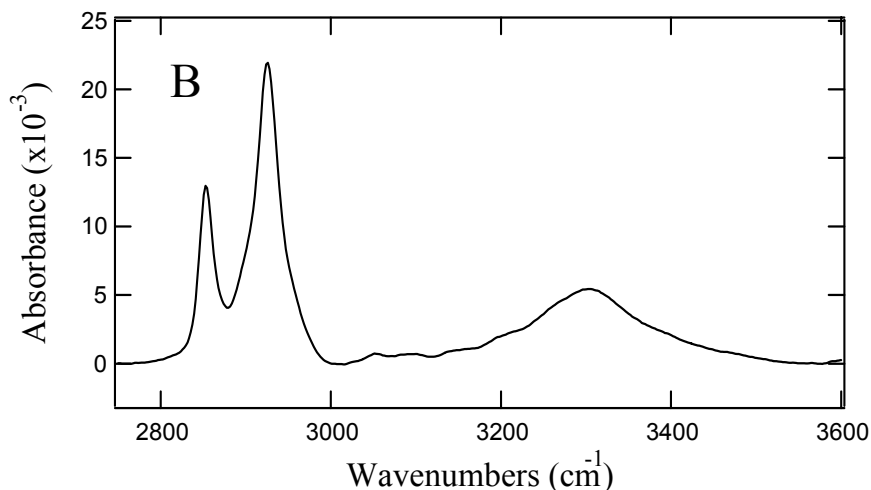


**Figure 4.3: Single – pass ATR – FTIR spectra of a 3 mM PBA solution in ethanol allowed to evaporate on the ATR element in the low (A) and high (B) wavenumber region.**

In order to verify further the assignments of the observed vibrational modes, a comparison was done with FTIR spectra in solution (Figure 4.3). A 3 mM solution of PBA was allowed to concentrate on the ATR element before measuring. The spectra shown in Figure 4.3A and 4.3B are for the low and high wavenumber regions, respectively. The characteristic modes including the C=O stretch and N-H bending at  $1663\text{ cm}^{-1}$  and  $1549\text{ cm}^{-1}$ , respectively. Also, the mode present at  $1427\text{ cm}^{-1}$  is most likely due to a combination of several vibrational motions in the molecule, while the B-O stretching modes are seen in solution by the band centered at  $1342\text{ cm}^{-1}$ . The methylene symmetric and asymmetric stretching modes are present at  $2853$  and  $2926\text{ cm}^{-1}$ . At  $3304\text{ cm}^{-1}$ , the B – OH stretching mode is present. These strong, clear modes are indicative of a PBA – SAM formation on the gold surface. In addition, these peak positions and intensities are well in line with reported monolayers.

#### *4.3.1b) Cyclic Voltammetry*

Cyclic voltammograms (CV) were obtained for both the bare gold surface (no formation of any monolayer) and the PBA- SAM (Figure 4.4A and 4.4B). The CV for the gold surface before and after deposition was measured at room temperature in 1.0 M HClO<sub>4</sub>, at a scan rate of 100 mV/s. The resulting voltammogram in Figure 4.4A displayed the expected shape for bare gold.

In Figure 4.4B, the graph shows a voltammogram of PBA-SAM. This SAM contains an aminophenylboronic acid group that is hydrophilic and nonelectroactive. Consequently, electrons are not expected to transfer across the electrode-solution interface, which in turn should result a nonfaradaic electrochemical behavior. For that reason, there should be an absence of a redox peak. Moreover, as SAMs reduce interfacial capacitance, the height of the charging current in the CV should decrease dramatically after the deposition of the PBA – SAM (Figure 4.4B). The PBA-SAM interfacial capacitance observed in the Figure 4.4B shows a decrease in its capacitance compared to that of the bare gold in Figure 4.4A and there is no evidence of a redox peak. Thus the results of both IR and CV experiments are consistent with the formation of a PBA – SAM on the gold electrode.

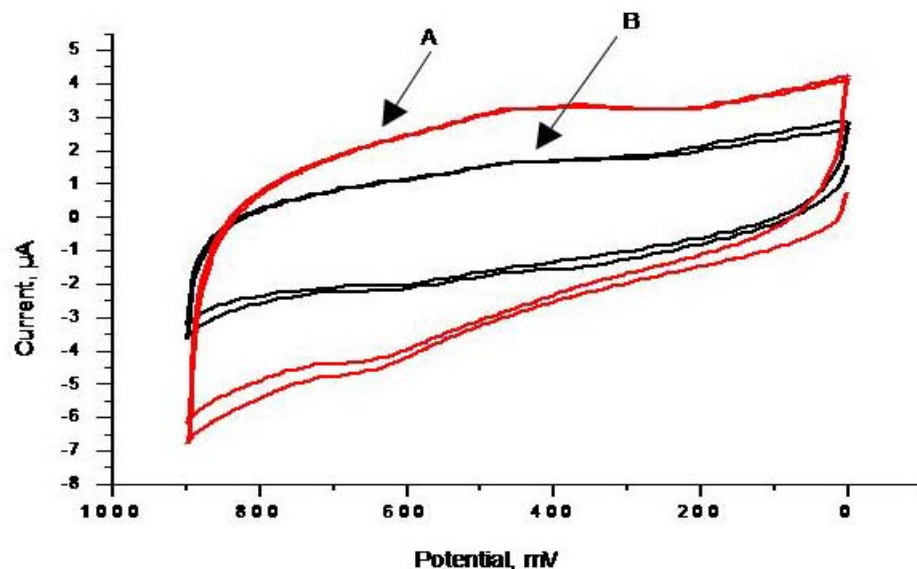
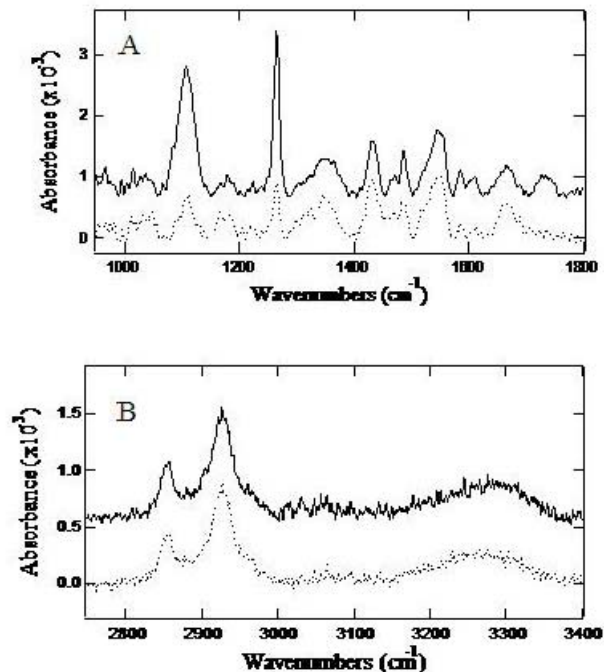


Figure 4.4: Cyclic voltammogram overlay of bare gold (A) and boronic acid terminated-SAM (B). Experiments were performed in 1.0 M HClO<sub>4</sub> and at room temperature. Scan rate, 100 mV/s; electrode area, 0.32 cm<sup>2</sup>.

#### 4.2.3 Binding interaction between PBA – SAM and D-glucose<sup>77</sup>

The ability of the phenylboronic acid terminated self-assembled monolayers to selectively recognize and form covalent bonds with sugars such as glucose is well known in literature. PM – IRRAS was further used to examine the recognition of glucose by the PBA – SAM. When the PBA – SAM was placed in a 3 mM glucose solution in ethanol for 30 minutes, detection of the boronate ester formation was observed once glucose bound to the boronic acid moiety of the PBA – SAM. The formation of a boronate ester displayed characteristic vibrational modes of this molecule.



**Figure 4.5: PM – IRRAS spectra of a PBA – SAM exposed (solid spectrum) to 3 mM glucose solution for 30 minutes and a PBA – SAM not exposed (dashed spectrum).**

Figures 4.5A and 4.5B show the PM – IRRAS spectra in the 950 – 1800  $\text{cm}^{-1}$  and 2750 – 3400  $\text{cm}^{-1}$  regions, respectively. Figure 4.5A displays the PM – IRRAS spectra in the lower wavenumber region where PBA – SAM on gold exposed to glucose ( solid) and not exposed (dashed), while Figure 5B displays the same two samples in the higher wavenumber region. The identification of the PBA – SAM has described previously. However, the spectra relating to the glucose bound to the PBA – SAM through the phenylboronic acid moiety shows modes characteristic similar to the PBA – SAM while establishing several new vibrational modes and peak shifts upon binding with glucose. For example, a C-O stretching mode is observed at 1107  $\text{cm}^{-1}$  after exposure of the PBA – SAM to glucose, in turn is suggestive of the presence of glucose. In addition, shifts and changes in peak profiles occur in the B-O stretching modes around 1342  $\text{cm}^{-1}$ ,

which is suggestive of a boronate ester formation. As observed before, the mode at  $1264\text{ cm}^{-1}$  is likely due to silicon oxide stretching motions in the glass substrate due to imperfections (i.e., scratches) in the gold surface or it could be due to the skin depth of the IR beam being larger than the thickness of the gold film on the glass slide at these IR wavelengths. For this reason, the intensity differences observed for the  $1264\text{ cm}^{-1}$  mode are primarily due to the number of imperfections (either scratches or variation of thickness) on the gold surface. Another major difference in the spectra upon addition of glucose to the PBA – SAM is the presence of a mode at  $1734\text{ cm}^{-1}$ . The significant rise in intensity of this mode upon glucose binding is relative to the other vibrational modes of this molecule (boronate formation) compared to the PBA – SAM on a gold surface. In Figure 4.5B, the spectra in high wavenumber region exhibits the symmetric and asymmetric methylene stretching modes at  $2857$  and  $2927\text{ cm}^{-1}$ , respectively, before and after glucose has been exposed to the PBA – SAM. Also observed is a shift in the O-H stretching region upon exposure and binding with glucose compared to no exposure the sugar. Upon glucose binding, a shift in the O-H stretching mode of boronic acid shifts  $\sim 11\text{ cm}^{-1}$  higher to the peak centered at  $3274 \pm 0.7\text{ cm}^{-1}$  (determined by Gaussian band fitting) indicative of the O-H stretching mode of glucose and the subsequent disappearance of the O-H stretching mode of the phenylboronic acid moiety of PBA prior to binding. The detection of glucose binding to a PBA – SAM on a gold surface was made possible by PM – IRRAS and verified by solution FTIR (Figure 4.6).

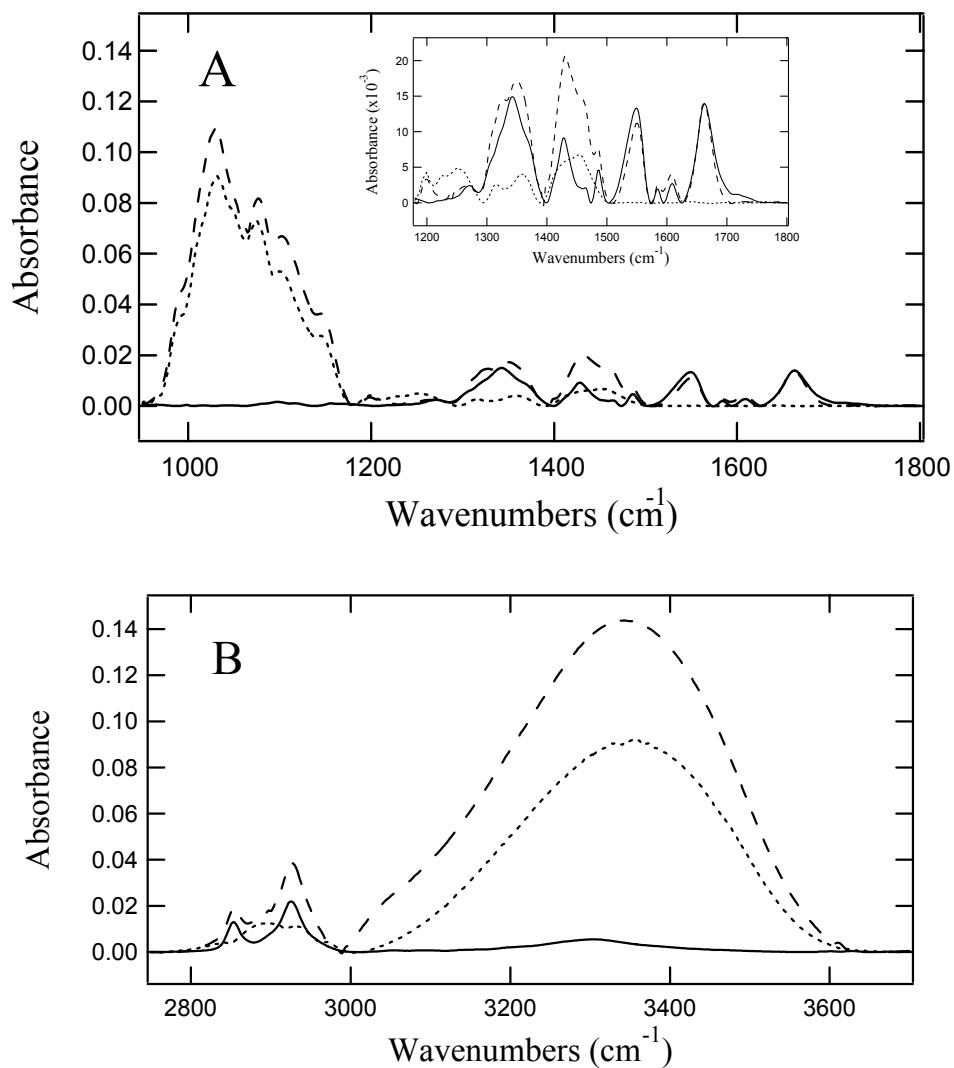


**Figure 4.6: Single-pass ATR-FTIR spectra of a 3 mM solution of PBA (solid), 3 mM solution of glucose (short dashed), and the 1:1 molar ratio of both in the low (A) and high (B) wavenumber region. All solutions were allowed to evaporate on the ATR element.**

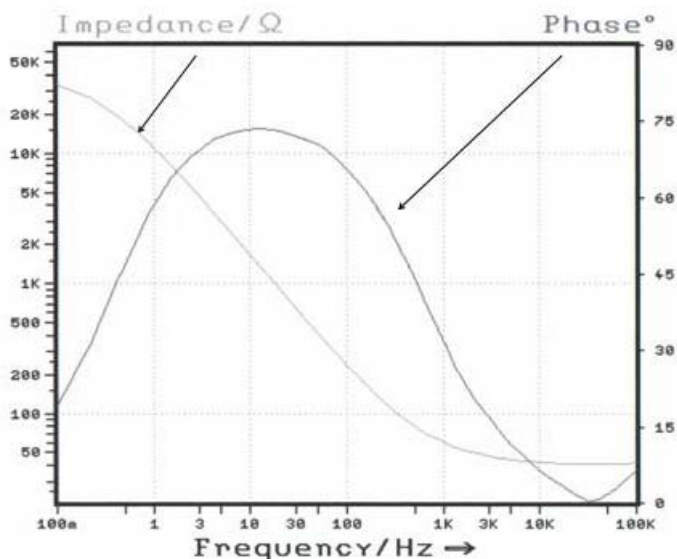
To confirm the vibration modes of PBA and glucose bound to PBA on the gold recorded for both species. The single-pass ATR-FTIR spectra of a 3 mM ethanolic solution of PBA (solid), glucose (short dashed) and an 1:1 molar ratio of PBA and glucose (long dashed) in the low (A) and high (B) wavenumber region are shown in Figure 4.6A and 4.6B. The spectra were obtained by allowing these solutions to evaporate onto the ATR element before acquiring the spectra.

The modes from PBA have already been assigned above. The most notable modes from glucose are the C-O stretching band centered at  $1099\text{ cm}^{-1}$  with several modes with a C-O stretching component in the  $950 - 1180\text{ cm}^{-1}$  region and the O-H stretching mode centered at  $3352\text{ cm}^{-1}$ . The spectra of glucose bound to PBA shows a shift in the O-H stretching mode from  $3304\text{ cm}^{-1}$  of the boronic acid component of PBA to  $3343\text{ cm}^{-1}$  of the O-H stretching mode of glucose bound to PBA. There is also a large intensity increase in the O-H stretching mode with glucose bound relative to PBA without glucose bound. However this intensity difference is not observed on the gold surface likely due to the orientation of the O-H transition dipole moment relative to the surface. The B-O stretching modes are also shifted and have a different peak profile with glucose bound to PBA compared to PBA without glucose bound. These two observations are suggestive that glucose is binding to PBA through the phenylboronic acid moiety. The C-O stretching mode of glucose is also evident in the glucose bound to PBA solution FTIR spectra. These differences between PBA and glucose bound to PBA are consistent with those observed on the gold surface (Figure 4.5). Lastly, the solution spectrum shows a combination mode centered at  $1734\text{ cm}^{-1}$  (low intensity) for glucose bound to PBA compared to the mode in PBA centered at  $1717\text{ cm}^{-1}$ . The presence of the mode at  $1734\text{ cm}^{-1}$  is in accordance with the experimental results on a gold surface; however, this mode is considerably less intense compared to the carbonyl-stretching mode in solution at  $1663\text{ cm}^{-1}$  in contrast to the PM-IRRAS spectra. Therefore the orientation of these molecules on the surface, the binding of glucose and the

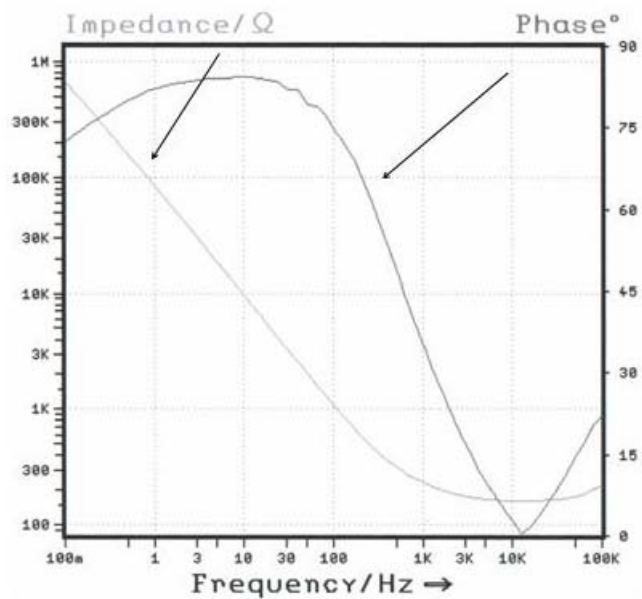
presence of the gold surface results in the increase in intensity of this combination mode that allows for the detection of glucose to be performed.

#### 4.3.3. EIS measurements of the PBA – SAM system

To follow the recognition of sugars by the PBA – SAM, electrochemical impedance was utilized. Specifically, it was sought to determine what changes would occur when different glucose concentrations were introduced to a cell containing the SAM electrode. Boronic acid moieties are nonelectroactive species, as shown previously in this chapter; therefore, impedance allows a way to determine how the capacitance will alter upon introducing different glucose concentrations to the PBA – SAM. As the glucose binds with the phenylboronic acid, it was hypothesized that the change in the interfacial capacitance as glucose concentration increase would yield impedance that increases linearly.



**A**



**B**

**Figure 4.7: Representations of Bode plots by the Thales software. Plots represent impedance on bare gold (A) and impedance on a PBA – SAM (B). All experiments were performed in 0.1 M HClO<sub>4</sub> at 5mV amplitude.**

The Bode plot showing the impedance of a bare gold electrode, immersed in a 0.10 M HClO<sub>4</sub> electrolyte solution, is displayed in Figure 4.7A. The absolute impedance,  $|Z|$ , shows a plateau in the frequency region of 100 kHz – 1 kHz, followed by a linear increase until 100 mHz. The phase shift,  $\Phi$ , does not reach  $-90^\circ$ , but it reaches its maximum angle around  $-80^\circ$  (1 Hz – 6 Hz) and then it decreases as the frequency increases. At higher frequencies, the system behaves like a resistor and the capacitive component is much smaller than the resistive which is observed by the linear consistency of the phase angle around  $0^\circ$  at those frequencies. Also, the Figure 4.7A show that, at lower frequencies, the system behave like a resistor again which is observed by the decrease in the

phase angle after 600 mHz. In the intermediate frequency range or the region where the impedance increases linearly and the phase angle approaches  $-90^\circ$ , the system behaves like a capacitor. Therefore the following studies will be carried out at intermediate frequencies, 1 – 10 Hz, in order to examine processes in the capacitance region.

In the literature, there are studies that examine frequencies within these regions for modified surfaces. Impedance measurements were performed with different glucose concentrations in supporting electrolyte solution for the modified gold electrodes. The influence of the PBA – SAM on the impedance is very noticeable. Figure 4.7B shows a Bode plot of a PBA – SAM after a 4 hour incubation time period. There are some distinct differences when compared to the bare gold graph. For instance, the phase angle curve remains constant at  $\sim 85^\circ$  over a longer frequency range, (8 mHz – 10 Hz). Within these intermediate frequencies, the absolute impedance reveals a linear relationship as a function of the frequency. This range suggests the system will be performing in a capacitive regime, whereupon the focus will be on the PBA – SAM. For instance, the phase angle reveals two distinct sections that correlate with the resistive behavior of the electrolyte at the very high and very low frequency regions.

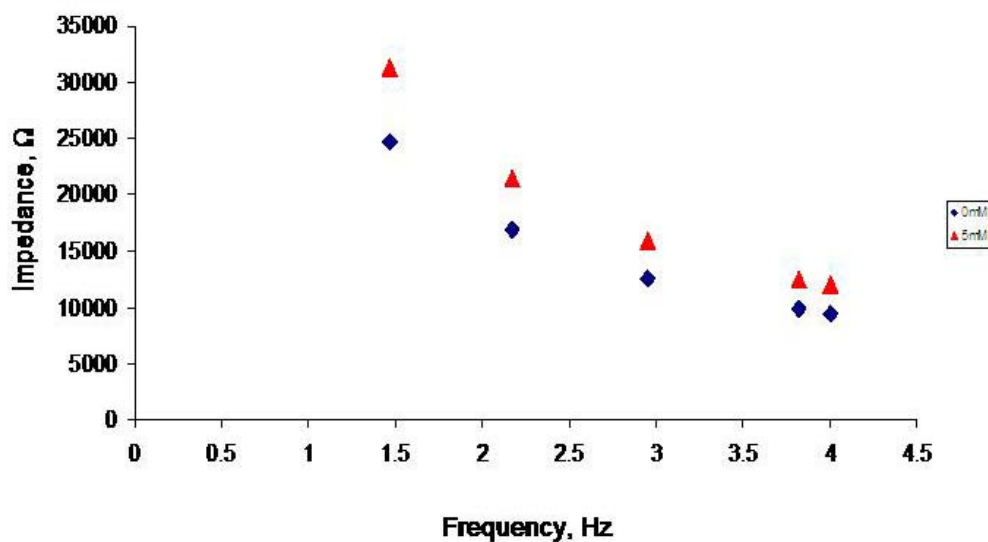
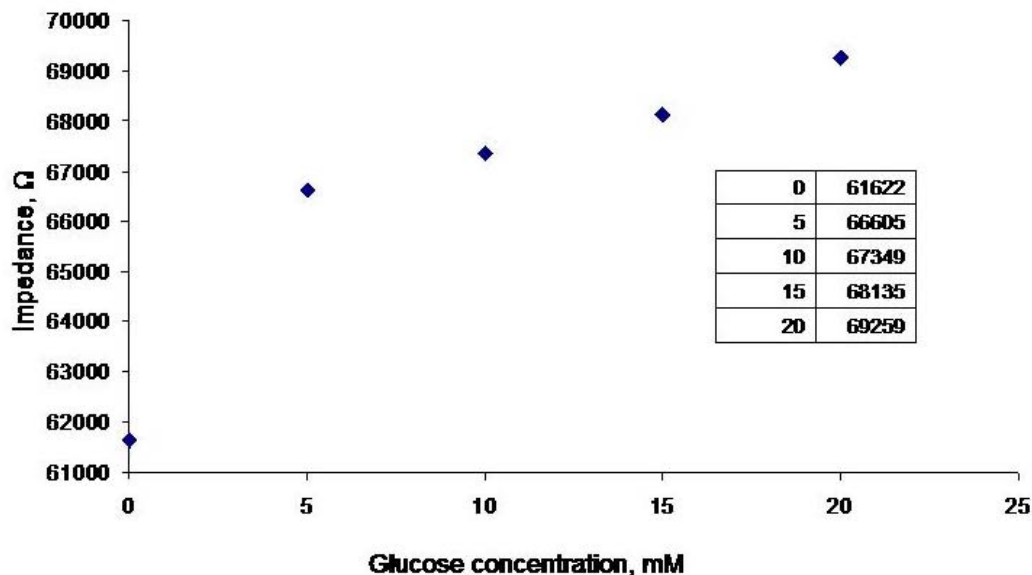


Figure 4.8: Graph representing the changes that occur in the absence and the presence of glucose in the intermediate region. An experiment ran in 0.1 M HClO<sub>4</sub> at 5 mV amplitude and at room temperature.

To affect glucose binding to the PBA –SAM, *D* – glucose was dissolved using the supporting electrolyte of 0.1 M HClO<sub>4</sub>. Analyses were performed with a range of frequencies in the intermediate region. The objective was to determine at which frequency the maximum change would occur when glucose was introduced to the cell. Impedance data taken from a cell in the absence and presence of glucose was used to decide this frequency. Figure 4.8 shows the maximum change in impedance at a frequency near 1 Hz. As the time decreases (frequency increases), the impedance change between the two glucose concentrations became smaller. So for further studies, measuring impedance at 1.5 Hz performed experiments.



**Figure 4.9: Plot of impedance against glucose concentration. The experiment was done in 0.1 M HClO<sub>4</sub> solution at 5 mV amplitude and at room temperature. Data obtained at 1.47 Hz.**

It is expected that the impedance would increase in value as the capacitance decrease, as noted in Figure 4.8 and related studies. Thus, it was hypothesized that when the glucose concentration expands beyond the physiological range, the increase of impedance will show an asset of the responsiveness of the proposed biosensor. Figure 4.9 shows a graph in which the impedance is graphed versus glucose concentrations from 0 to 20 mM (increments of 5) at 1.47 Hz. The increasing impedance values demonstrated a change occurring in the interfacial capacitance as different glucose concentrations were tested. The binding phenomenon of glucose to boronic acid can be correlated to the change in the interfacial capacitance that was seen by the increase in the impedance value.

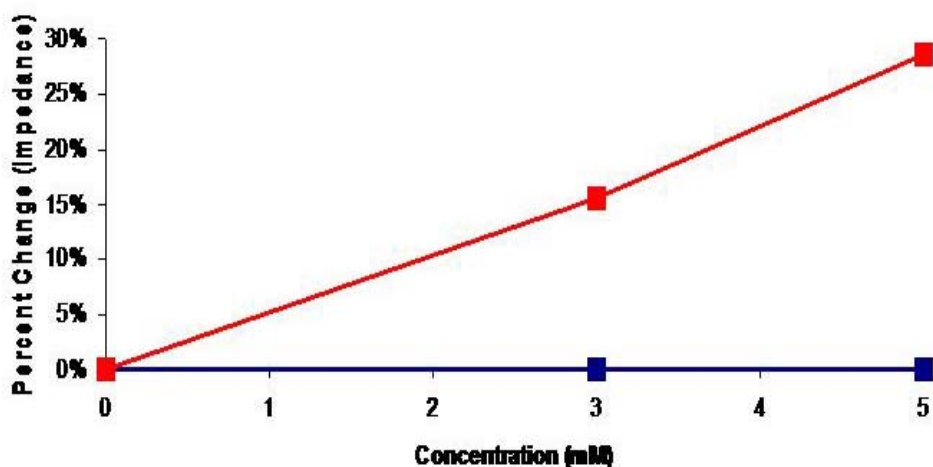


**Figure 4.10: Comparisons of impedance plots for mercaptoundecanoic acid –terminated SAM (blue) and phenylboronic acid –terminated SAM (red) at different glucose concentrations. Impedance measurements done at an amplitude of 5 mV and at room temperature. Plots were taken at 1.47 Hz.**

A mercaptoundecanoic acid - terminated self-assembled monolayer (OH-SAM) was utilized in a control experiment to verify that any changes observed in the PBA – SAM was due to the binding between glucose and phenylboronic acid.<sup>81,82</sup> The system was subjected to the physiological concentration range of glucose and compared to PBA – SAM at the exact concentrations. Figure 4.10 shows a plot of percent changes versus glucose concentrations for both the OH – SAM and PBA – SAM. In order to calculate the percent change (% change); the following equation (1) was used:  $\% \text{ change} = [Z_{0\text{mM}} - Z_{\text{conc}} / Z_{0\text{mM}}] \times 100$ . The percent changes show significant differences between the OH – SAM and PBA – SAM as glucose was introduced to each system. The OH – SAM illustrates absolute no change as different glucose concentrations were introduced to its cell, denoted by the unchanged percent change values. On the other hand, the PBA – SAM illustrates a considerable percent change as different glucose

concentrations were added to its cell, denoted by the linear increase in the percent change values. This linearly increase indicates a binding phenomenon with glucose. When observing impedance versus glucose concentration Bode plot, it showed that the impedance values for the OH – SAM to be higher than that of the PBA – SAM, which indicating that more of the OH – thiol attaches to the surface, bringing about a more well packed SAM. This denoted by observing an increase in the impedance values (not shown).

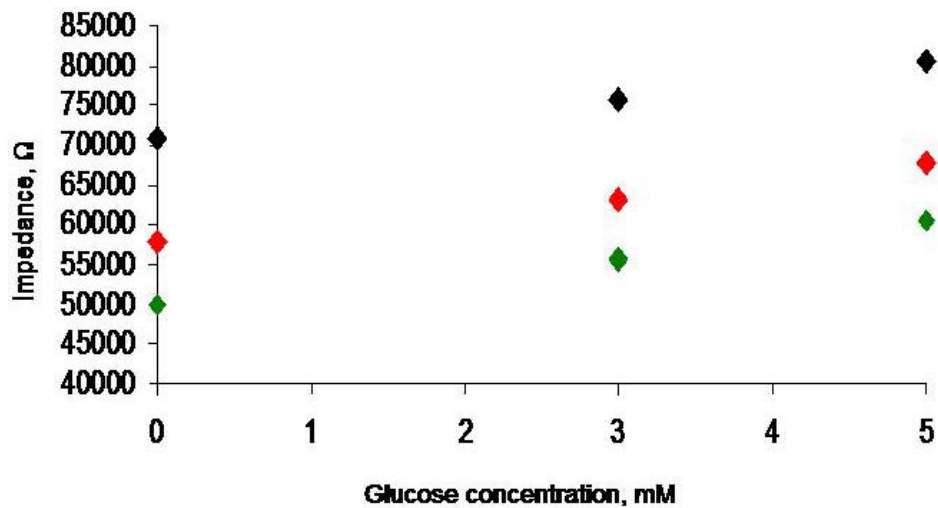
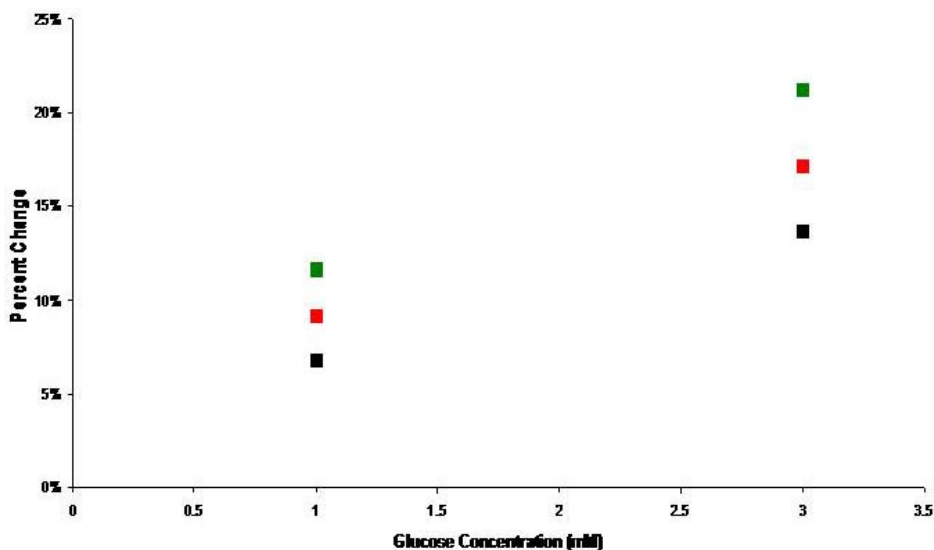


Figure 4.11: Graphs representing comparisons of PBA – SAMs. Experiments done in 0.1 M HClO<sub>4</sub> at an amplitude of 5 mV and room temperature.



**Figure 4.12:** A plot of how each cell differs in percent as different glucose concentrations are added. Each cell is represented by the same color as in Figure 4.11.

Additional studies were conducted to investigate the reproducibility among several cells. Figure 4.11 shows several representative plots in which the impedance of different PBA – SAM cells was plotted versus the concentration of glucose to the cells. The figure reveals that, even at a given glucose concentration, there is variation in the impedance from cell to cell. The source of this variation is currently unknown. However, variations may have resulted from unidentified differences in the method of cell cleaning or monolayer formation. To determine if the variation between cells was merely a result of differences in the initial impedance, Figure 4.12 was constructed to show the percent change in impedance versus glucose concentration for each of the cells shown in Figure 4.11. The percent change for each cell also showed variation. Thus, no conclusions were drawn about the source of cell-to-cell variation.

**Table 4.2: Two – way ANOVA results on impedance data for PBA<sub>11</sub>-SAMs**

Source of Variation	SS	df	MS	F	Fcrit
Concentration	2E+08	2	8E+07	919	7
Cell	6E+08	2	3E+08	3845	7
Error	3E+05	4	8E+04		
Total	8E+08	8			

**SS = Sum of Squares, df = degrees of freedom, MS = mean square, F= variance factor, F<sub>crit</sub> = variance limit**

Table 4.2 shows another analysis that was performed on the impedance data (Figure 4.11) to determine if the nature of the variation in the measurements was random or not for two independent variables: glucose concentration and the cell used. Two – way analysis of variance (ANOVA) was performed. This analysis showed that variation of both glucose concentration and cell resulted in a variation in impedance that was statistically greater than just random error. Specifically, the variance factor ( $F_{\text{calculated}}$ ) was larger than the variance limit ( $F_{\text{critical}}$ ), indicating that the cause of variation was real or determinate. As there is a statistically significant relationship between impedance and glucose concentration, it is concluded that glucose binding to the boronic acid groups in the SAM could be detected by impedance. However, the variation between cells obscures this trend.

#### **4.4 Conclusion**

Investigations on the formation of phenylboronic acid - terminated thiol on gold surfaces were evaluated through infrared spectroscopy (PM – IRRAS) and cyclic voltammetry (CV). PM – IRRAS confirmed the formation of a PBA – SAM. Additional confirmation was established through means of CV where the double layer capacitance change dramatically after incubation in the thiol. PM – IRRAS results also displayed the ability of glucose to bind with boronic acid moiety.

Examining how the boronic acid moiety recognizes glucose in solution studies by ATR – FTIR, reinforced the binding ability. The results obtained through impedance spectroscopy showed that the addition of glucose generated a change in the absolute impedance. Furthermore, subjecting glucose concentrations to another SAM terminated with –OH suggests that the change in impedance must be due to the binding process that occurs with boronic acid and glucose. Subjecting ANOVA to the impedance data showed that the variation observed was real and caused by factors that could be determined. As a result, the studies suggest that further investigations were needed in determining the factor(s) of why variation occurs from cell to cell.

## 4.5 References

- (1) Bain, C.; Whitesides, G. *Angew. Chem. Int. Ed. Engl.* **1989**, *28*, 5897.
- (2) Chidsey, C.; Loiacono, D. *Langmuir* **1990**, *6*, 682.
- (3) Finklea, H., Ed. *Self-assembled monolayers on electrodes*; John Wiley & Sons Ltd., 1997.
- (4) Springsteen, G.; Ballard, E.; Gao, S.; Wang, W.; Wang, B. *Bioorg. Chem.* **2001**, *29*, 259.
- (5) Springsteen, G.; Wang, B. *Tetrahedron* **2002**, *58*, 5291.
- (6) Yang, W.; Gao, X.; Wang, B. *Med. Res. Rev.* **2003**, *23*, 346.
- (7) Tony James: *C&E News* **2000**, 79.
- (8) Adhikiri, D.; Heagy, M. *Tetrahedron Lett.* **1999**, *40*, 7893.
- (9) Arimori, S.; Ushiroda, S.; Peter, L.; Jenkins, A.; James, T. *Chem. Commun.* **2002**, 2368.
- (10) Arimori, S.; James, T. *Tetrahedron Lett.* **2002**, *43*, 507.
- (11) DiCesare, N.; Lakowicz, J. *J. Phys. Chem.* **2001**, *105*, 6834-6840.
- (12) DiCesare, N.; Lakowicz, J. *Anal. Biochem.* **2001**, *294*, 154-160.
- (13) DiCesare, N.; Lakowicz, J. *Org. Lett.* **2001**, *3*, 3891.
- (14) DiCesare, N.; Lakowicz, J. *Tetrahedron Lett.* **2001**, *42*, 9105.
- (15) DiCesare, N.; Lakowicz, J. *J. Phys. Chem. A* **2001**, *105*, 6834.
- (16) DiCesare, N.; Pinto, M.; Schanze, K.; Lakowicz, J. *Langmuir* **2002**, *18*, 7785.
- (17) Gabai, R.; Sallacan, N.; Chegel, V.; Bourenko, T.; Katz, E.; Willner, I. *J. Phys. Chem. B* **2001**, *105*, 8196.
- (18) Kanayama, N.; Kitano, H. *Langmuir* **2000**, *16*, 577.
- (19) Karnati, V.; Gao, X.; Gao, S.; Yang, W.; Ni, W.; Sankar, S.; Wang, B. *Bioorg. Med. Chem. Lett.* **2002**, *12*, 3373.
- (20) Kitano, H.; Morokoshi, S.; Ohhori, K.; Gemmei-Ide, M.; Yokoyama, Y.; Ohno, K. *J. Colloid Interface Sci.* **2004**, *273*, 106.
- (21) Koh: Lee, M.; Hur, Y.; Kim, T. *Microchem. J.* **2002**, *72*, 315-321.
- (22) Murakami, H.; Akiyoshi, H.; Wakamata, T.; Nakashima, N. *Chem. Lett.* **2000**, 940.
- (23) Pavey, K.; Olliff, C.; Baker, J.; Paul, F. *Chem. Commun.* **1999**, 2223.
- (24) Bain, C.; Whiteside, G. *Langmuir* **1989**, *5*, 1370.
- (25) Brewer, S.; Allen, A.; Lappi, S.; Chasse, T.; Breggman, K.; Gorman, C.; Franzen, S. *Langmuir* **2004**, *20*, 5512.
- (26) Macdonald, J. *Impedance Spectroscopy*, 1987.
- (27) Bowden, E.; Nahir, T. *J. Electroanal. Chem.* **1196**, 410, 9.
- (28) Han, S.; Seo, H.; Chung, Y.; Kim, K. *Langmuir* **2000**, *16*, 9493.
- (29) Lee, M.; Kim, T.; Kim, K.; Kim, J.; Choi, M.; Choi, H.; Koh, K. *Anal. Biochem.* **2002**, *310*, 163.
- (30) Shen, H.; Mark, J.; Seliskar, C.; Mark, H.; Heineman, W. *J. Solid State Electrochem* **1997**, *1*, 148-154.
- (31) Sinniah, K.; Cheng, J.; Terrettaz, S.; Robey, J.; Miller, C. *J. Phys. Chem.* **1995**, *99*, 14500.
- (32) Anal. Calcd. for C<sub>17</sub>H<sub>28</sub>O<sub>3</sub>NSB: C, 60.54; H, 8.37. Found : C, 60.86; H, 9.11.

# CHAPTER 5: THE INFLUENCE OF INSERTING ELECTROACTIVE MOLECULES INTO THE PBA – SAMS

## 5.1 Introduction

---

The previous chapter relies on electrochemical impedance spectroscopy to determine the binding interactions between a PBA – SAM and glucose. Even though the interactions showed noticeable responses as glucose was added, the cause of variation from cell to cell is a concern. Implementing another thiol component to a surface has been widely studied in the field of self – assembly chemistry as mixed monolayers.<sup>20</sup> One reason for this introduction is the immobilization of biological materials onto surfaces that sequentially geared to the preparation of chemical sensors.<sup>20,22,24</sup> Another example deals with the reduction of disorder on SAMs by immobilizing nonelectroactive molecules and electroactive molecules that adjusts the selectivity of the electrode surfaces.<sup>20,22,24</sup> This new approach uses mixed SAMs to fabricate a biosensor capable of detecting glucose. Phenylboronic acid terminated thiols were molecules that demonstrated nonelectroactive characteristics. On the other hand, the adjunction of ferrocene terminated thiols demonstrated electroactive characteristics. Electroactive characteristics consist of a charge – transfer reaction that can occur at an electrode – surface interface.<sup>51,56,63,64</sup> This reaction causes a reduction and an oxidation (redox) to transpire which causes electrons to transfer among electrodes.<sup>51,56,63,64</sup> Cyclic voltammetry and other electrochemical techniques are preferred in the investigation of molecules attached to surfaces that possess electroactive properties.<sup>83</sup> However, there has not been an extensive study where

ferrocene moieties and boronic acid moieties are used in the attempts to develop electrochemical sensors for saccharides. One study by Shinkai et al. reported the properties of a chiral ferroceneboronic acid.<sup>84</sup> The compound was found to have little or no interaction with *D* – glucose, but strong interactions with another sugar based molecule. Norrild et al. showed that sensors based on boronic acid – appended ferrocenes interacts with glucose due to intramolecular B – N bonds.<sup>85</sup> These studies attempt to take those ideas further by constructing mixed SAMs of boronic acid and ferrocene moieties on gold surfaces.

Efforts in this investigation by inserting an electroactive molecule into a nonelectroactive SAM will be studied in terms of improving the conditions of reproducibility and sensitivity.<sup>54,86,87</sup> In this new approach, there are two distinct components of interest; the molecular recognition portion and the electroactive portion. As the bioactive material recognizes the analyte of interest, the electron transfer between the electroactive molecules and the gold electrode will be altered. Mixed self – assembled monolayers involving ferrocene moieties have been widely investigated, in which most studies deal with the use of cyclic voltammetry (CV) to examine the how the electron transfer is affected at the interface of the SAM.<sup>52,58,86-94</sup> For example, Rowe and Creager studied the electron transfer of mixed SAMs having ferrocenehexathiol and alkanethiols of varying lengths. They noted that the longer the alkane chain was, the slower the electron transfer became causing unusual behavior in the electrochemistry.<sup>90</sup> Chidsey and co – workers reported how the relative concentrations of the mixed SAM (ferrocene – terminated thiols and unsubstituted alkanethiols) played a role in the interfacial electron transfer.<sup>52,87</sup> They concluded that the defect sites were reduced as the mole ratio of

ferrocene decreased in the mixture creating better path for the electron transfer.

Reinhoudt, Veggel and Auletta reported mixed SAMs containing ferrocene – terminated thiols and hydroxyl – terminated thiols (OH – SH) where the rate of electron transfer is related to the different moieties on the surfaces.<sup>86</sup> Their findings were similar of those for mixed SAMs containing alkanethiols.

The introduction of ferrocene widens the studies that involve monitoring the difference in the electrochemical responses as a function of glucose binding with the surface bound PBA through means of impedance spectroscopy as well as CV. This chapter outlines another approach to detect glucose interaction with the boronic acid moiety by observing the changes in electrochemical activities of the co-component, ferrocene. Preliminary results first evaluate the surface IR and CV studies on the mixed SAM. Next, to observe more explicit effects on the interfacial capacities, electrochemical impedance spectroscopy was applied. At this time of investigation, it was brought to our attention that increasing the pH of the system can cause an increase in the chance for binding to occur. Literature has stated the ability to enhance signal, as well as, binding between boronic acid and glucose at pH levels higher than the pKa of boronic acid (pKa  $\approx$  8.8).<sup>27,28,71,85,95,96</sup> Finally, the impedance was analyzed by ANOVA to show agreements with findings.

## **5.2 Experimental Section**

### **5.2.1. Materials and substrates**

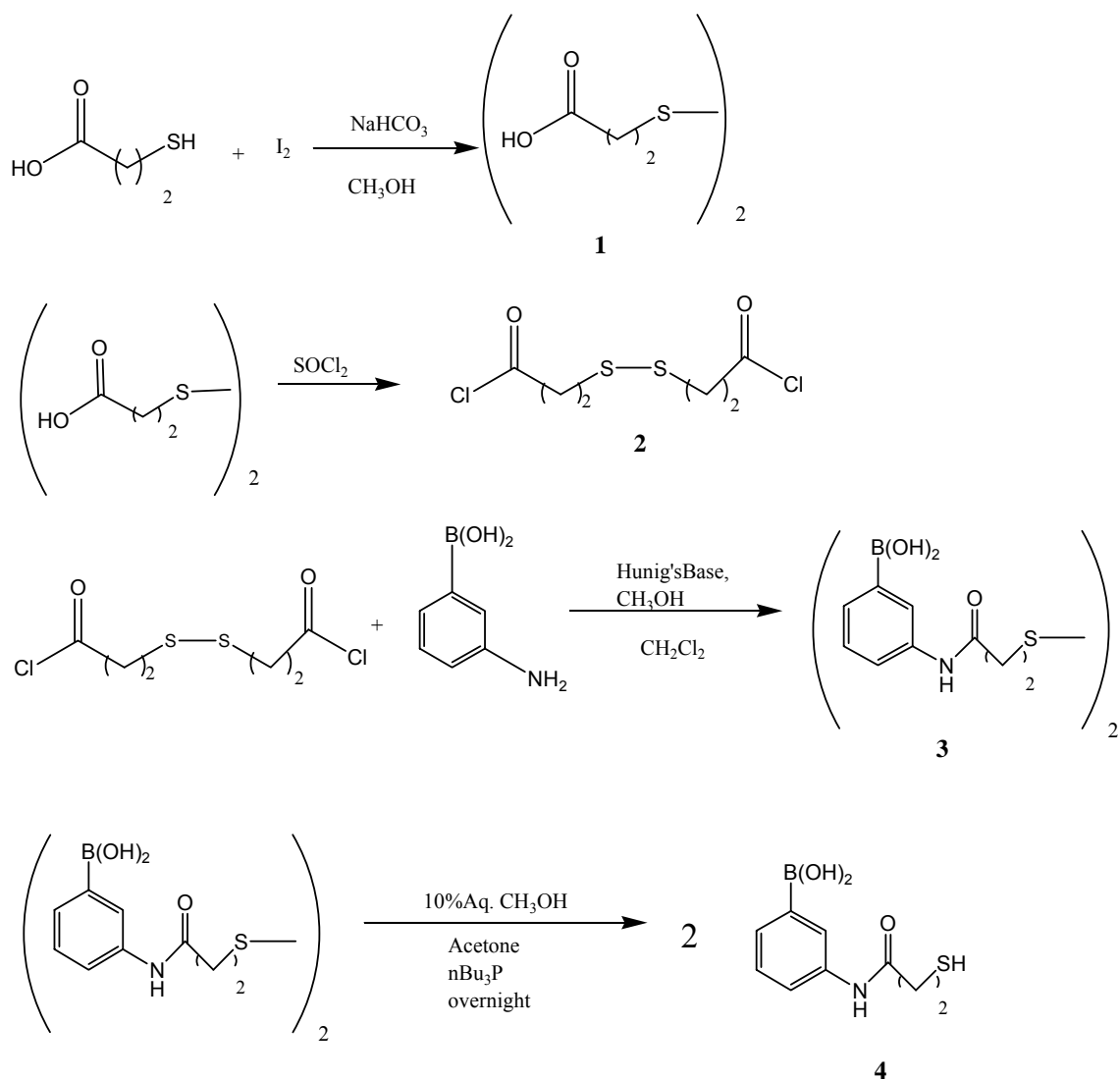
The synthesis of N-(3-dihydroxyborylphenyl)-11-mercaptoundecanamide (PBA<sub>11</sub>), can be found in 4.2.2. The synthesis of ferrocenylundecanethiol (Fc<sub>11</sub>) and ferrocenylhexanethiol (Fc<sub>6</sub>) of these experiments were synthesized by other members in

the group. All chemicals and reagents for the synthesis of N-(3-dihydroxyborylphenyl)-3-mercaptopropionicamide (PBA<sub>3</sub>) were commercially available and purchased from Acros Organics or Sigma – Aldrich. Glucose and other sugars (all *D* – chirality) were also purchased from Sigma-Aldrich. Milli-Q grade water (18 MΩ·cm) was used for preparation of solutions and monolayers. Absolute ethanol (200 proof) was also used for the preparation of the monolayer formation and solutions.

### 5.2.2. Synthesis of N-(3-dihydroxyborylphenyl)-3-mercaptopropionamide

PBA<sub>3</sub>

The synthesis of N-(3-dihydroxyborylphenyl)-3-mercaptopropionicamide (abbreviated PBA<sub>3</sub>) is shown in Scheme 5.1. 3-mercaptopropionic acid (2g, 18.8mmol) was added to a suspension of methanol (5ml), sodium bicarbonate (4.75 g, 56.5mmol) and molecular iodine (2.63g, 10.4mmol) to yield disulfide **1** which precipitated from solution and was used without further purification. This molecule (1g, 4.8mmol) was converted to the bis-acid disulfide **2** by refluxing for 30 minutes in thionyl chloride (11.32g, 95.1mmol). The excess thionyl chloride was removed by distillation. Subsequently, a substitution reaction was performed to give the bis-amide disulfide **3** where the white precipitate of **2** (0.65g, 2.6mmol) was added to a mixture containing 3-aminophenylboronic acid hemisulfate (0.98g, 5.3mmol) and Hunig's base (3mL). Separation of **3** (0.58g, 1.3mmol) with tributylphosphine (1.1mL) yielded the final product **4**. The identity and purity of the final product was confirmed by: <sup>1</sup>H NMR [( 400 MHz, CD<sub>3</sub>OD, δ) 1.33 (s, 12H), 1.67 (m, 4H), 2.36 (t, 2H, J = 7.3 Hz), 2.66 (t, 2H, J = 7.2 Hz), 7.30 (m, 1H), 7.48 (m, 1H), 7.61 (m, 1H), 7.78 (m, 1H)], and elemental analysis.



**Scheme 5.1:** Synthesis of N-(3-dihydroxyborylphenyl)-3-mercaptopropionamide (abbreviated PBA<sub>3</sub>)

### 5.2.3. Pretreatment of gold substrates and formation of SAM

Evaporated gold substrates (with Ti adhesion layer) were purchased from Evaporated Metal Films, Inc. All gold substrates used to prepare the monolayers were first cleaned in a piranha solution (3:1 ratio of concentrated H<sub>2</sub>SO<sub>4</sub> and 30% H<sub>2</sub>O<sub>2</sub>) for approximately 30 seconds (CAUTION: piranha solution reacts violently with organic chemicals), immediately rinsed with 18 MΩ·cm deionized water and dried under N<sub>2</sub> gas.

The monolayers were then rinsed with ethanol and water, and then dried under N<sub>2</sub> gas prior to further pretreatment of the surface.

#### **5.2.4. Electrochemical measurements**

Impedance spectroscopy experiments were done on a BAS – Zahner IM6e impedance system, in which the same type of electrochemical cell and electrodes as above were used. The cell was enclosed in the Faraday cage, whereupon any outside electrical noise is reduced. Impedance measurements were performed at a bias potential of 300 mV (an arbitrary value) and then at a bias potential equal to the formal potential of the redox for ferrocene, in the frequency range from 400 mHz to 4 Hz (or 100 mHz to 100 kHz), using an alternating voltage, 5 mV. The data were analyzed using the Origin Pro software.

In addition, the use of analysis of variance (ANOVA) provided a statistical based technique capable of producing meaningful factors studied in this work. A two – way ANOVA analysis using Excel was selected to investigate factors that effect reproducibility of cells and response to different glucose concentration. ANOVA was performed on impedance data after measurements were taken on cells after the addition of glucose concentrations. The aim was to determine if the nature of the variations was due to random error or not. In ANOVA, the F – ratio is the statistic used to test the hypothesis that the variation observed is real. In other words, if the variance factor (F) is smaller than the variance limit ( $F_{crit}$ ), then the variation is due to random error. However, if F is larger than  $F_{crit}$ , then the variation is not due to random error and the effects are real.

## 5.3 Results and Discussion

Clean gold surfaces were subjected to a mixed solution of (1 mM each) a ferrocene and a boronic acid moiety, resulting chemisorbed monolayers. Characterization by cyclic voltammetry and infrared reflection – absorption spectroscopy (IRRAS) established the formation of these monolayers.

### 5.3.1. Characterization of Fc<sub>11</sub> and PBA<sub>11</sub> coadsorbed on gold surface<sup>79,97</sup>

#### 5.3.1a) Surface IR

After the Fc<sub>11</sub> and PBA<sub>11</sub> molecules were coadsorbed onto a gold surface, the resulting SAMs were studied by PM – IRRAS. This study was performed in order to get an idea on the presence of the components formed on the electrode. Infrared spectra of ferrocene-based molecules have been thoroughly examined. However, mode assignments have not been well examined into for mixed monolayers containing ferrocene. Figure 5.1 shows the stretching modes observed in two regions: 950 – 1800 cm<sup>-1</sup> region (5.1A) and 2750 – 3400 cm<sup>-1</sup> region (5.1.B), respectively. The strong absorption peaks at 2856 cm<sup>-1</sup> and 2927 cm<sup>-1</sup> observed in Figure 1B are consistent with the methylene symmetric and asymmetric stretching modes comparable with single monolayer formation. The modes suggest that the monolayer formation is well – ordered. In addition, the broad mode around 3263 cm<sup>-1</sup> corresponds to the O –H stretching modes of the B(OH)<sub>2</sub> moiety of PBA. Noticeable bands in this low region are associated with the stretching modes of the ferrocene rings and phenylboronic acids are observable in Figure 1A. Peaks in the region of 950 – 1100 cm<sup>-1</sup> can be assigned to the stretching modes of the asymmetric cyclopentadiene ring of the ferrocene, however, there can be uncertainty when looking in this lower region due the existence of multiple vibrational frequencies associated with bending and/or scissoring modes. Peak modes in the region of 1200 – 1800 cm<sup>-1</sup> consist

of bands at  $1280\text{ cm}^{-1}$ ,  $1396\text{ cm}^{-1}$ , and  $1466\text{ cm}^{-1}$ . The mode at  $1280\text{ cm}^{-1}$  is the ester on the ferrocene. Modes at  $1396\text{ cm}^{-1}$  and  $1420\text{ cm}^{-1}$  are related to the stretching modes of the ferrocene ring, along with the addition of the B – O stretching mode around  $1340\text{ cm}^{-1}$ .

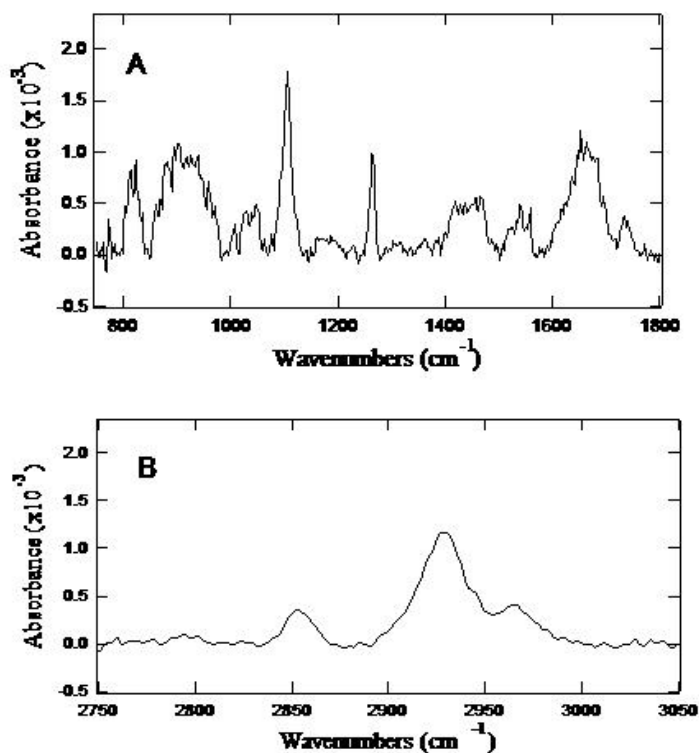


**Figure 5.1: PM – IRRAS spectra of a mixed SAM, having a 50/50 feed ratio, on gold in the (A) low and (B) high wavenumber regions, respectively.**

In addition, there is an intense peak observed at  $1466\text{ cm}^{-1}$  for the C – C stretch corresponding to the cyclopentadiene of the ferrocene molecule, which may include the modes from boronic acid molecules observed at  $1430\text{ cm}^{-1}$ . The peak at  $1663\text{ cm}^{-1}$  signifies a combination of the N – H bending mode. The peak at  $1733\text{ cm}^{-1}$  apparently represents the carbonyl (C = O) stretching mode. The peak intensities and modes suggest formation of a mixed monolayer on the gold surface.

### 5.3.1b) Electrochemical studies

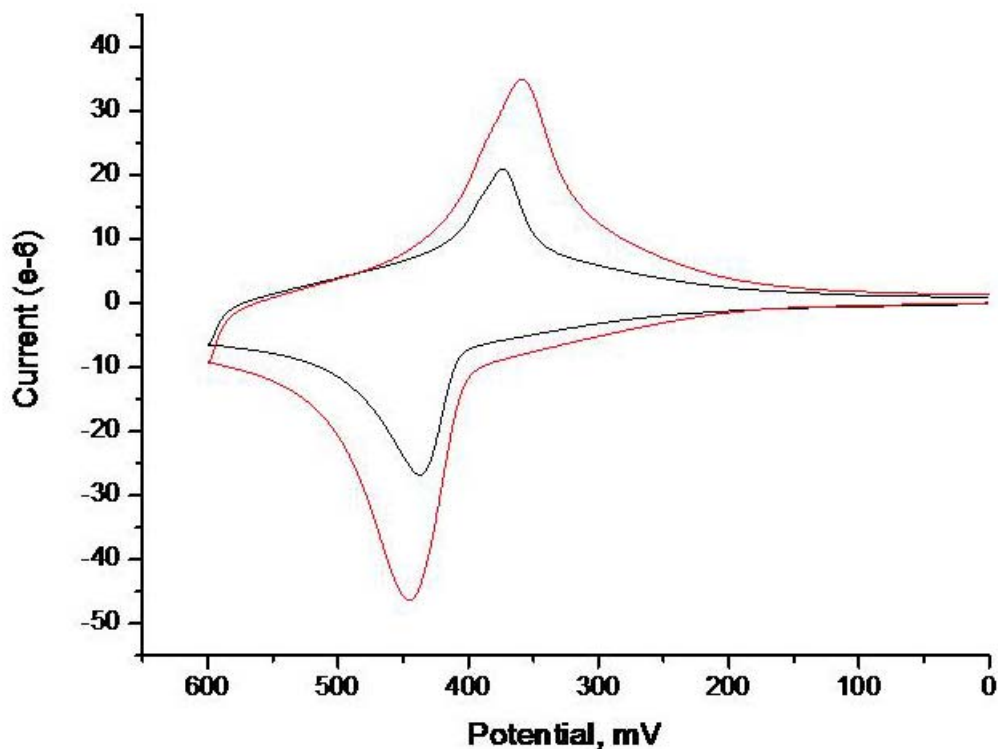


**Figure 5.2:** An overlay of cyclic voltammograms of (red) ferrocenylthiolate on gold and (black) a 50/50 feed ratio of a mixed SAM [PBA<sub>11</sub> and Fc<sub>11</sub>]; experiment done in 0.1 M NaClO<sub>4</sub> (pH 11 w/ 10 mM NaOH) at a scan rate of 100 mV/s and at room temperature.

Cyclic voltammetry was used to characterize the formation of the mixed monolayer since it allows for the determination of the quantity of electroactive species in surface – confined monolayers. Figure 5.2 shows representative cyclic voltammograms in aqueous 0.1 M NaClO<sub>4</sub> (plus 10 mM NaOH to increase the pH level to 11) of SAMs prepared from 1 mM solution of ferroceneundecanethiol in ethanol and from a mixed 1 mM solution of Fc<sub>11</sub> and PBA<sub>11</sub> in ethanol. In all the experiments, the potential applied was cycled between 0 and 600 mV. The SAMs resulting from the adsorption was characterized with respect to peak positions and surface coverage. The voltammograms features in Figure 5.2 are comparable to those of other ferrocene – derivatived SAMs in

the literature. Conversely, the peak splitting is further apart than most literature indicating nonideal behavior such as slow kinetics. On the other hand, the redox peak position agrees with several ferrocene derivatives where the peak positions were between + 400 and + 200 mV (vs SCE). Therefore, the redox peaks observed in the present work are due to the redox reaction of ferrocene that is immobilized on the gold electrode. The amount of ferrocene incorporated onto the mixed SAM can be determined by the feed ratios of each component. An ideal mixed monolayer should show a 50/50 feed ratio which shows that both the components having relative interactions of adsorbates with the gold. The surface coverage,  $\Gamma$ , was estimated for each voltammogram using equation 1:

$$\Gamma = Q/ nFA \quad (1)$$

where, the values of Q were obtained by integrating the area underneath the cathodic wave, n is the number of electrons transferred per redox event, F is the Faraday's constant, and A is the area of the working electrode.<sup>42</sup> The current associated with the reduction of each formation yielded surface coverage of  $5.78 \times 10^{-10}$  and  $2.68 \times 10^{-10}$  mol/cm<sup>2</sup> for Fc<sub>11</sub> and Fc<sub>11</sub>/PBA<sub>11</sub>, respectively. Full coverage of a ferrocene monolayer predicted in the literature is  $4.5 \times 10^{-10}$  mol/cm<sup>2</sup>, wherein the ferrocene group is treated to a sphere with a diameter of 0.66 nm.<sup>54,86,87,92</sup> Even though the experimental coverage value for Figure 5.2(red) was higher than expected, it was agreeable with what Chidsey and co – workers reported their maximum surface coverage to be for a ferrocene monolayer with a longer alkyl chain ( $5.8 \times 10^{-10}$  mol/cm<sup>2</sup>).<sup>88</sup> As a result, the coverage calculated can be used in comparing with the coverage of mixed monolayers. In the case of the mixed monolayer, the coverage value indicates that the choice of using a 50/50

feed ratio for other studies to be a reasonable one due coverage being near half of that for the Fc – SAM.

### **5.3.2. Performance of the mixed SAM**

The idea of inserting electroactive molecules into the system was to create a SAM that would be more responsive to a binding event . Specifically, the goal was to generate a more sensitive sensor in which the exchange of electrons between the ferrocene and surface would be altered as binding occurs between boronic acid and glucose. Until now, the electrochemical study of self – assembled monolayer containing just PBA was measured in 0.1 M HClO<sub>4</sub> aqueous solution as seen in previous chapter.

During this study, literature reported findings to improve the binding ability between boronic acid and glucose by working at pH levels higher than the expected pKa (reported ~8). Lorand and Edwards investigated the structure of a phenylboronic acid group in its neutral and anionic forms.<sup>25</sup> Their results showed that the stability of the boronate ester was pH – dependent in which there was increased in the emission intensity observed for the formation of the anionic form of the boronic acid group.

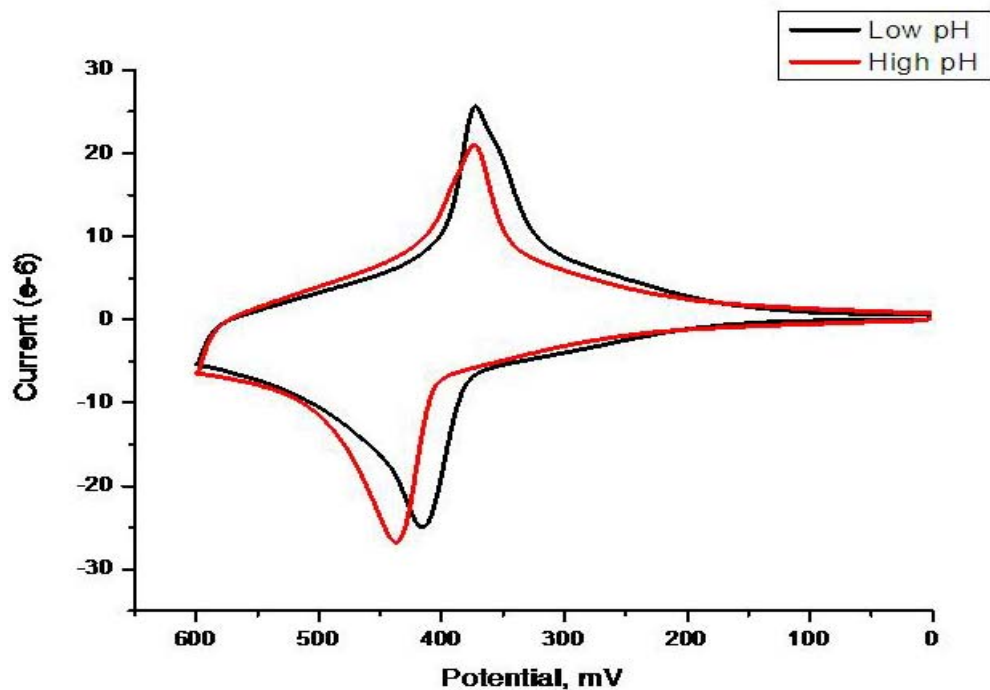


**Figure 5.3: Comparisons of cyclic voltammograms in high pH (red) and low pH (black) electrolyte solutions for Fc<sub>11</sub>/PBA<sub>11</sub> SAMs. Experiments done at scan rate of 100 mV/s and at room temperature. (Data for graphs were taken at different times)**

Other laboratories have observed the effect of binding on a co-adsorbed electroactive molecule and have indicated its use in developing sensors.<sup>27,85,95,98</sup> Beulen, Veggel, and Reinhoudt reported that a mixed carboxylic acid-ferrocene self-assembled monolayer on gold has a pH-dependent electrochemical response through space communication between the carboxylate ‘receptor’ and ferrocene readout unit.<sup>99</sup> The electrochemical behavior of the substrate changed as the pH of the electrolyte solution varied, providing a way to detect nonelectroactive species. Figure 5.3 illustrates the electrochemical response observed for 50/50 mixed monolayers influenced by high and low pH of the electrolyte solution, (0.1 M NaClO<sub>4</sub> plus 10mM NaOH and 0.1 M HClO<sub>4</sub>, respectively). It is known that the pKa for surface bound molecules increase by 3 to 4 compared to molecules in solution.<sup>100</sup> Therefore, the pH 11 was selected for usage in this work by adjusting 0.1 M NaClO<sub>4</sub> with 10 mM NaOH. Results show that as the pH

increased, the deprotonation of the acid creates negative charges, in turn stabilizing the ferrocenium ions and causing a shift of the redox peak positions in cathodic shift. The electrochemical response shows a slight shift occurring. This slight shift indicates that the deprotonation of the acid presence is influenced by the ferrocene moiety; however, overall the ferrocene in the mixed monolayer was pH – independent. Thus, the remaining works will all be done in pH 11 electrolyte.

#### **5.3.4. Binding abilities of boronic acid after incorporating ferrocene – terminated thiol**

Infrared spectroscopic and cyclic voltammogram data indicated the formation of a mixed monolayer. Cyclic voltammograms also illustrated ferrocene – terminated thiolate shifting cathodically as the pH was increased from low to high. Before investigating the binding abilities with the mixed SAM, an experiment was done to determine if there was any binding capabilities between ferrocene and glucose.

Ideally, there should be no binding interactions between the incorporated ferrocene and glucose. Figure 5.4 shows an overlay of an Fc – SAM with and without glucose. Ferrocene monolayers were subjected to the presence of *D* – glucose in solution. There are no specific behavior changes in the voltammogram as different glucose concentration was added; which indicates that there are no interactions happening between ferrocene and glucose.

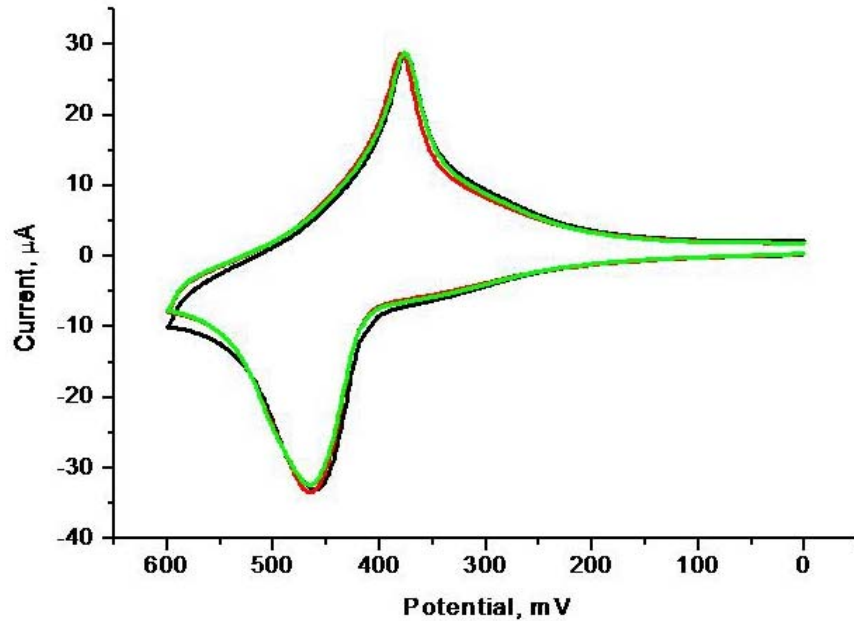


Figure 5.4: Overlays of Fc – SAM cyclic voltammograms at different glucose concentrations: 0 mM (black), 5 mM (red) and 20 mM (green); scan rates at 100 mV/s

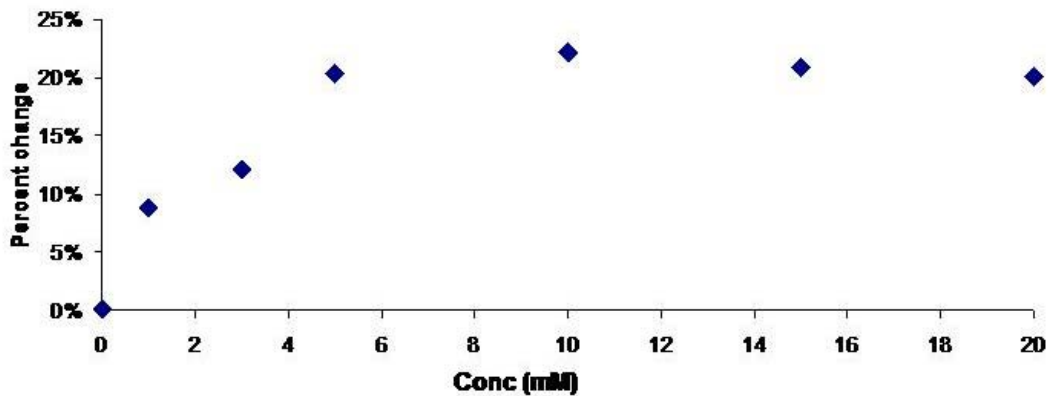


Figure 5.5: Graph of the percent change in the impedance data obtained in 0.1 NaClO<sub>4</sub> (pH 11, adjusted with 10 mM NaOH); observed at 1.5 Hz

Unlike the others, impedance measurements can provide valuable information about how the ferrocene influences the capacitance. Figure 5.5 illustrates the percent change in the impedance data of an Fc<sub>11</sub>/PBA<sub>11</sub> – SAM observed at 1.5 Hz. The percent change gives a more insight on how the impedance is affected by the addition of glucose. The graph displays an increase of change until the system reaches 10 mM glucose where

the change becomes steady. Apparently, the cell has reached its limits due to saturation of the surface.

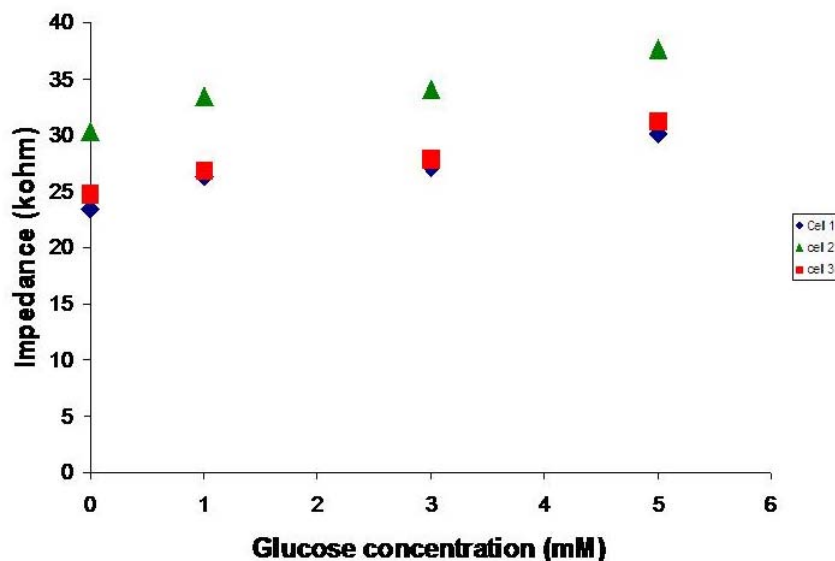


Figure 5.6: Plots that represent the reproducibility of  $\text{Fc}_{11}/\text{PBA}_{11}$  – SAMs; experiments done in pH 11 solution at an amplitude of 5 mV and at room temperature.

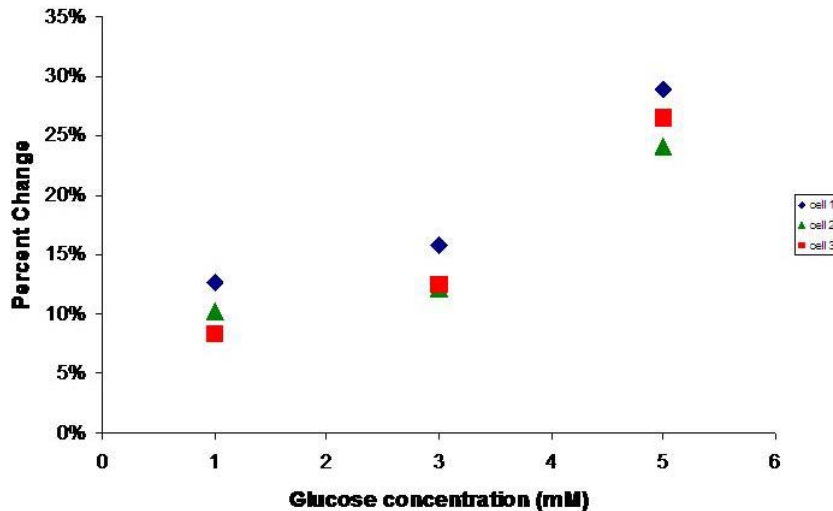


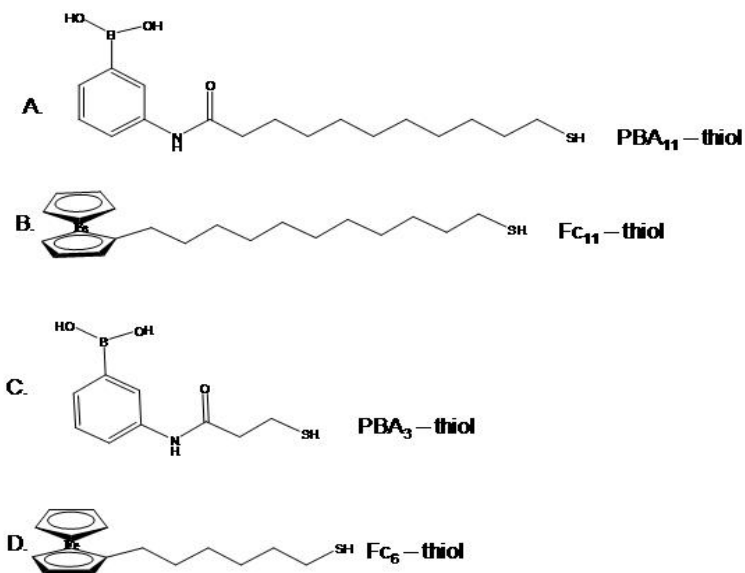
Figure 5.7: A graph representing the cells from Figure 5.5 (with respect to colors) of the impedance changes in the presence of glucose .

Figure 5.6 shows a two – component mixed monolayer observed at a frequency that has impedance values increasing in the presence of glucose. The variation from cell to cell seems to have reduced compared to the values on just the PBA – SAM alone.

Figure 5.7 shows the percent changes of the impedance values in the presence of glucose. Although, the variation has been reduced among cells, there is now variation observed in how each cell changes with the addition of glucose. This variation probably is due to organization of monolayers on the gold surfaces.

### 5.3.5. Optimizing parameters in order to produce a more proficient biosensor

In order to optimize the use of mixed monolayers, there were several options that could be explored. One obvious option was to shorten the methylene chain length so that distance between the electrodes (working and reference). Another option was to vary the methylene chain lengths.



**Scheme 5.2: Molecules used in the formation of mixed monolayers in order to optimize the organization of the SAM.**

Understanding how mixed monolayers having electroactive and nonelectroactive components of different alkyl chain lengths affect the electrochemical properties of the SAM have been investigated extensively. Scheme 5.2 shows the selected carbon chain lengths of both the ferrocene and phenylboronic acid that will be used to form mixed

monolayers. The mixed monolayers (Fc<sub>6</sub>/PBA<sub>11</sub> and Fc<sub>6</sub>/PBA<sub>3</sub>) will also be prepared as a 50: 50 feed ratio.

*5.3.5a) Effects of electrochemical properties by CV*

Investigating the effects of decreasing the methylene chain length of the ferrocene, while maintaining the same methylene chain length for boronic acid was studied through cyclic voltammetry.

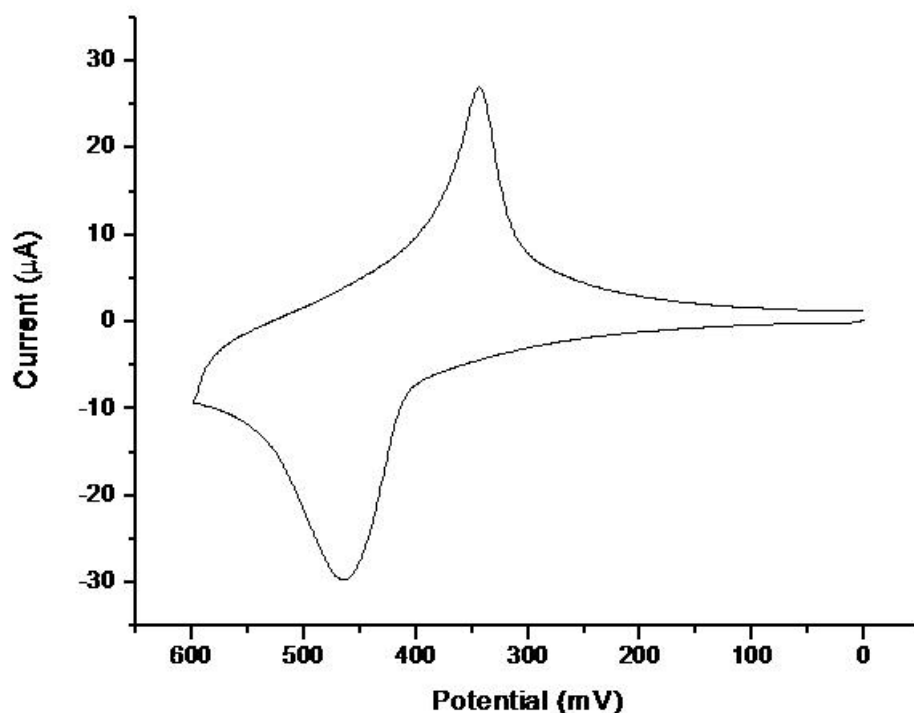


**Figure 5.8: Cyclic voltammogram of a Fc<sub>6</sub>/PBA<sub>11</sub> - SAM on a gold surface in pH 11 solution; scan rate of 100 mV/s at room temperature.**

Figure 5.8 shows a cyclic voltammogram of Fc<sub>6</sub>/PBA<sub>11</sub> – SAM on gold in 0.1 M NaClO<sub>4</sub> of pH 11 (adjusted with NaOH). The peak positions agree with reported values found in literature. The formations of peaks are agreeable accordingly to literature. The coverage of ferrocene adsorbed onto the gold surface was calculated to be  $2.10 \times 10^{-10}$ , which was not much smaller than the coverage for the ferrocenylhexanethiolates adsorbed onto the surface ( $2.64 \times 10^{-10}$ ). These findings contradict literature for mixed monolayers where the component with the longer alkyl chain usually attaches the surface faster. In this case, the

size of the terminal group may play a role in how the thiolates are organized on the surface.

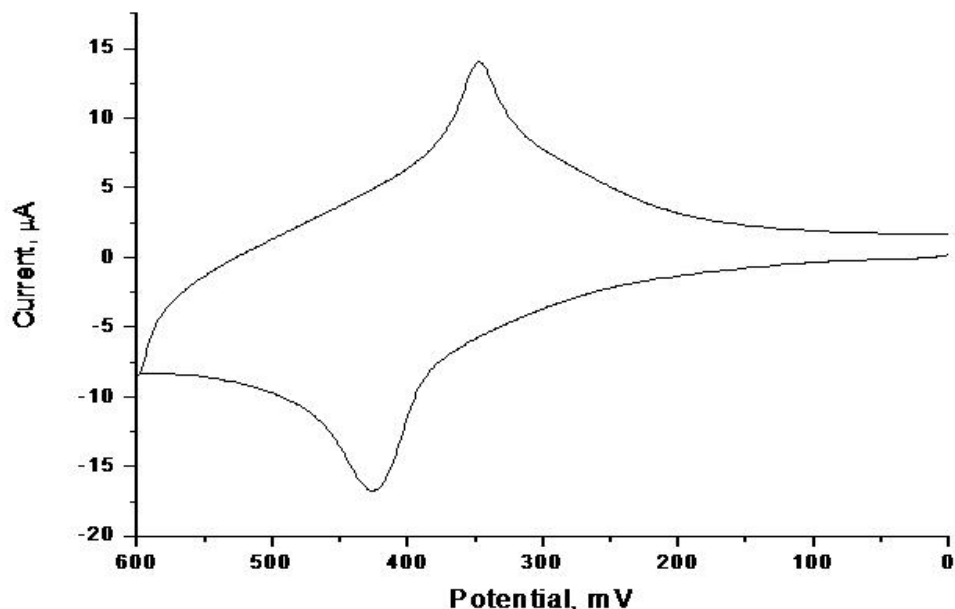


**Figure 5.9: Cyclic voltammogram of a  $\text{Fc}_6/\text{PBA}_3$  - SAM on a gold surface in pH 11 solution; scan rate of 100 mV/s at room temperature.**

To increase coverage of boronic acid on the SAM, the length of the alkyl chains were switched. Figure 5.9 shows a voltammogram of an  $\text{Fc}_6/\text{PBA}_3$  – SAM in a pH solution of 0.1 M  $\text{NaClO}_4$  (adjusted with  $\text{NaOH}$ ). The amount of ferrocene calculated for this SAM was  $1.42 \times 10^{-10}$  mol/cm<sup>2</sup>. Not only are the redox peaks observable, the coverage is almost half that of an  $\text{Fc}_6$  – SAM.

The inconsistency of ferrocene coverage in the formation of these two mixed monolayers made it difficult to reproduce SAMs that showed redox peaks in the voltammograms.

#### *5.3.5b) Effects of electrochemical properties by EIS*

The influence on impedance when the carbon chain lengths were altered should give more insight into the function of the faradaic portion in the mixed monolayers. The idea was to decrease the alkyl chain of the ferrocene as well as to increase it, in order to determine the distinction within the electron transfer that occur through the ferrocene when binding happens between the boronic acid and glucose. Bode plots were generated from the Thales software.

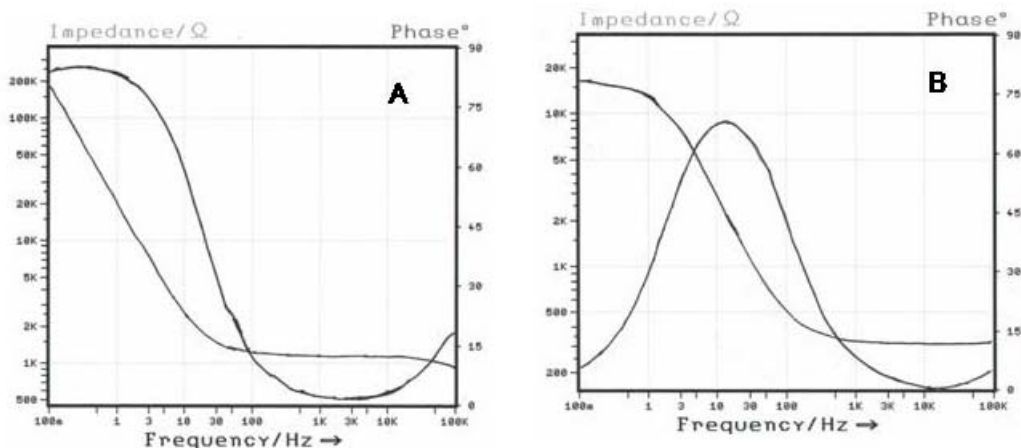


**Figure 5.10: Bode plots of both mixed monolayers: (A) Fc<sub>6</sub>/PBA<sub>11</sub> – SAM and (B) Fc<sub>6</sub>/PBA<sub>3</sub> – SAM.**

The Bode plots for the two other proposed systems are presented in Figure 5.9. A difference to point out in the two is the shape of the phase angles. Observing data at 1Hz, the degree in the phase angles has lowered dramatically in both the Fc<sub>6</sub>/PBA<sub>11</sub> (Figure 5.10A) and Fc<sub>6</sub>/PBA<sub>3</sub> (Figure 5.10B) compared to the PBA – SAM in chapter 4. This suggests that the ordering has lessened within the formation of the mixed SAMs. Furthermore, the increase in the electrolyte pH can cause electrostatic repulsion due to the charges on the boron causing ion permeability becomes more accessible. Another observation is the difference in the shape of the impedance curve. The impedance shape in figure 5.10A is similar to that of the PBA –SAM; thus suggesting there PBA thiolates attached to the surface. However, in figure 5.10B, the impedance shape has a appearance of bare gold; thus suggesting that the surface is not well ordered or that the coverage of the absorbates is low. Further studies were investigated by implementing the impedance data observed at 1.47 Hz to percent change values.

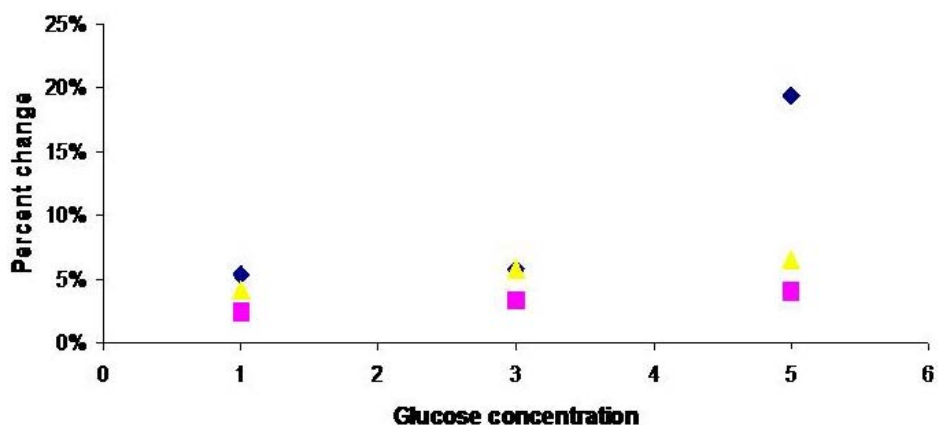


Figure 5.11: Impedance plots of representative data from  $\text{Fc}_6/\text{PBA}_{11}$  – SAMs at different glucose concentrations. Impedance measurements done at an amplitude of 5 mV and at room temperature. Plots were taken at 1.47 Hz.

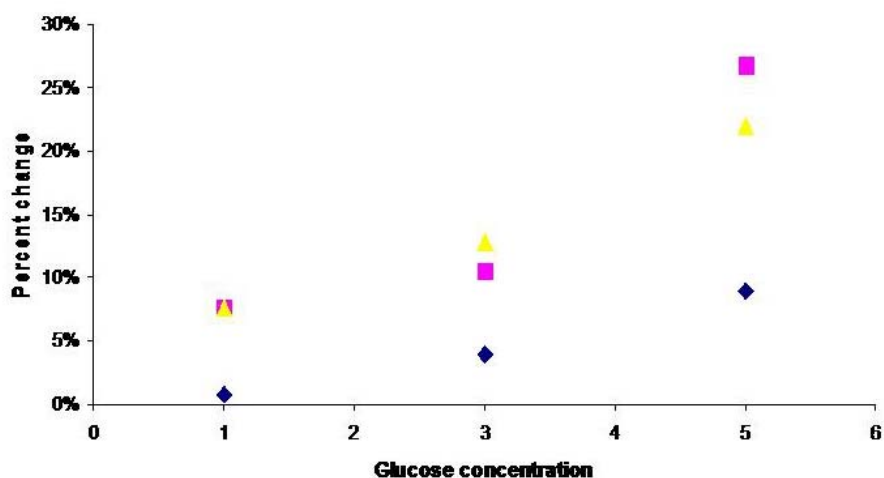
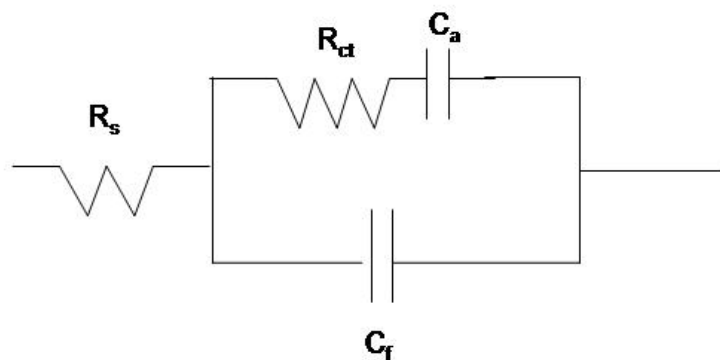


Figure 5.11: Impedance plots of representative data from  $\text{Fc}_6/\text{PBA}_3$  – SAMs at different glucose concentrations. Impedance measurements done at an amplitude of 5 mV and at room temperature. Plots were taken at 1.47 Hz.

Figures 5.11 and 5.12 illustrate the percentage change of representative data of cells as different glucose concentrations were added. The binding in interactions displays lower percent changes when an electroactive molecule (Fc) is co – absorbed with a nonelectroactive molecule (PBA). Furthermore, the changes show results opposite than expected since the original impedance data suggests less variation from cell to cell.



**Figure 5. 12: A proposed circuit model to investigate the physical characteristics of the mixed SAMs; which includes four components: uncompensated solution resistance,  $R_s$ , film capacitance,  $C_f$ , charge transfer resistance,  $R_{ct}$ , and pseudocapacitance,  $C_a$ .**

To develop an understanding of physical characteristics, such as resistance and capacitance, of the mixed monolayers, a circuit model was proposed. Figure 5.13 illustrates a circuit deem appropriate for modeling a monolayer having an electroactive molecule bound to a surface and having its electrochemical properties altered when binding with another molecule occur. Fits for the data were achieved by using the complex nonlinear least – squares (CNLS) method, a feature in Origin Pro 7 software. The results were inconclusive in this study due to the occurrence of large errors. Subsequently, the impedance data was subjected to the analysis of ANOVA.

Tables 5.1, 5.2 and 5.3 show two – way ANOVA analyses for the cells containing the three different mixed SAM compositions, again to determine if the variations in both concentration and cell were statistically significant. For the  $Fc_6/PBA_{11}$  – SAMs, the analysis showed that the response variation as glucose concentrations was varied was statistically less significant than random error. However, for the  $Fc_6/PBA_3$  – SAMs and the  $Fc_{11}/PBA_{11}$  – SAMs, the analysis showed the same result obtained for monocomponent  $PBA_{11}$  – SAMs shown in Table 4.2. Specifically, both glucose concentration and cell had a statistically significant effect on impedance. Again, the

effect of cell variation is unclear. However, the results suggest that impedance associated with these mixed SAMs is sensitive to glucose.

**Table 5.1: Two – way ANOVA results on impedance data on Fc<sub>11</sub>/PBA<sub>11</sub> - SAMs**

Source of Variation	SS	df	MS	F	F <sub>crit</sub>
Concentration	2.9E+07	2	1.4E+07	364	7
Cell	9.3E+07	2	4.6E+07	1157	7
Error	1.6E+05	4	4.1E+04		
Total	1.2E+08	8			

SS = Sum of Squares, df = degrees of freedom, MS = mean square, F= variance factor, F<sub>crit</sub> = variance limit

**Table 5.2: Two – way ANOVA results on impedance data on Fc<sub>6</sub>/PBA<sub>11</sub> – SAMs**

Source of Variation	SS	df	MS	F	F <sub>crit</sub>
Concentration	1.4E+08	3	4.6E+07	3	5
Cell	3.7E+09	2	1.8E+09	128	5
Error	8.7E+07	6	1.4E+07		
Total	3.9E+09	11			

SS = Sum of Squares, df = degrees of freedom, MS = mean square, F= variance factor, F<sub>crit</sub> = variance limit

**Table 5.3: Two – way ANOVA results on impedance data on Fc<sub>6</sub>/PBA<sub>3</sub> – SAMs**

Source of Variation	SS	df	MS	F	F <sub>crit</sub>
Concentration	2.4E+08	2	1.2E+08	682	5
Cell	1.4E+07	3	4.7E+06	27	5
Error	1.1E+06	6	1.8E+05		
Total	2.6E+08	11			

SS = Sum of Squares, df = degrees of freedom, MS = mean square, F= variance factor, F<sub>crit</sub> = variance limit

## 5.4 Conclusion

Mixed self – assembled monolayers composed of ferrocene and boronic acid derivative thiolates were prepared and characterized on gold electrodes. The PM – IRRAS experiment provided information on the composition, which indeed suggested that both molecules were present. Cyclic voltammetry confirmed the formation of ferrocene for all the proposed systems used for assembly. Impedance measurements

supplied insight on how the length of the ferrocenylalkane thiolate played a role in the sensitivity of the proposed sensor as glucose concentrations were added. Since the percent change showed distinct variations in the representative data, the frequency was extended from 100 mHz to 100 kHz in order to rule out any the possibilities of resistance playing a role. Nonetheless, the circuit did not furnish a better understanding into the resistance and capacitance of our system. The ANOVA method showed that there were distinct factors that contributed to the variation in responses in both areas: cell to cell and addition of different glucose concentrations; except the  $\text{Fc}_6/\text{PBA}_{11} - \text{SAM}$  showed that the responses as glucose was added to the cell were due to random error. Unfortunately, this concept of detecting glucose with the mixed SAMs studied appear to give non-ideal behaviors. For example, the voltammograms of the mixed monolayers exhibited inconsistent peak shapes which could be related to the amount of the absorbates on the surface. This behavior may have been due to surface roughness or/and to adsorption process. The nature of all the non-ideal behaviors observed has not been sorted out; thus, this leads to other alternatives. One alternative could be the investigation of employing other electroactive molecules to form mixed monolayers. Another alternative conveys the use of more surface techniques such as SPR. Overall, these preliminary findings suggest that EIS alone does not disclose enough information to fabricate a glucose biosensor.

## 5.5 References

- (1) Clark, L. *Biosens. Bioelectron.* **1993**, *8*, iii.
- (2) Cass, A.; Davis, G.; Francis, G.; Hill, H.; Aston, W.; Higgins, I.; Plotkin, E.; Scott, L.; Turner, A. *Anal. Chem.* **1984**, *56*, 667.
- (3) Hunter, I.; Jones, L.; Kanigan, T.; Brenan, C.; Sambol, L.; Sosnowski, L. In *MIT Home Automation and Healthcare Consortium*, 2000.
- (4) Mohanty, S. At URL: <http://citeseer.ist.psu.edu/mohanty01biosensor.html>
- (5) Ohara, T.; Rajagopalan, R.; Heller, A. *Anal. Chem.* **1994**, *65*, 2451-2457.
- (6) Reach, G.; al., e. *Anal. Chem.* **1996**, *68*, 3822-3826.
- (7) Rishpon, J.; Gottesfeld, S.; Campbell, C.; Davey, J.; Zawodzinski, T. *Electroanalysis* **1994**, *6*, 17.
- (8) Vo-Dinh, T.; Cullum, B. *Fresenius J. Anal. Chem.* **2000**, *366*, 540.
- (9) Wang, J. *Electroanalysis* **2001**, *13*, 983.
- (10) Wisniewski, N.; Moussy, F.; Reichert, W. *Fresenius J. Anal. Chem.* **2000**, *366*, 611-621.
- (11) Woedtko, T.; Julich, W.; Hartmann, V.; Stieber, M.; Abel, P. *Biosensors & Bioelectronics* **2002**, *17*, 373-382.
- (12) Badugu, R.; Lakowicz, J.; Geddes, C. *Anal. Chem.* **2004**, *76*, 610-618.
- (13) Claremont, D.; Penton, C.; Pickup, J. *J. Biomed. Eng.* **1986**, *8*, 272.
- (14) McDonald, W.; Kopeland, R. At URL: <http://www.ieee.org/organizations/pubs/newsletters/leos/apr98/invitro.htm>
- (15) Kobos, R. *Trends Anal. Chem.* **1987**, *6*, 6.
- (16) Clark, L.; Lyons, C. *Ann. NY Acad. Sci.* **1962**, *102*, 29.
- (17) Frew, J.; Hill, H. *Anal. Chem.* **1987**, *59*, 933A.
- (18) He, B. At URL: [www.glue.umd.edu](http://www.glue.umd.edu)
- (19) Rinken, T.; Tenno, T. *Biosens. Bioelectron.* **2001**, *16*, 53.
- (20) Murray, R.; Ewing, A.; Durst, R. *Anal. Chem.* **1987**, *59*, 379.
- (21) Tierney, M.; Kim, H.; Burns, M.; Tamada, J.; Potts, R. *Electroanalysis* **2000**, *12*, 666.
- (22) Wang, J. *Electroanalysis* **1991**, *3*, 255.
- (23) Vreeke, M. At URL: <http://www.devicelink.com>
- (24) Wink, T.; Zuilen, S.; Bult, A.; Benneken, W. *The Analyst* **1997**, *122*, 43R.
- (25) Lorand, J.; Edwards, J. *J. Am. Chem. Soc.* **1959**, *24*, 769.
- (26) Springsteen, G.; Ballard, E.; Gao, S.; Wang, W.; Wang, B. *Bioorg. Chem.* **2001**, *29*, 259.
- (27) Springsteen, G.; Wang, B. *Tetrahedron* **2002**, *58*, 5291.
- (28) Yang, W.; Gao, X.; Wang, B. *Med. Res. Rev.* **2003**, *23*, 346.
- (29) Adhikiri, D.; Heagy, M. *Tetrahedron Lett.* **1999**, *40*, 7893.
- (30) Arimori, S.; Ushiroda, S.; Peter, L.; Jenkins, A.; James, T. *Chem. Commun.* **2002**, 2368.
- (31) Carey, R.; Folkers, J.; Whitesides, G. *Langmuir* **1994**, *10*, 2228.
- (32) Czarnik, A. *J. Am. Chem. Soc.*, 117.
- (33) DiCesare, N.; Lakowicz, J. *Org. Lett.* **2001**, *3*, 3891.
- (34) Gabai, R.; Sallacan, N.; Chegel, V.; Bourenko, T.; Katz, E.; Willner, I. *J. Phys. Chem. B* **2001**, *105*, 8196.

- (35) Karnati, V.; Gao, X.; Gao, S.; Yang, W.; Ni, W.; Sankar, S.; Wang, B. *Bioorg. Med. Chem. Lett.* **2002**, *12*, 3373.
- (36) Murakami, H.; Akiyoshi, H.; Wakamata, T.; Nakashima, N. *Chem. Lett.* **2000**, 940.
- (37) Tong, A.; Yamauchi, A.; Hayashita, T.; Zhang, Z.; Smith, B.; Teramae, N. *Anal. Chem.* **2001**, *73*, 1530.
- (38) Kitano, H.; Morokoshi, S.; Ohhori, K.; Gemmei-Ide, M.; Yokoyama, Y.; Ohno, K. *J. Colloid Interface Sci.* **2004**, *273*, 106.
- (39) Kanayama, N.; Kitano, H. *Langmuir* **2000**, *16*, 577.
- (40) Sherwood, L. *Human Physiology: From cells to systems*; Second ed.; West Publishing Company, 1993.
- (41) Saudek, C.; Rubin, R.; Shump, C. *The John Hopkins guide to diabetes for today and tomorrow*; The John Hopkins University Press: Baltimore, 1997.
- (42) Kissinger, P.; Bott, A. *Current Separations* **2002**, *20*, 2.
- (43) Prevention, C. f. D. C. a. At URL: <http://www.diabetes.org> Accessed: 2003.
- (44) Gough, D.; Armour, J. *Diabetes* **1995**, *44*, 1005.
- (45) Heller, A. *Annu. Rev. Biomed. Eng.* **1999**, *1*, 153.
- (46) Technology, M. D. At URL: <http://www.fraserclan.com/biosen2.htm> Accessed: 2002.
- (47) Centre, C. B. At URL: <http://www.cranfield.ac.uk/biotech/sensors/events.htm> Accessed: 2004.
- (48) Tonnesen, C.; Withrow, G. At URL: <http://www.hitl.washington.edu/sciww/EVE/I.D.1.c.Biosensors.html> Accessed: 2002.
- (49) Kissinger, P.; Heineman, W. *Laboratory Techniques in Electroanalytical Chemistry*; 2nd ed.; Marcel Dekker, Inc, 1996.
- (50) Bain, C.; Whitesides, G. *Angew. Chem. Int. Ed. Engl.* **1989**, *28*, 5897.
- (51) Brett, O.; Brett *Electrochemistry*; Oxford University Press: New York, 1998.
- (52) Chidsey, C.; Loiacono, D. *Langmuir* **1990**, *6*, 682.
- (53) Finklea, H., Ed. *Self-assembled monolayers on electrodes*; John Wiley & Sons Ltd., 1997.
- (54) Bain, C.; Whitesides, G. *J. Am. Chem. Soc.* **1989**, *111*, 7164.
- (55) Schreiber, F. *Prog. Surf. Sci.* **2000**, *65*, 151.
- (56) Vassos, B.; Ewing, G. *Electroanalytical Chemistry*; John Wiley & Sons, Inc., 1983.
- (57) Gunzler, H.; Williams, A. *Handbook of Analytical Techniques*; Wiley-VCH, 2001; Vol. II.
- (58) Bain, C.; Troughton, E.; Tao, Y.; Evall, J.; Whitesides, G.; Nuzzo, R. *J. Am. Chem. Soc.* **1989**, *111*, 321.
- (59) Flink, S.; van Veggel, C.; Reinhoudt, D. *Adv. Mater.* **2000**, *12*, 1315.
- (60) Ju, H. *Phys. Chem. Chem. Phys.* **1999**, *1*, 1549.
- (61) Oldham, Myland *Fundamentals of Electrochemical Studies*, 1994.
- (62) Porter, M.; Bright, T.; Allara, D. *J. Am. Chem. Soc.* **1987**, *109*, 3559-3568.
- (63) Monk, P. *Electroanalytical Chemistry*; John Wiley & Sons, Inc., 2001.
- (64) Wang, J. *Analytical Electrochemistry*; 2nd ed.; Wiley-VCH, 2000.
- (65) Macdonald, J. *Impedance Spectroscopy*, 1987.

- (66) Yoo, J.; Park, S. *Anal. Chem.* **2000**, *72*, 2035.
- (67) Skoog, D.; Holler, F.; Nieman, T. *Principles of Instrumental Analysis*; Fifth ed.; Saunders College Publishing, 1998.
- (68) Tony James: *C&E News* **2000**, 79.
- (69) Arimori, S.; James, T. *Tetrahedron Lett.* **2002**, *43*, 507.
- (70) DiCesare, N.; Lakowicz, J. *J. Phys. Chem.* **2001**, *105*, 6834-6840.
- (71) DiCesare, N.; Lakowicz, J. *Anal. Biochem.* **2001**, *294*, 154-160.
- (72) DiCesare, N.; Lakowicz, J. *Tetrahedron Lett.* **2001**, *42*, 9105.
- (73) DiCesare, N.; Pinto, M.; Schanze, K.; Lakowicz, J. *Langmuir* **2002**, *18*, 7785.
- (74) Koh: Lee, M.; Hur, Y.; Kim, T. *Microchem. J.* **2002**, *72*, 315-321.
- (75) Pavey, K.; Olliff, C.; Baker, J.; Paul, F. *Chem. Commun.* **1999**, 2223.
- (76) Bain, C.; Whiteside, G. *Langmuir* **1989**, *5*, 1370.
- (77) Brewer, S.; Allen, A.; Lappi, S.; Chasse, T.; Breggman, K.; Gorman, C.; Franzen, S. *Langmuir* **2004**, *20*, 5512.
- (78) Bowden, E.; Nahir, T. *J. Electroanal. Chem.* **1196**, *410*, 9.
- (79) Han, S.; Seo, H.; Chung, Y.; Kim, K. *Langmuir* **2000**, *16*, 9493.
- (80) Lee, M.; Kim, T.; Kim, K.; Kim, J.; Choi, M.; Choi, H.; Koh, K. *Anal. Biochem.* **2002**, *310*, 163.
- (81) Shen, H.; Mark, J.; Seliskar, C.; Mark, H.; Heineman, W. *J. Solid State Electrochem* **1997**, *1*, 148-154.
- (82) Sinniah, K.; Cheng, J.; Terrettaz, S.; Robey, J.; Miller, C. *J. Phys. Chem.* **1995**, *99*, 14500.
- (83) Hsueh, C.; Lee, M.; Freund, M.; Ferguson, G. *Angew. Chem. Int. Ed. Engl.* **2000**, *39*, 1228.
- (84) Mizuno, T.; Fukumatsu, T.; Takeuchi, M.; Shinkai, S. *J. Chem. Soc., Perkin Trans. 1* **2000**, 407.
- (85) Norrild, J.; Sotofte, I. *J. Chem. Soc., Perkin Trans. 2* **2002**, *2*, 303.
- (86) Auletta, T.; van Veggel, F.; Reinhoudt, D. N. *Langmuir* **2002**, *18*, 1288.
- (87) Chidsey, C. E. D.; Bertozzi, C. R.; Putvinski, T. M.; Muijsce, A. M. *J. Am. Chem. Soc.* **1990**, *112*, 4301.
- (88) Chidsey *J Am Chem Soc* **1989**, *109*, 3559.
- (89) Chidsey, C. *Science* **1991**, *251*, 919.
- (90) Creager, S.; Rowe, G. *Anal. Chim. Acta* **1991**, *246*, 233.
- (91) Creager, S.; Clarke, J. *Langmuir* **1994**, *10*, 3675.
- (92) Creager, S.; Rowe, G. *J. Electroanal. Chem.* **1997**, *420*, 291.
- (93) David Grosser, J. *Cyclic Voltammetry*; VCH, 1993.
- (94) Long, H. D.; Donohue, J.; Buttry, D. *Langmuir* **1991**, *7*, 2196-2202.
- (95) Yoon, J.; Czarnik, A. *J. Am. Chem. Soc.* **1992**, *114*, 5874.
- (96) Wiskur, S.; Lavinge, J.; Ait-Haddou, H.; al., e. *Organic Letters* **2001**, *3*, 1311-1314.
- (97) Hsu, Y.; Penner, T.; Whitten, D. *Langmuir* **1994**, *10*, 2757.
- (98) Nakazawa, I.; Suda, S.; Masuda, M.; Asai, M.; Shimizu, T. *Chem. Commun.* **2000**, 881.
- (99) Beulen, M.; Veggel, F. v.; Reinhoudt, D. *Chem. Comm.* **1999**, 503.
- (100) Finklea, H.; Yoon, K.; Chamberlain, E.; Allen, J.; Haddox, R. *J. Phys. Chem. B* **2001**, *105*, 3088.